

PREPARATION AND CHARACTERIZATION OF CONDUCTIVE POLYMER
COMPOSITES, AND THEIR ASSESSMENT FOR ELECTROMAGNETIC
INTERFERENCE SHIELDING MATERIALS AND CAPACITORS

A THESIS SUBMITTED TO
THE GRADUATE SCHOOL OF NATURAL AND APPLIED SCIENCES
OF
MIDDLE EAST TECHNICAL UNIVERSITY

BY

ÖZCAN KÖYSÜREN

IN PARTIAL FULFILLMENT OF THE REQUIREMENTS
FOR
THE DEGREE OF DOCTOR OF PHILOSOPHY
IN
CHEMICAL ENGINEERING

APRIL 2008

Approval of the thesis:

**PREPARATION AND CHARACTERIZATION OF CONDUCTIVE
POLYMER COMPOSITES, AND THEIR ASSESSMENT FOR
ELECTROMAGNETIC INTERFERENCE SHIELDING MATERIALS AND
CAPACITORS**

submitted by **ÖZCAN KÖYSÜREN** in partial fulfillment of the requirements for
the degree of **Doctor of Philosophy in Chemical Engineering Department,**
Middle East Technical University by,

Prof. Dr. Canan Özgen
Dean, Graduate School of **Natural and Applied Sciences**

Prof. Dr. Gürkan Karakaş
Head of Department, **Chemical Engineering**

Assoc. Prof. Dr. Göknur Bayram
Supervisor, **Chemical Engineering Dept., METU**

Examining Committee Members:

Prof. Dr. Ülkü Yılmaz
Chemical Engineering Dept., METU

Assoc. Prof. Dr. Göknur Bayram
Chemical Engineering Dept., METU

Prof. Dr. Zuhâl Küçükyavuz
Chemistry Dept., METU

Prof. Dr. Teoman Tinçer
Chemistry Dept., METU

Prof. Dr. Nursel Dilsiz
Chemical Engineering Dept., Gazi University

Date: 01.04.2008

I hereby declare that all information in this document has been obtained and presented in accordance with academic rules and ethical conduct. I also declare that, as required by these rules and conduct, I have fully cited and referenced all material and results that are not original to this work.

Name, Last name: Özcan Köysüren

Signature :

ABSTRACT

PREPARATION AND CHARACTERIZATION OF CONDUCTIVE POLYMER COMPOSITES, AND THEIR ASSESSMENT FOR ELECTROMAGNETIC INTERFERENCE SHIELDING MATERIALS AND CAPACITORS

Köysüren, Özcan

Ph.D., Department of Chemical Engineering

Supervisor: Assoc. Prof. Dr. Göknur Bayram

April 2008, 197 pages

The aim of this study was to improve electrical properties of conductive polymer composites. For this purpose, various studies were performed using different materials in this dissertation. In order to investigate the effect of alternative composite preparation methods on electrical conductivity, nylon 6/carbon black systems were prepared by both in-situ polymerization and melt-compounding techniques. When compared with melt compounding, in-situ polymerization method provided enhancement in electrical conductivity of nylon 6 composites.

Furthermore, it was aimed to improve electrical conductivity of polymer composites by modifying surface chemistry of carbon black. 1 wt. % solutions of 3-Aminopropyltriethoxysilane and formamide were tried as chemical modifier, and treated carbon black was melt mixed with low-density polyethylene (LDPE) and

nylon 6. According to electron spectroscopy for chemical analysis (ESCA), chemicals used for surface treatment may have acted as doping agent and improved electrical conductivity of polymer composites more than untreated carbon black did. Formamide was more effective as dopant compared to the silane coupling agent. In order to investigate electromagnetic interference (EMI) shielding effectiveness and dielectric properties of conductive polymer composites, 1, 2 and 3 wt. % solutions of formamide were tried as chemical modifier and treated carbon black was melt mixed with poly(ethylene terephthalate) (PET). Composites containing formamide treated carbon black exhibited enhancement in electrical conductivity, EMI shielding effectiveness and dielectric constant values compared to composites with untreated carbon black.

In order to enhance electrical conductivity of polymer composites, the selective localization of conductive particles in multiphase polymeric materials was aimed. For this purpose, carbon nanotubes (CNT) were melt mixed with polypropylene (PP)/PET. Grinding, a type of solid state processing technique, was applied to PP/PET/CNT systems to reduce the average domain size of blend phases and to improve interfacial adhesion between these phases. Grinding technique exhibited improvement in electrical conductivity and mechanical properties of PP/PET/CNT systems at low PET compositions.

To investigate application potential of conductive polymer composites, polyaniline (Pani)/carbon nanotubes (CNT) composites were synthesized and electrochemical capacitance performances of these systems, as electrode material in electrochemical capacitors, were studied. Polyaniline/carbon nanotubes composites resulted in a higher specific capacitance than that of the composite constituents. Pseudocapacitance behavior of Pani might contribute to the double layer capacitance behavior of nanotubes. Additionally, as an alternative to Pani/CNT systems, polyaniline films were deposited on treated current collectors and electrochemical capacitance performances of these electrode systems were investigated. The highest

specific capacitance of polyaniline/carbon nanotubes composites was 20 F/g and this value increased to 35.5 F/g with polyaniline film deposited on treated current collector.

Keywords: Conductive Polymer Composites, Electrical Conductivity, Microwave Properties, Electrochemical Capacitance

ÖZ

İLETKEN POLİMER KOMPOZİTLERİNİN HAZIRLANMASI VE KARAKTERİZASYONU, VE BUNLARIN ELEKTROMANYETİK PARAZİT KALKANLARI VE KAPASİTÖRLER İÇİN DEĞERLENDİRİLMESİ

Köysüren, Özcan

Doktora, Kimya Mühendisliği Bölümü

Tez Yöneticisi : Doç. Dr. Göknur Bayram

Nisan 2008, 197 sayfa

Bu çalışmanın amacı, iletken polimer kompozitlerinin elektriksel özelliklerini geliştirmektir. Bu amaçla, tez kapsamında değişik malzemeler kullanılarak farklı çalışmalar yapılmıştır. Alternatif kompozit hazırlama yöntemlerinin elektriksel iletkenliğe olan etkisini incelemek için, naylon 6/karbon siyahı sistemleri yerinde polimerizasyon ve eriyik karıştırma yöntemleri ile hazırlanmıştır. Eriyik karıştırma yöntemi ile karşılaştırıldığında, yerinde polimerizasyon yöntemi naylon 6 kompozitlerinin elektriksel iletkenliğinde gelişme sağlamıştır.

Ayrıca, karbon siyahının yüzey özelliklerini değiştirerek, polimer kompozitlerin elektriksel iletkenliğini geliştirmek amaçlanmıştır. Ağırlıkça % 1'lik 3-Aminopropyltriethoxysilane ve formamid solüsyonları, kimyasal işlem elemanı olarak denenmiştir ve işlem görmüş karbon siyahı, alçak-yoğunluklu polietilen

(LDPE) ve naylon 6 ile ayrı ayrı eriyik halde karıştırılmıştır. Kimyasal analiz için elektron spektroskopu'na (ESCA) göre, yüzey işlemi için kullanılan kimyasalların, doping etkisi gösterdiği ve polimer kompozitlerin elektriksel iletkenliğini işlem görmemiş karbon siyahından daha fazla geliştirdiği anlaşılmıştır. Silan tip bağlayıcıya göre, formamid'in doping etkisi daha fazladır. İletken polimer kompozitlerinin elektromanyetik parazit (EMI) kalkanı etkililiği ve dielektrik özelliklerini incelemek için, ağırlıkça % 1, 2 ve 3'lük formamid solüsyonları kimyasal işlem elemanı olarak denenmiştir ve işlem görmüş karbon siyahı, poli (etilen tereftalat) (PET) ile eriyik halde karıştırılmıştır. Formamid ile işlem görmüş karbon siyahı içeren kompozitler, işlem görmemiş karbon siyahı içeren kompozitlere göre, elektriksel iletkenlik, EMI kalkanı etkililiği ve dielektrik sabiti değerlerinde gelişme göstermiştir.

Polimer kompozitlerin elektriksel iletkenliğini artırmak için, iletken dolgu maddesinin çok fazlı polimer malzemelerde tercihli dağılımı amaçlanmıştır. Bu plan doğrultusunda karbon nanotüp, polipropilen (PP)/PET ile eriyik halde karıştırılmıştır. Karışım fazlarının ortalama boyutlarını küçültmek ve bu fazlar arasındaki yapışmayı artırmak için PP/PET/CNT sistemlerine, bir çeşit katı hal proses yöntemi olan öğütme uygulanmıştır. Öğütme tekniği, PP/PET/CNT sistemlerinin düşük PET kompozisyonlarında elektriksel iletkenlik ve mekanik özellikler bakımından gelişme sağlamıştır.

İletken polimer kompozitlerinin uygulama potansiyelini incelemek için, polianilin (Pani)/karbon nanotüp (CNT) kompozitleri sentezlenmiştir ve bu sistemlerin elektrokimyasal kapasitörlerde elektrot malzemesi olarak elektrokimyasal kapasitans performansları çalışılmıştır. Polianilin/karbon nanotüp kompozitleri, kendi bileşenlerine göre daha fazla özgül kapasitans sağlamıştır. Pani'nin pseudokapasitans davranışı, nanotüp'ün çift katmanlı kapasitans davranışına katkıda bulunmuş olabilir. Ayrıca, Pani/CNT sistemlerine alternatif olarak, işlem görmüş akım kollektörlerine polianilin filmler kaplanmıştır ve bu elektrot sistemlerinin elektrokimyasal

kapasitans performansları incelenmiştir. Polianilin/karbon nanotüp kompozitlerinin en yüksek özgül kapasitans değeri 20 F/g olarak elde edilmiştir ve bu değer işlem görmüş akım kollektörü üzerine kaplanan polianilin film ile 35.5 F/g'a yükselmiştir.

Anahtar Kelimeler: İletken Polimer Kompozitleri, Elektriksel İletkenlik, Mikrodalga Özellikleri, Elektrokimyasal Kapasitans

To My Family

ACKNOWLEDGEMENTS

I wish to express my sincere appreciation to my thesis supervisor Assoc. Prof. Dr. Göknur Bayram for her valuable guidance, encouragement and support for this study. In addition, I wish to thank Prof. Dr. Ülkü Yılmaz and Prof. Dr. Zuhâl Küçükyavuz for their helpful advice necessary for the completion of this work.

I am thankful to Prof. Ning Pan from the University of California at Davis for giving me the opportunity to study in his laboratories in the field of nano supercapacitors investigation and characterization.

I would like to thank Prof. Dr. H. Önder Özbelge for his valuable advice during my teaching assistantship for many semesters.

I would also like to acknowledge Sertan Yeşil for his great help both in research and experiments.

I want to thank my previous lab mates Dr. Güralp Özkoç, Dr. Işıl Işık Gülsaç, Elif Alyamaç, Aslı Tolga and my present lab mates Mert Kılınç, İlknur Çakar, Fatma Işık Çoşkunes, Damla Eroğlu, Filiz Cengiz, Canan Yeniova and Tijen Seyidoğlu who have been a constant source of support and inspiration for me.

Finally, a very special thanks to my family for their encouragement and support throughout my life and education.

TABLE OF CONTENTS

ABSTRACT.....	iv
ÖZ.....	vii
ACKNOWLEDGMENTS.....	xi
TABLE OF CONTENTS.....	xii
LIST OF TABLES.....	xix
LIST OF FIGURES.....	xxi
LIST OF ABBREVIATIONS.....	xxxii
CHAPTER	
1. INTRODUCTION.....	1
2. BACKGROUND.....	7
2.1. Conductive Polymer Composites.....	7
2.1.1. Conductive Fillers.....	8
2.1.1.1. Carbon Black (CB).....	9
2.1.1.2. Carbon Nanotubes (CNT).....	10
2.1.2. Polymer Matrices.....	12
2.1.2.1. Nylon 6.....	13
2.1.2.2. Low-Density Polyethylene (LDPE).....	16
2.1.2.3. Poly(ethylene terephthalate) (PET).....	17

2.1.2.4. Polypropylene (PP).....	18
2.1.2.5. Polyaniline (Pani).....	18
2.1.3. Polymer Composites and Blends.....	23
2.1.3.1. Polymer Composite and Blend Preparation Methods...	25
2.1.3.1.1. Extrusion.....	25
2.1.3.1.2. In-Situ Polymerization (Polymerization Filling).	26
2.1.3.1.3. Solid State Grinding.....	27
2.1.4. Surface Treatment of Composite Constituents.....	28
2.1.4.1. Surface Energy of Composite Constituents.....	28
2.1.4.2. Interfacial Strength and Selective Localization of Filler.....	29
2.1.4.3. Doping.....	30
2.2. Experimental Techniques for Material Characterization.....	32
2.2.1. Solution and Melt Viscosity, and Average Molecular Weights	32
2.2.2. Electrical Conductivity.....	34
2.2.3. Mechanical Properties.....	37
2.2.3.1. Tensile Test.....	37
2.2.3.2. Impact Test.....	38
2.2.4. Scanning Electron Microscopy (SEM) and Transmission Electron Microscopy (TEM).....	39
2.2.5. Electron Spectroscopy for Chemical Analysis (ESCA).....	40

2.2.6. X-Ray Diffraction (XRD).....	40
2.2.7. Microwave Properties.....	41
2.2.7.1. Electromagnetic Interference (EMI) Shielding Effectiveness (SE).....	41
2.2.7.2. Dielectric Constant.....	44
2.2.8. Fourier Transform Infrared (FTIR) Spectroscopy.....	45
2.2.9. Electrochemical Capacitance Performances.....	45
2.2.9.1. Cyclic Voltammetry.....	48
2.2.9.2. Charge-Discharge Test.....	50
2.2.9.3. AC Impedance Analysis.....	51
3. EXPERIMENTAL.....	53
3.1. Preparation of Nylon 6/Carbon Black Composites.....	53
3.1.1. Materials.....	54
3.1.2. Composite Preparation Techniques	55
3.2. Effect of Surface Treatment of Filler on LDPE/Carbon Black, Nylon 6/Carbon Black and PET/Carbon Black Composites.....	59
3.2.1. Materials.....	59
3.2.2. Surface Treatment of Carbon Black.....	60
3.2.3. Composite Preparation.....	61
3.3. Effect of Grinding on PP/PET and PP/PET/CNT Systems.....	63
3.3.1. Materials.....	64
3.3.2. Blend and Composite Preparation and Grinding.....	65

3.4. Characterization of Conductive Polymer Composites and Blends...	67
3.4.1. Intrinsic Viscosity Measurement.....	67
3.4.2. Melt Flow Index Test.....	68
3.4.3. Electrical Conductivity Characterization.....	68
3.4.4. Mechanical Property Characterization.....	69
3.4.4.1. Tensile test.....	69
3.4.4.2. Impact test.....	70
3.4.5. Morphology Analysis.....	70
3.4.5.1. Scanning Electron Microscopy (SEM).....	70
3.4.5.2. Transmission Electron Microscopy (TEM).....	71
3.4.6. Electron Spectroscopy for Chemical Analysis.....	71
3.4.7. Contact Angle Measurement.....	72
3.4.8. X-Ray Analysis.....	73
3.4.9. Microwave Property Characterization.....	73
3.4.9.1. EMI Shielding Effectiveness Analysis.....	73
3.4.9.2. Dielectric Constant Measurement.....	74
3.5. Electrochemical Capacitance Performances of Polyaniline/Carbon Nanotubes Composites and Polyaniline Films on Treated Current Collectors.....	76
3.5.1. Materials.....	77
3.5.2. Growth of Carbon Nanotubes.....	78

3.5.3. Synthesis of Polyaniline and Polyaniline/Carbon Nanotubes Composites.....	79
3.5.4. Preparation of Polyaniline Films on Treated Current Collectors.....	80
3.5.5. Characterization of Polyaniline/Carbon Nanotubes and Polyaniline Films on Treated Current Collectors.....	81
3.5.5.1. Fourier Transform Infrared (FTIR) Spectroscopy.....	81
3.5.5.2. Electrochemical Capacitance Characterization.....	82
3.5.5.3. Scanning Electron Microscopy (SEM).....	82
4. RESULTS AND DISCUSSION.....	84
4.1. Preparation of Nylon 6/Carbon Black Composites.....	84
4.1.1. Intrinsic Viscosity and Melt Flow Index Measurements.....	85
4.1.2. Electrical Conductivity Characterization.....	86
4.1.3. Mechanical Property Characterization.....	88
4.1.4. Morphology Analysis.....	93
4.2. Effect of Surface Treatment of Filler on LDPE/Carbon Black, Nylon 6/Carbon Black and PET/Carbon Black Composites.....	95
4.2.1. Electron Spectroscopy for Chemical Analysis.....	96
4.2.2. Effect of Surface Treatment of Filler on LDPE/Carbon Black and Nylon 6/Carbon Black.....	104
4.2.2.1. Electrical Conductivity Characterization.....	104
4.2.2.2. Surface Energy Analysis.....	106

4.2.2.3. X-Ray Diffraction Analysis.....	107
4.2.2.4. Mechanical Property Characterization.....	108
4.2.3. Effect of Surface Treatment of Filler on PET/Carbon black (EMI shielding and Dielectric Material Applications of Conductive Polymer Composites).....	109
4.2.3.1. Electrical Conductivity Characterization.....	110
4.2.3.2. Microwave Property Characterization.....	112
4.2.3.2.1. EMI Shielding Effectiveness Analysis.....	112
4.2.3.2.2. Dielectric Constant Measurement.....	119
4.2.3.3. Morphology Analysis.....	121
4.3. Effect of Grinding on PP/PET and PP/PET/CNT Systems.....	122
4.3.1. Surface Energy Analysis and Selective Localization of CNT.....	122
4.3.2. Electrical Conductivity Characterization.....	124
4.3.2.1. High Temperature Processing of Ground PP/PET/CNT Systems.....	126
4.3.2.2. Effect of Carbon Nanotubes Content on PP/PET/CNT System.....	128
4.3.3. Mechanical Property Characterization.....	129
4.3.3.1. High Temperature Processing of Ground PP/PET/CNT Systems	134
4.3.4. Morphology Analysis.....	136

4.4. Electrochemical Capacitance Performances of Pani/CNT and Pani Films on Treated Current Collectors.....	140
4.4.1. Fourier Transform Infrared (FTIR) Spectroscopy.....	140
4.4.2. Electrochemical Capacitance Performances of Pani/CNT Composites.....	144
4.4.3. Scanning Electron Microscopy of Pani/CNT Composites...	150
4.4.4. Electrochemical Capacitance Performances of Pani Films on Treated Current collectors.....	155
5. CONCLUSIONS.....	164
5.1. Preparation of Nylon 6/Carbon Black Composites.....	164
5.2. Effect of Surface Treatment of Filler on LDPE/Carbon Black, Nylon 6/Carbon Black and PET/Carbon Black Composites.....	164
5.3. Effect of Grinding on PP/PET and PP/PET/CNT Systems.....	165
5.4. Electrochemical Capacitance Performances of Pani/CNT and Pani Films on Treated Current Collectors.....	166
6. RECOMMENDATIONS.....	167
REFERENCES.....	169
APPENDICES.....	190
A. X-RAY DIFFRACTION PATTERNS.....	190
B. ELECTROCHEMICAL CAPACITANCE PERFORMANCES OF POLYANILINE/CARBON NANOTUBES COMPOSITES.....	192
CURRICULUM VITAE.....	195

LIST OF TABLES

TABLES

Table 3.1 Chemicals for ring opening polymerization of nylon 6.....	54
Table 3.2 Properties of commercial grade nylon 6 and carbon black.....	54
Table 3.3 Physical properties of materials.....	60
Table 3.4 Extrusion process condition of LDPE/carbon black, nylon 6/carbon black and PET/carbon black composites.....	62
Table 3.5 Compression molding process condition of LDPE/carbon black, nylon 6/carbon black and PET/carbon black composites.....	63
Table 3.6 Physical properties of materials	64
Table 3.7 Surface energy components of probe liquids, (mN/m) [127].....	72
Table 3.8 Chemicals used for polyaniline synthesis.....	77
Table 3.9 Chemicals used to treat the current collector and to coat it with polyaniline film.....	77
Table 4.1 Intrinsic viscosity $[\eta]$ and viscosity average molecular weight M_v ..	85
Table 4.2 Melt Flow Index results of composites prepared by method A and B.....	86
Table 4.3 Surface energy components of carbon black, (mJ/m ²).....	107

Table 4.4 Structural properties of untreated, APS treated and formamide treated carbon black (CB) in nylon 6 and LDPE matrices.....	108
Table 4.5 Tensile properties of composites containing untreated and treated carbon black (CB) with (\pm) standard deviations.....	109
Table 4.6 The surface energy components of PP, PET and CNT at 20 °C, (mJ/m ²).....	123
Table 4.7 The surface energy components of PP and PET calculated using theoretical equations for 20 and 260 °C, (mJ/m ²).....	123
Table 4.8 The interfacial tension between PP/PET/CNT composite constituents, (mJ/m ²).....	124

LIST OF FIGURES

FIGURES

Figure 2.1 Crystal structure of carbon black particle.....	9
Figure 2.2 Three types of single-walled carbon nanotubes with differing chirality [79].....	11
Figure 2.3 Reaction of caprolactam with sodium hydride in the initiation step of ring opening polymerization [86].....	14
Figure 2.4 Reaction of initiated caprolactam with N-acetylcaprolactam in the initiation step of ring opening polymerization [86].....	14
Figure 2.5 Reaction between growing chain and caprolactam in the propagation step of ring opening polymerization [86].....	15
Figure 2.6 Ring opening of growing chain by amide anion of initiated caprolactam [86].....	16
Figure 2.7 (a) Branching characteristic and (b) chemical structure of polyethylene.....	17
Figure 2.8 Chemical structure of poly(ethylene terephthalate).....	17
Figure 2.9 Chemical structure of polypropylene.....	18
Figure 2.10 Emeraldine salt (ES) form of polyaniline [88].....	19
Figure 2.11 Leucoemeraldine form of polyaniline [89].....	19

Figure 2.12 Pernigraniline form of polyaniline [89].....	20
Figure 2.13 Oxidation reaction of aniline and reduction of peroxydisulfate....	20
Figure 2.14 Dimer formation reaction of aniline radical cation.....	21
Figure 2.15 Oxidation of dimer into quinoidal diimine structure.....	21
Figure 2.16 The growth reaction of dimer to form trimer structure.....	22
Figure 2.17 The growth reaction of trimer to form polyaniline molecule.....	22
Figure 2.18 Illustration of a single-screw extruder [37].....	26
Figure 2.19 Bonding structures of (a) n-type dopant atom and (b) p-type dopant atom [78].....	31
Figure 2.20 Energy band scheme for (a) intrinsic semiconductor, (b) n-type semiconductor and (c) p-type semiconductor [78].....	32
Figure 2.21 Two common types of capillary viscometers, Ostwald and Ubbelohde [3].....	33
Figure 2.22 Resistance components of two point probe technique.....	35
Figure 2.23 Four point probe head.....	36
Figure 2.24 Illustration of a typical dumbbell test specimen [37].....	37
Figure 2.25 Idealized stress-strain curve for a polymer undergoing ductile failure [37].....	38
Figure 2.26 Illustration of a shield enclosure (a) to contain radiated emission and (b) to exclude radiated emissions.....	42
Figure 2.27 Polarization of conventional capacitor (a) without a dielectric material and (b) with a dielectric material.....	46

Figure 2.28 Polarization of electrochemical capacitor.....	47
Figure 2.29 Cyclic voltammogram of (a) an ideal double layer capacitor and (b) a pseudocapacitor.....	49
Figure 2.30 Galvanostatic charge-discharge plot of an ideal electrochemical capacitor.....	50
Figure 2.31 Impedance plots of (a) an ideal capacitor and (b) a real electrochemical capacitor [122].....	52
Figure 3.1 Experimental setup of nylon 6 synthesis	56
Figure 3.2 A photograph of the co-rotating twin screw extruder.....	57
Figure 3.3 A photograph of the compression molding device.....	58
Figure 3.4 A photograph of the injection molding device (Daca Instruments).....	58
Figure 3.5 Chemical structures of surface treatment agents (a) 3- Aminopropyltriethoxysilane (APS) and (b) formamide.....	59
Figure 3.6 A photograph of the laboratory scale injection molding instrument (DSM Micro 10 cc Injection Molding Machine)	63
Figure 3.7 A photograph of the Wiley mill intermediate model grinder.....	66
Figure 3.8 Experiment setup of dielectric constant measurement.....	75
Figure 3.9 Schematic illustration of experimental setup for carbon nanotubes synthesis.....	78
Figure 4.1 The electrical resistivity values of carbon black filled nylon 6 composites prepared by method A and method B.....	87

Figure 4.2 The tensile strength values of carbon black filled nylon 6 composites prepared by method A and method B.....	89
Figure 4.3 The tensile modulus values of carbon black filled nylon 6 composites prepared by method A and method B.....	90
Figure 4.4 The elongation at break values of carbon black filled nylon 6 composites prepared by method A and method B.....	91
Figure 4.5 Charpy impact strength values of carbon black filled nylon 6 composites prepared by method A and method B.....	92
Figure 4.6 SEM micrographs of impact fractured samples containing 6 wt. % carbon black, (a) Method A (x5000) and (b) Method B (x5000).....	93
Figure 4.7 TEM micrographs of impact samples containing 3 wt. % of carbon black, (a) Method A and (b) Method B	94
Figure 4.8 TEM micrographs of impact samples containing 3 wt. % of carbon black, (a) Method A and (b) Method B.....	95
Figure 4.9 High resolution spectrum of oxygen (O_{1s}) of untreated carbon black (UCB).....	97
Figure 4.10 High resolution spectrum of nitrogen (N_{1s}) of untreated carbon black (UCB).....	97
Figure 4.11 High resolution spectrum of oxygen (O_{1s}) of 1 wt. % APS solution treated carbon black (APS1-CB).....	98
Figure 4.12 High resolution spectrum of oxygen (O_{1s}) of 1 wt. % formamide solution treated carbon black (FA1-CB).....	99

Figure 4.13 High resolution spectrum of oxygen (O_{1s}) of 2 wt. % formamide solution treated carbon black (FA2-CB).....	99
Figure 4.14 High resolution spectrum of oxygen (O_{1s}) of 3 wt. % formamide solution treated carbon black (FA3-CB).....	100
Figure 4.15 High resolution spectrum of nitrogen (N_{1s}) of 1 wt. % APS solution treated carbon black (APS1-CB).....	102
Figure 4.16 High resolution spectrum of nitrogen (N_{1s}) of 1 wt. % formamide solution treated carbon black (FA1-CB).....	102
Figure 4.17 High resolution spectrum of nitrogen (N_{1s}) of 2 wt. % formamide solution treated carbon black (FA2-CB).....	103
Figure 4.18 High resolution spectrum of nitrogen (N_{1s}) of 3 wt. % formamide solution treated carbon black (FA3-CB).....	103
Figure 4.19 Doping mechanism of nitrogen atom during surface treatment of carbon black [134].....	104
Figure 4.20 The electrical resistivity values of (a) LDPE based composites....	105
Figure 4.20 (Cont'd) The electrical resistivity values of (b) nylon 6 based composites.....	106
Figure 4.21 Comparison of the electrical resistivity values of LDPE, nylon 6 and PET based composites containing untreated carbon black.....	110
Figure 4.22 The electrical resistivity values of PET based composites.....	111
Figure 4.23 Variation of absorption loss of PET/UCB and PET/FA1-CB systems in X-band range.....	113

Figure 4.24 Variation of absorption loss of composites containing 8 wt. % UCB, FA1-CB, FA2-CB and FA3-CB, respectively, in X-band range	114
Figure 4.25 Variation of return loss of PET/UCB and PET/FA1-CB systems in X-band range	115
Figure 4.26 Variation of return loss of composites containing 8 wt. % UCB, FA1-CB, FA2-CB and FA3-CB, respectively, in X-band range.....	116
Figure 4.27 Variation of insertion loss of PET/UCB and PET/FA1-CB systems in X-band range	117
Figure 4.28 Variation of insertion loss of composites containing 4 wt. % UCB, FA1-CB, FA2-CB and FA3-CB, respectively, in X-band range	117
Figure 4.29 Variation of insertion loss of composites containing 6 wt. % UCB, FA1-CB, FA2-CB and FA3-CB, respectively, in X-band range	118
Figure 4.30 Variation of insertion loss of composites containing 8 wt. % UCB, FA1-CB, FA2-CB and FA3-CB, respectively, in X-band range	118
Figure 4.31 Dielectric constant values of PET based composites at 8.5 GHz...	120
Figure 4.32 Dielectric constant values of PET based composites at 10 GHz...	120
Figure 4.33 SEM micrographs of impact fractured samples of PET containing (a) 6 wt. % UCB (x5000) and (b) 6 wt. % FA1-CB (x5000).....	121
Figure 4.34 Electrical resistivity of conventional and ground PP/PET/CNT systems.....	125
Figure 4.35 Electrical resistivity of ground PP/PET/CNT systems, prepared at 230 °C and 280 °C.....	127

Figure 4.36 Electrical resistivity of conventional and ground PP/PET/CNT systems containing 30 wt. % PET and different amount of carbon nanotubes..	128
Figure 4.37 Tensile strength values of conventional and ground PP/PET systems without carbon nanotubes	129
Figure 4.38 Tensile modulus values of conventional and ground PP/PET systems without carbon nanotubes.....	130
Figure 4.39 Tensile strength values of conventional and ground PP/PET/CNT systems.....	131
Figure 4.40 Tensile modulus values of conventional and ground PP/PET/CNT systems.....	132
Figure 4.41 Impact strength values of conventional and ground PP/PET systems.....	133
Figure 4.42 Impact strength values of conventional and ground PP/PET/CNT systems.....	134
Figure 4.43 Tensile strength values of ground PP/PET/CNT systems, prepared at 230 °C and 280 °C.....	135
Figure 4.44 Tensile modulus values of ground PP/PET/CNT systems, prepared at 230 °C and 280 °C.....	136
Figure 4.45 SEM micrographs of impact fractured samples of PP/PET/CNT (90/10/1) systems, etched with trifluoroacetic acid, (a) ground and (b) conventional.....	137

Figure 4.46 SEM micrographs of impact fractured samples of PP/PET/CNT (80/20/1) systems, etched with trifluoroacetic acid, (a) ground and (b) conventional.....	138
Figure 4.47 SEM micrographs of impact fractured samples of PP/PET/CNT (70/30/1) systems, etched with trifluoroacetic acid, (a) ground and (b) conventional.....	138
Figure 4.48 SEM micrographs of impact fractured samples of ground PP/PET/CNT (90/10/1) systems, etched with trifluoroacetic acid, (a) molded at 230 °C and (b) molded at 280 °C.....	139
Figure 4.49 Comparison of FTIR spectra of (a) pure carbon nanotubes, (b) pure polyaniline and (c) polyaniline/carbon nanotubes composite containing 40 wt. % polyaniline.....	141
Figure 4.50 Possible reaction between polyaniline and carbon nanotubes during polymerization process [132, 153].....	142
Figure 4.51 Comparison of FTIR spectra of polyaniline/carbon nanotubes composites containing (a) 10 wt. % polyaniline, (b) 20 wt. % polyaniline, (c) 60 wt. % polyaniline and (d) 80 wt. % polyaniline.....	143
Figure 4.52 Cyclic voltammetry curves of (a) pure carbon nanotubes, (b) polyaniline/carbon nanotubes composite containing 20 wt. % polyaniline and (c) pure polyaniline.....	145

Figure 4.53 Charge-discharge plots of (a) pure carbon nanotubes, (b) polyaniline/carbon nanotubes composite containing 20 wt. % polyaniline and (c) pure polyaniline.....	146
Figure 4.54 Relationship of polyaniline content of polyaniline/carbon nanotubes systems with the specific capacitance, calculated from charge/discharge plots.....	147
Figure 4.55 Electrochemical impedance spectra of (a) pure carbon nanotubes, (b) polyaniline/carbon nanotubes composite containing 20 wt. % polyaniline and (c) pure polyaniline.....	148
Figure 4.56 SEM micrographs of carbon nanotubes, (a) (x100000) and (b) (x300000).....	151
Figure 4.57 SEM micrographs of polyaniline/carbon nanotubes composite containing 20 wt. % polyaniline, (a) (x100000) and (b) (x300000).....	152
Figure 4.58 SEM micrographs of polyaniline/carbon nanotubes composite containing 40 wt. % polyaniline, (a) (x100000) and (b) (x300000).....	153
Figure 4.59 SEM micrographs of polyaniline/carbon nanotubes composite containing 60 wt. % polyaniline, (a) (x100000) and (b) (x300000).....	154
Figure 4.60 SEM micrograph of pure polyaniline, (x100000).....	155
Figure 4.61 Treatment of nickel foil with sulfuric acid and then with alizarin [163, 164].....	156
Figure 4.62 Coating of treated nickel foil with polyaniline base using alizarin [163, 164].....	157

Figure 4.63 Cyclic voltammetry plots of polyaniline based electrochemical capacitors	158
Figure 4.64 Specific capacitance values of polyaniline based electrochemical capacitors.....	159
Figure 4.65 Charge/discharge plots of polyaniline based electrochemical capacitors.....	160
Figure 4.66 Impedance spectra of polyaniline based electrochemical capacitors.....	161
Figure 4.67 Cyclic voltammetry plots of polyaniline based electrochemical capacitors and nickel (Ni) current collectors as a reference.....	162
Figure A.1 Diffraction pattern of 2 wt. % (a) formamide treated carbon black, (b) untreated carbon black and (c) APS treated carbon black in LDPE	190
Figure A.2 Diffraction pattern of 2 wt. % (a) formamide treated carbon black, (b) untreated carbon black and (c) APS treated carbon black in nylon 6.....	191
Figure B.1 Cyclic voltammetry curves of polyaniline/carbon nanotubes composites containing (a) 10 wt. % polyaniline, (b) 40 wt. % polyaniline, (c) 60 wt. % polyaniline and (d) 80 wt. % polyaniline.....	192
Figure B.2 Charge/discharge plots of polyaniline/carbon nanotubes composites containing (a) 10 wt. % polyaniline, (b) 40 wt. % polyaniline, (c) 60 wt. % polyaniline and (d) 80 wt. % polyaniline	193

Figure B.3 Electrochemical impedance spectra of polyaniline/carbon nanotubes composites containing (a) 10 wt. % polyaniline, (b) 40 wt. % polyaniline, (c) 60 wt. % polyaniline and (d) 80 wt. % polyaniline..... 194

LIST OF ABBREVIATIONS

Alizarin	Monosodium salt of 1,2-dihydroxyanthraquinone-3-sulphonic acid
APS	3-Aminopropyltriethoxysilane
APS1-CB	Carbon black treated with 1 wt. % APS solution
CB	Carbon black
CNT	Carbon nanotubes
EMI	Electromagnetic interference
ESCA	Electron spectroscopy for chemical analysis
FA1-CB	Carbon black treated with 1 wt. % formamide solution
FA2-CB	Carbon black treated with 2 wt. % formamide solution
FA3-CB	Carbon black treated with 3 wt. % formamide solution
FTIR	Fourier transform infrared
LDPE	Low-density polyethylene
Method A	Synthesis of nylon 6/carbon black masterbatch by in-situ polymerization technique and dilution with commercial nylon 6 in an extruder
Method B	Preparation of nylon 6/carbon black composite by melt mixing method

Ni	Nickel
NPA25	Untreated nickel electrodes deposited with polyaniline base solution, including 25 mg of polymer in 10 ml solvent
Pani	Polyaniline
PA6.7	Alizarin treated electrodes deposited with polyaniline base solution, including 6.7 mg of polymer in 10 ml solvent
PA16.7	Alizarin treated electrodes deposited with polyaniline base solution, including 16.7 mg of polymer in 10 ml solvent
PA25	Alizarin treated electrodes deposited with polyaniline base solution, including 25 mg of polymer in 10 ml solvent
PA50	Alizarin treated electrodes deposited with polyaniline base solution, including 50 mg of polymer in 10 ml solvent
PA100	Alizarin treated electrodes deposited with polyaniline base solution, including 100 mg of polymer in 10 ml solvent
PA250	Alizarin treated electrodes deposited with polyaniline base solution, including 250 mg of polymer in 10 ml solvent
PET	Poly(ethylene terephthalate)
PP	Polypropylene
SEM	Scanning electron microscopy
TEM	Transmission electron microscopy
UCB	Untreated carbon black
XRD	X-ray diffraction

CHAPTER 1

INTRODUCTION

One of the present aims of material research is to produce new materials with properties adapted to a particular application and to receive knowledge about the physical processes, determining the final properties of the materials [1]. For a long time, polymer application area has been limited by the branches that do not require high electrical conductivity from these materials [2]. Recently, there is a strong necessity to create polymer based materials with relatively higher electrical conductivity than that of conventional ones, without compromising the superior mechanical and processing properties [1]. The limitation in application area of polymeric materials has been ended after invention of conductive polymer composites [2]. These materials have a great importance among all engineering materials, since their electrical properties can be altered by changing the composite constituents and their compositions which give them the chance to have a wide range of application area [3]. They can be used in static dissipative, transducer, adhesive and electromagnetic interference shielding applications [2].

When electrically conductive filler is incorporated to a polymer matrix, electrical, mechanical and other properties of the pure material may change depending on the properties of individual components, the shape, size, and amount of the filler, the morphology of the system, and the interface between the components [4]. Especially, electrical conductivity of composite systems increases by several orders when the content of conductive filler reaches a definite value that is high enough for the formation of current conductive structures. This critical filler concentration is known

as percolation threshold. At that concentration, the filler particles are so close to each other that the electron transfer occurs from one particle to the neighboring one. Current conduction can be performed by tunneling process or direct contact of electrically conductive particles [2].

Electrical resistivity of conductive polymer composites depends on filler concentration, electrical resistivity of composite constituents, filler dispersion and process conditions [2]. In order to preserve properties of polymer matrix, conductive filler content of composites has to be as low as possible. For this purpose, different types of composite preparation methods have been applied to prepare electrically conductive polymer composites at lower filler composition. One of these methods is the formation of conductive polymer composites by melt mixing. In this method, conductive fillers are incorporated into polymer matrices using melt-compounding devices [5-10]. Another approach to reduce the percolation threshold concentration is to prepare conductive polymer composites by in-situ polymerization method, by which polymer is synthesized in the presence of conductive particles [6, 11-16]. This method, providing intimate contacts, improves the interfacial interaction between composite constituents by decreasing average agglomerate size of the conductive filler.

Electrical resistivity of conductive filler is the key for controlling the final properties of polymer composite [2]. Thus, any operation, resulting in a decrease in electrical resistivity of conductive filler also decreases the electrical resistivity of prepared composite. In the literature, carbon black is exposed to surface treatments to improve electrical conductivity of polymer composites [17, 18]. Bulk structure of carbon black, which consists of highly conductive graphene layers, and chemical nature of carbon black surface determine the electrical character of the filler. Hence, any type of functional groups present on carbon black surfaces and added by surface treatment, influence electrical conductivity of the filler [19]. Especially, surface

modifiers containing amine functional groups may improve electrical conductivity of carbon black and its composites [17, 20].

Surface treatment of conductive filler affects not only electrical conductivity but also electromagnetic interference (EMI) shielding effectiveness (SE) and dielectric property of conductive polymer composites, which possess high enough electric conductivity for their application as EMI shielding and dielectric material [21]. Electromagnetic radiation may interfere with the operation of electrical and electronic devices [22], which need to be shielded against transmission of electromagnetic wave. Shielding is the method to reduce or prevent interference of undesired electromagnetic radiation into devices [22, 23]. EMI shielding efficiency depends mostly on specific resistance of materials [2]. Hence, any attempt to increase electrical conductivity of composite may improve EMI shielding effectiveness [21, 22, 24-27]. Additionally, dielectric property is as important as electromagnetic interference shielding effectiveness of electronic and electrical devices since incident electric field from any source will affect operation performances of these equipment. This destructive effect of electric field may be diminished by using shielding material with high dielectric constant value [28, 29]. Electrical conductivity and dielectric constant value of insulating polymer can be improved by incorporation of conductive filler into the matrix [30-35]. Additionally, surface treatment, reducing electrical resistivity of filler, enhances both conductivity and dielectric constant value of polymer composites.

Another approach to decrease the percolation threshold concentration and electrical resistivity of conductive polymer composite relies upon the selective localization of conductive particles in immiscible polymer blends [36, 37]. However, blend phases tend to form large and inhomogeneous domains of homopolymers in incompatible system, resulting in poor interphase adhesion and also poor mechanical properties [36]. In literature, several techniques, such as reactive extrusion, in-situ polymerization and mechanical milling, have been developed to reduce coarse

domains of blend phases to nanoscale range [38-46]. Additionally, a new approach, solid-state shear pulverization method has been applied to obtain well dispersed and stable blend microstructure, composed of immiscible polymer phases [47-49]. Microstructured or nanostructured blend morphology is important in terms of electrical conductivity and mechanical properties of conductive polymer composites. Conventional melt mixing methods, e.g., extrusion, have limitations in preparation of microstructured or nanostructured blend systems [50]. As an alternative, grinding, a type of solid-state processing method, can be applied to reduce average domain size of conductive polymer composite, composed of two immiscible polymer phases, following the conventional melt mixing process. Grinding method will improve both electrical and mechanical properties of conductive polymer composite by increasing the contact probability between domains of blend phases.

In recent years, conductive polymer composites have attracted great attention due to their potential application as an electrode material in electrochemical capacitors, which are electrical energy storing devices similar to conventional batteries and dielectric capacitors. They can store energy by utilizing double layer and pseudocapacitance processes [51-53]. In order to achieve high performance as a capacitor, the electrode material should have a high surface area, a high double layer capacitance and pseudocapacitance [53]. Carbon nanotubes [54-62], possessing double-layer capacitance character, have been considered as ideal electrode material for electrochemical capacitors owing to high effective surface area, low electrical resistivity and nano-porous morphology to provide good electrolyte accessibility into the inner surface area of the electrode material, resulting in high specific capacitance (F/g). On the other hand, polyaniline, which possesses pseudocapacitance character and contributes to the double-layer capacitance by changing the number of mobile charges through pseudocapacitive redox reactions [63], has been thought as an alternative electrode material in electrochemical capacitors [64-71]. Recently, several attempts have been made to combine double layer capacitance behavior of carbon nanotubes with pseudocapacitance behavior of polyaniline by coating the

conducting polymer on nanoparticles [72-74]. Carbon nanotubes with high surface area and low resistivity turn coated polyaniline film into a nanoporous three-dimensional morphology [72, 73]. Polyaniline film with an enormous effective surface area results in enhanced double-layer capacitance and pseudocapacitance, since ions can diffuse and migrate easily in the active layer of this film [75].

The main aim of this dissertation was to develop conductive polymer composites with enhanced electrical properties and without sacrificing the mechanical properties. In the light of this purpose, different aspects were investigated in four main parts. In each part, different composite constituents were studied to obtain improved electrical properties. In the first part, two different composite preparation methods, melt mixing and in-situ polymerization, were developed to prepare nylon 6/carbon black systems in order to investigate their effects on conductivity and mechanical properties of prepared composites. In-situ polymerization method was attempted as an alternative to melt mixing method to improve electrical conductivity and mechanical properties of nylon 6 composites by reducing average agglomerate size of carbon black. Apart from the literature, masterbatch composite of nylon 6 was first synthesized by in-situ polymerization method and then diluted with commercial grade nylon 6 in an extruder. In the second part of the thesis, effect of surface treatment of carbon black on electrical conductivity of low-density polyethylene (LDPE) and nylon 6 composites was examined. Two different types of surface modifiers, 3-Aminopropyltriethoxysilane and formamide, were applied to carbon black particles to lower electrical resistivity of polymer composites. Additionally, surface treatment research was focused on developing and testing of conductive polymer composites for EMI shielding and dielectric material applications. Effect of surface treatment of carbon black on EMI shielding effectiveness and dielectric property of poly(ethylene terephthalate) (PET) composites was investigated. Only one type of surface modifier, formamide, with three different concentrations (1, 2 and 3 wt. %) was applied to carbon black particles to enhance electrical conductivity, EMI shielding effectiveness and dielectric constant value of PET composites. In the

third part, carbon nanotubes (CNT) were melt mixed with immiscible polypropylene (PP)/PET systems. Grinding, alternative to conventional melt mixing method, was carried out to improve both electrical conductivity and mechanical properties of PP/PET/CNT systems by reducing average domain size of blend phases and improving interfacial adhesion between these phases. In the last part, this thesis was focused on preparation and characterization of conductive polymer composite with high electrical conductivity and specific capacitance for electrochemical capacitor application. For this purpose, polyaniline/carbon nanotubes composites were developed and investigated for their electrochemical capacitance performances. Furthermore, apart from the studies reported in the literature, polyaniline films were deposited on treated current collectors, and their electrochemical capacitance behavior was studied.

CHAPTER 2

BACKGROUND

2.1 Conductive Polymer Composites

Materials can be divided into two main classes as conductors and insulators with respect to the electrical conductivity. Conductors and semiconductors, which are thermally excited insulators, are able to conduct electricity at a certain extent depending on the number of free charge carriers. The resistivity depends on the charge carrier concentration and its mobility [76]. Metal as a conductor has a resistivity range of 10^{-6} - 10^{-3} ohm.cm. Semiconductors are in the range of 10^{-3} - 10^7 ohm.cm. Materials with a resistivity in the range of 10^7 - 10^{12} ohm.cm are called as poor or semi-insulators [77]. If the resistivity is higher than 10^{12} ohm.cm, then the material is an insulator. Polymers are made up of molecules, whose atoms acquire a complete outer electron shell, with all the probable electron levels complete. If an energy band is completely full or completely empty, it plays no part in conductivity when an electric field is applied [2]. Electrons turn into conduction electrons only in case they are in a partially occupied band. This is a basis for classifying substances by conductivity types. As the temperature increases, the resistivity increases in conductors due to atomic vibrations. However, the resistivity decreases in insulators with the thermal effect due to an increase in the number of free charge carriers [78].

Polymer material can attain electric conductivity either by the synthesis of a polymer of definite chemical structure or by the introduction of electrically conductive filler. Conductive polymer composite consists of a polymer matrix and electrically

conductive particles dispersed in matrix. After introduction of conductive fillers, such as powders, flakes or fibers of different metals, graphite or carbon black, the electrical properties of composites change according to filling effect. In composite with low filler content, free charge carriers of conductive particles, which are electrons, have to pass through micro spaces between fillers, which are filled with the polymer matrix. Up to the percolation threshold concentration, tunneling distance is so much that insulating polymer will dominate the conduction mechanism. Beginning from the percolation content, conductive particles dominate the conduction mechanism and the direct contact may be provided at high filler concentrations. Conductive polymer composite has a nonlinear conduction character. Except for the percolation threshold concentration, electrical conductivity of composite exhibits small changes with increasing conductive filler composition. However, around the percolation content, the conductivity character changes suddenly following the filler chain structure [2].

Electrical conductivity and mechanical properties of conductive polymer composites depend on particle sizes of fillers and their agglomerate structure. Especially, small size of agglomerate structure is a required criterion for carbon based fillers to construct conductive networks at lower concentrations. However, due to strong agglomeration tendency, composites require large amounts of carbon based fillers and it is difficult to provide homogeneous distribution of these particles. In addition, mechanical properties of polymer composites change in a manner that they become fragile, and elasticity decreases with large amounts of filler addition [2].

2.1.1 Conductive Fillers

Many types of conductive filler in fiber or powder form can be added to polymeric materials to obtain the required degree of electrical conductivity. Carbon based filler, carbon black, carbon nanotubes, and carbon fibers, intrinsically conducting polymers, and metal particles are used in conductive polymer composites [79]. In the

content of this dissertation, two major types of carbonaceous fillers, carbon black and carbon nanotubes, were used as conductive fillers. In the first part of the thesis, carbon black was utilized to prepare nylon 6 composites by in-situ polymerization and melt mixing methods, respectively. In the second part, again carbon black was used as conductive filler. Surface treatment was applied to carbon black particles and treated filler was compounded with LDPE, nylon 6 and PET, respectively. In the third part of the dissertation, carbon nanotubes were utilized to prepare PP/PET/CNT composites. In the last part, polyaniline, type of conducting polymer, was used with carbon nanotubes as electrode material for electrochemical capacitor application.

2.1.1.1 Carbon Black (CB)

Carbon black is produced by burning of oil and natural gas. It has been used as a pigment and as reinforcing filler in rubber. Besides functioning in rubber, carbon black is also used as a UV stabilizer, antistatic and electromagnetic shielding agent, colorant, thermal antioxidant and conductive filler in plastics [80].

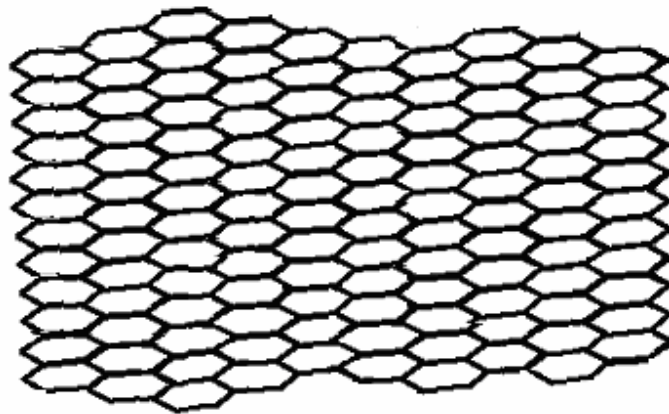


Figure 2.1 Crystal structure of carbon black particle

Carbon black has a structure similar to graphite. Each particle consists of separate crystal fragments with parallel layers (Figure 2.1). Carbon black particles connect with each other under the influence of van der Waals forces [2]. These particles are in agglomerate structure, which will affect physical properties of polymer composite by determining filler-matrix surface interactions. The reinforcing effect of filler can be estimated from the change of total interfacial area [80]. Carbon based fillers with high modulus and hardness values tend to increase the hardness and initial modulus of the polymer matrix. They also affect elongation, ultimate strength, toughness and processability of the polymer [3].

2.1.1.2 Carbon Nanotubes (CNT)

Carbon nanotubes, discovered by Iijima in 1991 [79], can be thought as being at the intersection of traditional carbon fiber and the fullerene [81]. They have unique structural and electronic properties [79]. Nanotubes can be classified into two types, multiwalled carbon nanotubes and single-walled carbon nanotubes (Figure 2.2). Multiwalled carbon nanotubes were discovered earlier than single-walled carbon nanotubes. They are composed of 2 to 30 concentric graphitic layers in diameters from 10 to 50 nm with an aspect ratio more than 1000. On the other side, single-walled carbon nanotubes have much thinner diameters from 1 to 1.4 nm [82].

Multiwalled carbon nanotubes have intrinsic properties suitable for field emitters in the form of a sharp tip with nanometer scale radius of curvature, chemical inertness, high mechanical stiffness and high electrical conductivity [82]. If the growth process of carbon nanotubes is optimized and controlled, the potential of these particles will be realized much more than today. For certain applications such as hydrogen storage and composite reinforcement, it is desired to obtain high quality carbon nanotubes at large scale with simple and inexpensive growth techniques. However, for electronic applications, it is required to produce nanotubes with controlled growth strategies.

Large scale production, defect-free nanotube structure and control of the nanotube growth are among challenging topics in the nanotube growth area [83].

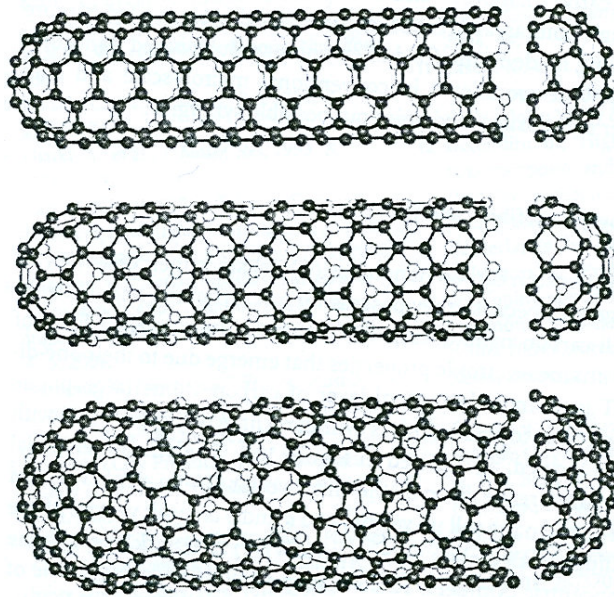


Figure 2.2 Three types of single-walled carbon nanotubes with differing chirality [79]

Multiwalled carbon nanotubes have been prepared by many kinds of methods including arc-discharge, laser ablation and thermal synthesis [84]. The arc-discharge method remains the most useful due to the ease with which significant quantities can be produced [81]. An arc is generated across a 1-mm gap between two graphite electrodes, 5 to 20 mm in diameter, with an inert gas such as helium or argon. Under a pressure of 100 to 1000 torr, nanotubes start to deposit on the cathode with the arc electric current of 80 amperes. Nanotubes produced by arc-discharge method need

extensive purification before use [84]. Laser ablation technique is similar to arc-discharge method in that both methods use graphite target to produce nanotubes. The graphite target is placed in a 1200 °C quartz tube furnace with an inert gas such as argon or helium. The growth of nanotubes starts with a laser pulse [84].

As an alternative to arc-discharge and laser ablation, carbon nanotubes can be produced by thermal synthesis method, which is based on mainly thermal energy and on active catalytic species. At a medium temperature, lower than 1200 °C, carbon source is exposed to break down on active catalysts such as Fe, Ni and Co for the growth of carbon nanotubes. Chemical vapor deposition can be considered as thermal synthesis method [84]. In the growth process of nanotubes at chemical vapor deposition technique, active catalytic species is heated to a certain temperature and a hydrocarbon gas flows through the reactor for a certain time period. Hydrocarbon molecules dissociate and precipitate on the catalyst particles to form tubular carbon solids in sp^2 structure, which is preferred over other carbon structures such as graphite since carbon solid in tubular structure is in a low energy state. Mostly, ethylene and acetylene are used as the carbon feedstock to produce multiwalled carbon nanotubes and the growth process takes place between 550-750 °C. Chemical vapor deposition is promising for growing high quality carbon nanotubes at large scales. The major drawback of this method is that nanotubes produced by using this technique possess high defect densities [83].

2.1.2 Polymer Matrices

In each part of this dissertation, different polymer-filler combinations were studied. In the first part, nylon 6 was utilized to prepare conductive polymer composites by melt mixing technique. Besides, nylon 6/carbon black composites were synthesized by in-situ polymerization method. At the surface treatment part of the thesis, low-density polyethylene (LDPE), commercial grade nylon 6 and poly(ethylene terephthalate) (PET) were used to combine treated carbon filler with polymer matrix.

In the third part, PET and polypropylene (PP) were studied to prepare composite systems composed of carbon nanotubes and different blends. In the final part of the dissertation, polyaniline was selected as matrix material for capacitor application of conductive polymer composites. Polyaniline was synthesized in the presence of carbon nanotubes by in-situ polymerization technique.

2.1.2.1 Nylon 6

Nylon 6, an engineering thermoplastic, have high modulus, tensile strength, hardness and impact resistance [3]. This polymer can be synthesized by ring opening polymerization, which is a type of chain growth polymerization mechanism. The active center responsible for the chain growth is combined with a single polymer molecule through the addition of many monomer units and relatively short reaction time is enough to obtain high molecular weight polymer, which are the general characteristics of chain growth polymerization mechanism [85].

In addition to caprolactam monomer, three more components, sodium hydride, N-acetylcaprolactam and polyethylene glycol, are required to perform nylon 6 synthesis. Sodium hydride is the initiator of this reaction, which initiates ring opening polymerization by reacting with caprolactam monomer. N-acetylcaprolactam is used as activator, which is essential for initiation step, especially. Polyethylene glycol is required to shield metallic initiator [86].

In the initiation step, sodium hydride reacts with monomer. Hydrogen is extracted from caprolactam and there will be a complex of sodium-caprolactam (Figure 2.3). Then, polyethylene glycol turns the metallic sodium into unreactive form by shielding it, which makes the initiated monomer more reactive with an amide anion [86].

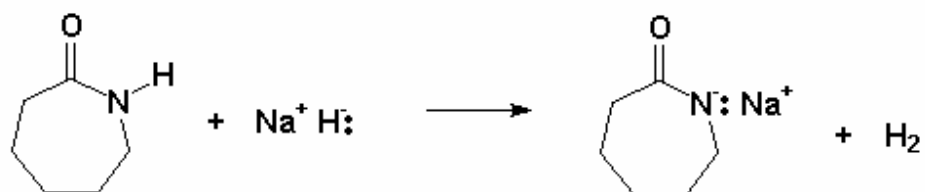


Figure 2.3 Reaction of caprolactam with sodium hydride in the initiation step of ring opening polymerization [86]

The initiation step continues with a reaction between initiated monomer and N-acetylcaprolactam, which leads to a fast reaction at relatively lower temperature. In this reaction, reactive amide anion opens the ring of the N-acetylcaprolactam, which will also complete the initiation step (Figure 2.4) [86].

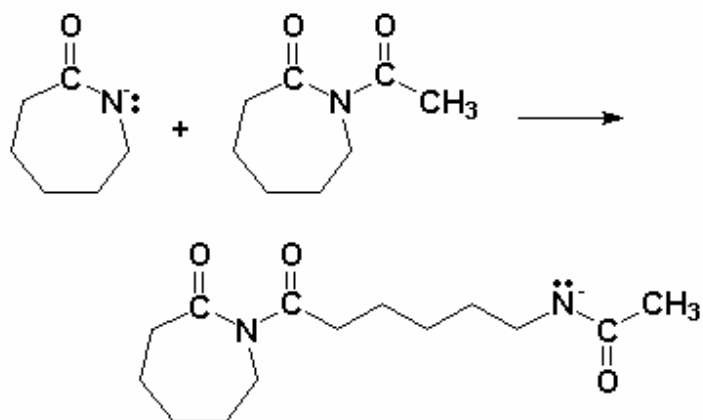


Figure 2.4 Reaction of initiated caprolactam with N-acetylcaprolactam in the initiation step of ring opening polymerization [86]

At the propagation step of ring opening polymerization, remaining caprolactam monomers are added to the growing chain. Amide anion of growing chain removes hydrogen of any caprolactam, which produces another amide anion on monomer, which opens the ring of the growing chain. Nylon 6 molecules continue to grow by addition of remaining monomers. Hence, propagation step continues until all monomers are used up. The reaction between growing chain and monomer are illustrated in Figures 2.5 and 2.6, respectively [86].

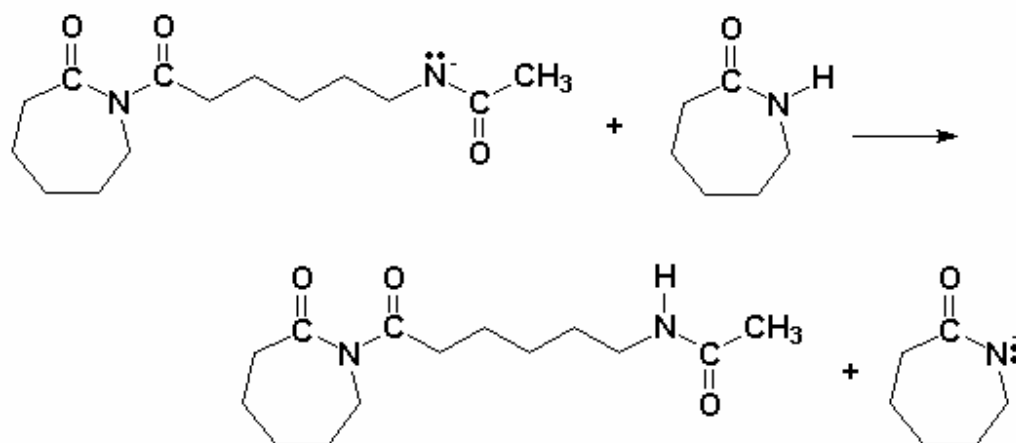


Figure 2.5 Reaction between growing chain and caprolactam in the propagation step of ring opening polymerization [86]

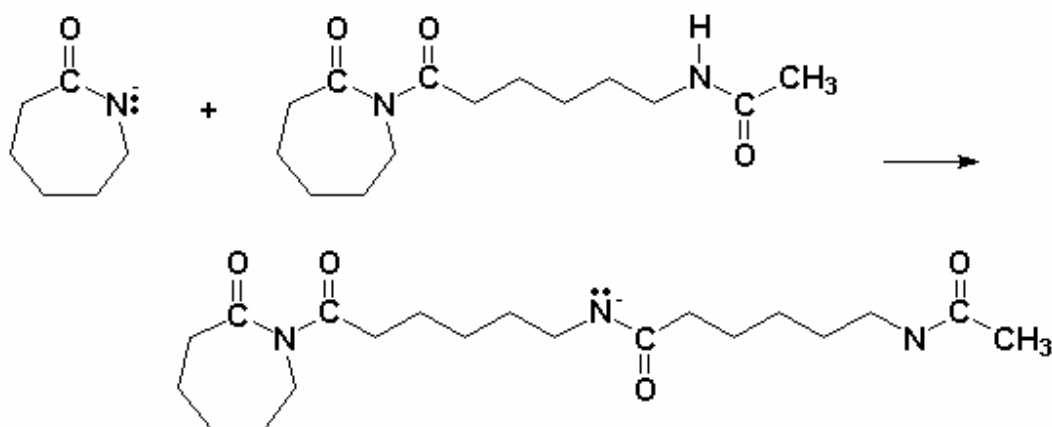


Figure 2.6 Ring opening of growing chain by amide anion of initiated caprolactam [86]

2.1.2.2 Low-Density Polyethylene (LDPE)

Low-density polyethylene (LDPE), which is composed of ethylene repeating units (Figure 2.7), is a partially crystalline polymer with a melting temperature around 115 °C [85]. It can be produced by free-radical bulk polymerization, which results in to a highly branched molecule. When compared with high-density polyethylene, LDPE provides low density and low crystalline-melting temperature due to its branching characteristic, reducing crystallinity [37, 87]. It is soluble only in a few solvent such as decalin, carbon tetrachloride, toluene and xylene at their boiling point temperatures. Polyethylene has good toughness and pliability over a wide temperature range. It has high electrical resistivity. In addition, it is a suitable material for dielectric application. Polyethylene is chemically inert and it has good resistance to water, acids and bases [85, 87]. Two-third of low density polyethylene is used in film and sheeting applications [85, 87]. The second largest market for low density polyethylene is extrusion coating for packaging materials [85].

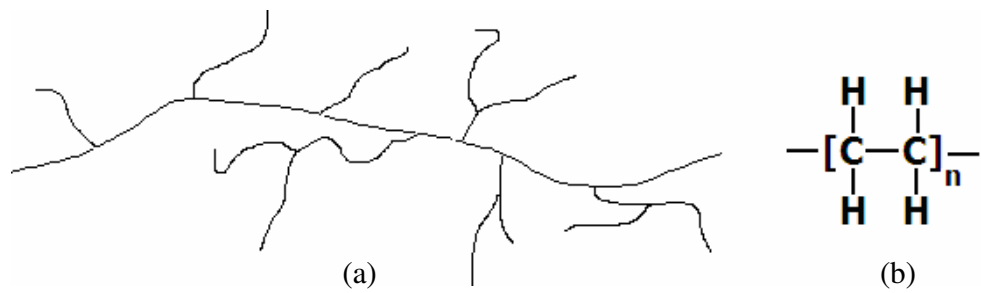


Figure 2.7 (a) Branching characteristic and (b) chemical structure of polyethylene

2.1.2.3 Poly(ethylene terephthalate) (PET)

Poly(ethylene terephthalate) (PET), whose chemical structure is illustrated in Figure 2.8, is among industrially important polyesters. It can be synthesized through ester interchange reactions of dimethyl terephthalic acid and ethylene glycol at around 200 °C [37]. PET can preserve its mechanical properties at temperatures near 150 °C due to its high crystalline melting point and glass transition temperature [85]. It illustrates high chemical and solvent resistance. Besides, PET is abrasion and oxidation resistant. Fiber, bottle and film applications constitute nearly the major use of this polymer in the world [37].

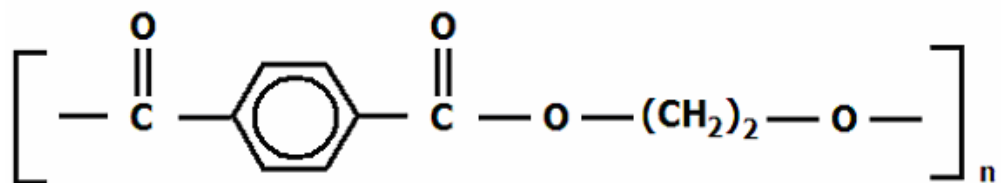


Figure 2.8 Chemical structure of poly(ethylene terephthalate)

2.1.2.4 Polypropylene (PP)

Polypropylene (Figure 2.9), the lightest major plastic, can be produced in isotactic form. It has 60 % to 70 % crystallinity in the isotactic structure [85, 87]. The existence of methyl side group gives the polymer a higher rigidity with elevated glass transition temperature, T_g . Besides, this side group causes higher sensitivity to oxidation or environmental exposure at elevated temperatures [87]. Due to its high crystallinity, polypropylene illustrates high tensile strength, stiffness and hardness, which leads to high utilization as packaging, containers, furniture, piping, electronic accessories, transportation, machinery parts and sanitary items [85, 87]. Polypropylene illustrates chemical inertness and moisture resistance as other hydrocarbon polymer does. In addition, it is free from environmental stress cracking [85].

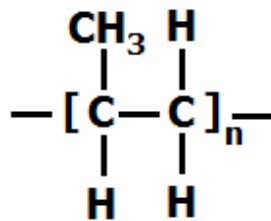


Figure 2.9 Chemical structure of polypropylene

2.1.2.5 Polyaniline (Pani)

Polyaniline, which is a conducting polymer, has an electrical resistivity of $\sim 10^{10}$ ohm.cm in emeraldine base form. During doping of the insulating form of

polyaniline, protons, H^+ , are added to a fraction of the formerly unprotonated nitrogen sites (Figure 2.10). Doping of emeraldine base with hydrochloric acid yields highly conducting emeraldine salt, having a resistivity of ~ 0.5 ohm.cm. Apart from other conducting polymers, the number of electrons on polyaniline backbone is held constant while the number of protons is varied [88].

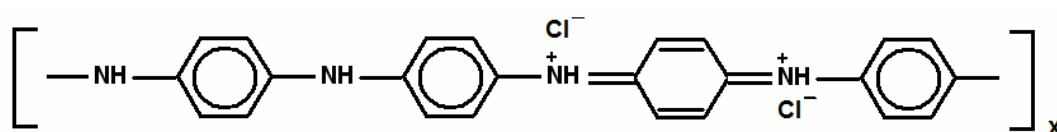


Figure 2.10 Emeraldine salt (ES) form of polyaniline [88]

In addition to emeraldine base form, polyaniline can be in the fully reduced poly(paraphenyleneamine) form, known as leucoemeraldine (Figure 2.11), and in the fully oxidized poly(paraphenyleneamine) form, known as pernigraniline, whose chemical structure is given in Figure 2.12 [89].

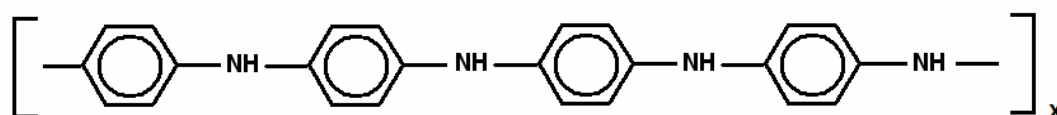


Figure 2.11 Leucoemeraldine form of polyaniline [89]

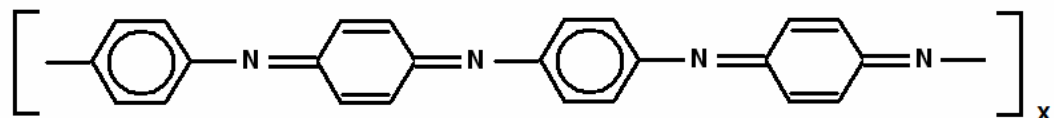


Figure 2.12 Pernigraniline form of polyaniline [89]

Aniline and peroxydisulfate are required to perform the synthesis of polyaniline. Aniline monomer exists in aqueous media as the anilinium cation and it turns to the aniline cation radical in the presence of the oxidizing agent, peroxydisulfate. This reaction is illustrated in Figure 2.13 [90].

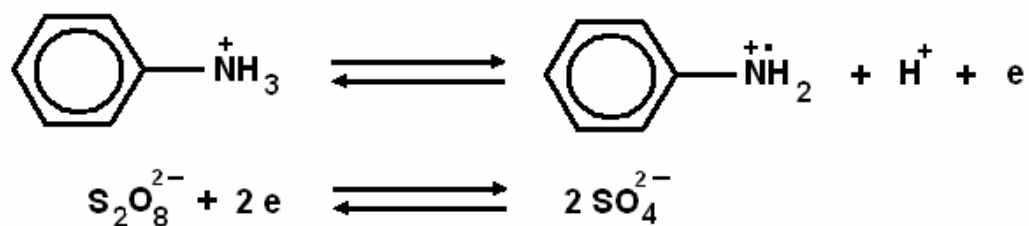


Figure 2.13 Oxidation reaction of aniline and reduction of peroxydisulfate

Aniline cation radicals combine to form dimer structure, which is known as pernigraniline [90]. The rate determining step of aniline polymerization process is the dimer formation step, which is illustrated in Figure 2.14 [91, 92].

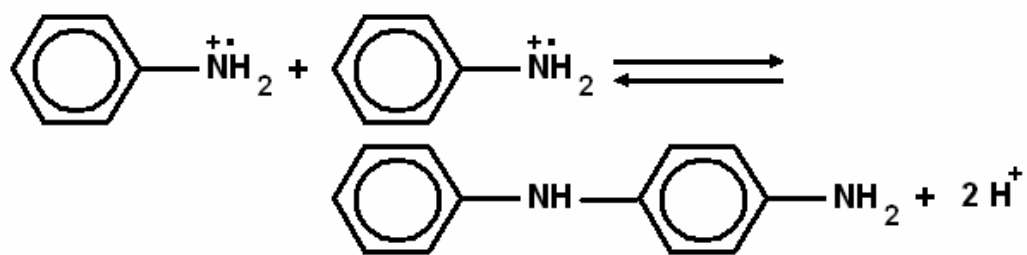


Figure 2.14 Dimer formation reaction of aniline radical cation

Then, the dimer is exposed to following oxidizing reaction to form quinoidal diimine structure. This reaction step, presented in Figure 2.15, takes place faster than the dimer formation step owing to lower oxidation potential of the dimer when compared with aniline [91, 92].

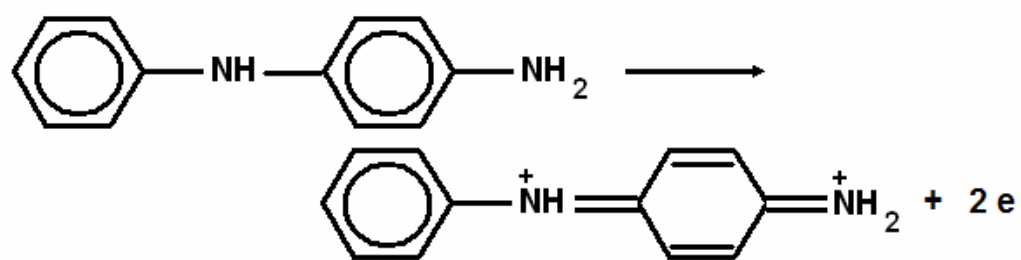


Figure 2.15 Oxidation of dimer into quinoidal diimine structure

Polymer chain continues to grow with the following reactions, which are given in Figures 2.16 and 2.17. In detail, the growth of polymer chain takes place through an electrophilic attack of the iminium cation on a neutral aniline monomer or through an electrophilic aromatic substitution reaction of nitrenium cation, intermediate product, with a neutral aniline monomer [92].

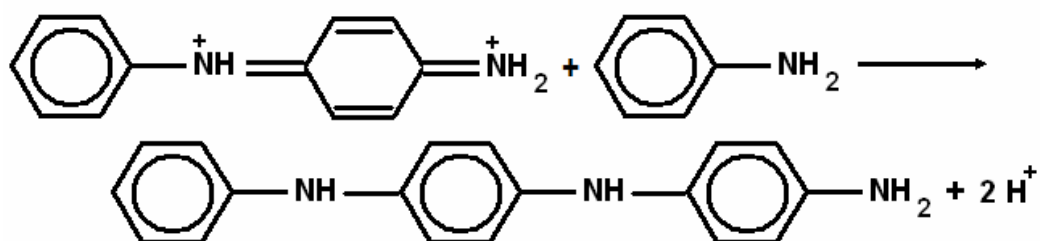


Figure 2.16 The growth reaction of dimer to form trimer structure

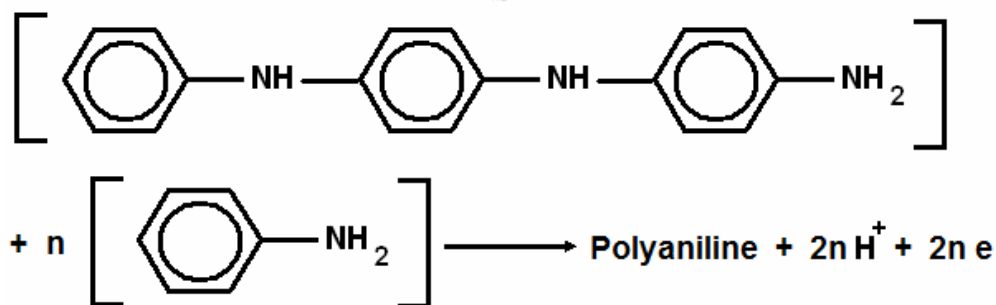


Figure 2.17 The growth reaction of trimer to form polyaniline molecule

As the chain length of polyaniline increases, the oxidation potential of formed oligomer structure decreases, resulting in faster reaction. Polymerization continues until all monomer, present in the reaction medium, is consumed. At the later stage of the polymerization, with a decrease in aniline concentration, dimer structures start to take part in the growth reactions instead of aniline monomers [92].

2.1.3 Polymer Composites and Blends

Polymer composites are mixtures of polymeric materials with organic or inorganic additives, which are fibers, flakes, spheres and particulates. Hence, they are composed of two or more phases. The additives can be continuous like long fibers, which are embedded in the matrix in regular arrangement. On the other hand, the additives can be discontinuous such as flakes and platelets, which are dispersed throughout the matrix. Additives can be classified as reinforcements, filler or reinforcing filler. Reinforcements, much stiffer and stronger than the matrix material, improve the modulus and strength of the polymer. At the same time, reinforcements affect thermal expansion, transparency and thermal stability of the matrix. Reinforcing fillers, which are discontinuous type of additives, are arranged in the matrix in different orientations [79].

Main reasons to prepare polymer composite are property modification or enhancement, overall cost reduction, and improving and controlling of processing characteristics. The parameters affecting the properties of polymer composites are the properties of the additives and their compositions, the interaction of components at the phase boundaries, and the method of fabrication [79]. To prepare polymer composite from thermoplastic polymer and solid additives, solution intercalation, melt intercalation, roll milling, emulsion polymerization, high shear mixing and in-situ polymerization (polymerization filling) methods are applied [93-95].

Most of the polymeric materials, which are used in many applications, are homopolymers. However, sophisticated applications require more complicated material systems, possessing combination of properties not attainable with simple homopolymer [36]. Development of new polymer systems to meet demands for high performance materials will take too long and will be too expensive. An alternative to the development of new polymer systems is the development of alloys and blends, which are a physical combination of two or more polymers to form a new material [96]. They are prepared to reduce the cost of an expensive homopolymer, to improve processability of an heat-sensitive homopolymer or to improve impact resistance [37].

Alloys and blends differ in the levels of inherent thermodynamic compatibilities and in resulting properties. Polymers in alloys tend to be mutually soluble over a limited concentration range; that is, individual polymeric components in alloys are intimately mixed on a molecular level through specific interactions between the polymer chains of the different components. On the other hand, polymeric components in blends separate into different phases, resulting in immiscible phases [96]. The simplest and economical technique to produce polymer blend is the physical blending of two or more polymers. The properties of physical blend depend on the degree of compatibility of homopolymers forming the blend system [36]. Compatible polymer blends form single phase systems with a single property. However, incompatible polymer blends are composed of a heterogeneous mixture of components and exhibit discrete polymer phases [96]. In incompatible blend system, constituents tend to form aggregations, resulting separated phases. Two phase morphological system possess large and inhomogeneous domains of homopolymers with poor interphase adhesion, resulting in poor mechanical properties. Large domains of phases result in stress concentrations at the phase boundaries. Hence, tensile strength, impact strength and elongation at break values of incompatible blend are relatively low. This two-phase morphology affects thermal and optical properties of the blend system. Opacity is also direct consequence of the phase

separation. The wavelength of light is smaller than domains of phases. Thus, light scattering occurs at the phase boundaries [36].

Polymer blends can be prepared by mechanical mixing, latex blending, fine powder mixing, dissolution in co-solvent then film casting, melt-compounding, and use of monomer as solvent for another blend component then polymerization.

2.1.3.1 Polymer Composite and Blend Preparation Methods

Various studies were performed to enhance electrical properties of conductive polymer composites. In light of this goal, several composite preparation methods were experimented using different materials. In the first part of the dissertation, commercial grade nylon 6 and carbon black were compounded in an extruder to prepare conductive polymer composites. Besides, as an alternative to melt mixing technique, nylon 6/carbon black composites were synthesized by polymerization filing method. At the surface treatment part of the thesis, low-density polyethylene (LDPE), commercial grade nylon 6 and poly(ethylene terephthalate) (PET), respectively, were compounded with treated carbon black particles in the extruder. In the following part, the same extruder was used to prepare polypropylene (PP)/PET/carbon nanotubes composites. In addition, solid state grinding was applied to PP/PET/CNT systems to obtain microstructured or nanostructured blend morphology. In the final part, polyaniline/carbon nanotubes composites were synthesized by in-situ polymerization method.

2.1.3.1.1 Extrusion

Extrusion is a melt-compounding technique by which thermoplastic materials in powdered or granular form are converted into a continuous melt. Extruder, shown in Figure 2.18, is widely used for shear sensitive materials and for compounding purposes. Adjustable and controllable parameters of extrusion processes are

temperature and shear rate, determining final properties of the extruder products. The screw, which is the moving part of the extruder, consists of three sections, which are melting, compression and metering. The melting section provides conveying solid pellets from the hopper and it converts the solid pellets into molten polymer. The compression section compacts and mixes the molten polymer to provide homogeneous melt to the metering section besides eliminating air bubbles in molten polymer. The metering section ensures a uniform flow rate and it generates the pressure needed to force the molten polymer out through the die. Some extruders feature two screws, co-rotating or counter rotating types. Twin screw extruder is preferable instead of single screw extruder to provide better mixing [93, 95, 96].

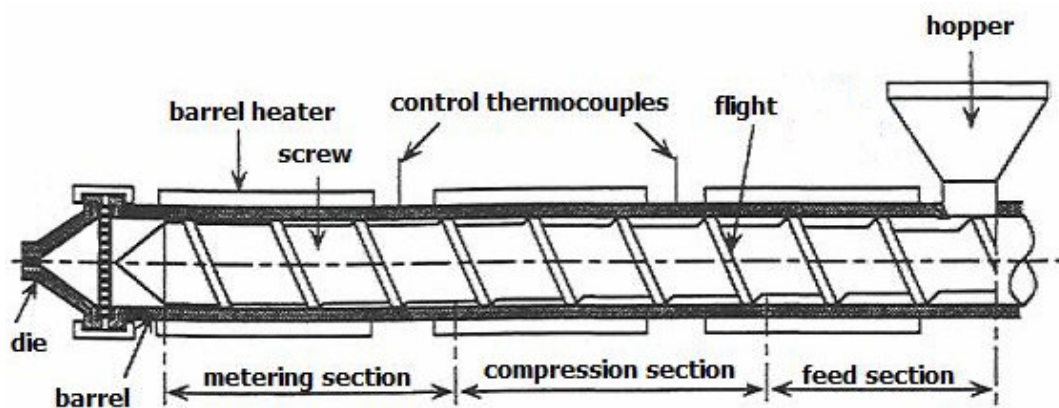


Figure 2.18 Illustration of a single-screw extruder [37]

2.1.3.1.2 In-Situ Polymerization (Polymerization Filling)

Composite can be prepared by synthesizing polymer matrix in the presence of organic or inorganic additives, which is known as in-situ polymerization method. In

this technique, low molecular weight monomers are able to penetrate into the agglomerate structure of fillers during synthesis, providing intimate contact between the filler and the polymer [11]. In-situ polymerization method provides the most homogeneous distribution of the filler in the polymer matrix; whereas, melt-compounded composite shows preferential orientation of the additives due to low melt viscosity and poor filler-matrix interactions [15]. Furthermore, in melt-compounding method, filler agglomerates cannot be broken into pieces due to the poor mobility of macromolecules in composite and limited shearing force of melt-compounding equipment [11]. Hence, in-situ polymerization method can be chosen as an alternative to melt-compounding technique to prepare composites with enhanced properties. Especially, with this method, electrical conductivity of polymer composites can be improved. In-situ polymerization technique provides a decrease in average agglomerate size of conductive filler, which leads to a reduction in percolation threshold concentration of conductive polymer composites [11].

2.1.3.1.3 Solid State Grinding

Grinding is a size reduction application in which particles of solids are cut or broken into smaller pieces. Grinder is a type of size reduction machine for intermediate duty. The chief types of grinders are hammer mills and impactors, rolling-compression machines, attrition mills, and tumbling mills. Among the grinders, the hammer mill can be used for general purposes. This type of grinder contains a high-speed rotor turning inside a cylindrical casing. Feed dropped into the top of the casing is broken and falls out through a bottom opening. Particles are broken by sets of swing hammers pinned to a rotor disk [97].

To reduce the domain size of phases and stabilize the morphology, an efficient and intensive mechanical dispersion of immiscible blend components is required. Mechanical mixing methods such as solid state grinding result in interlocking the polymer phases into a stable and desired morphology by physical means. High shear

mixing provided by solid state grinding can disrupt coarse domains of phases and convert immiscible blend morphology to microstructured or nanostructured form. According to final performance of the blend, the size of the dispersed phase can be optimized [98].

2.1.4 Surface Treatment of Composite Constituents

2.1.4.1 Surface Energy of Composite Constituents

Surface treatment of the filler may generate modified surface characteristics within the polymer matrix, which results in improved mechanical and electrical properties of the composite [79]. Contact angle measurements are used to investigate surface chemistry of materials. Any change in surface structure of filler can be noticed from a change in surface energy components of this particle.

The total surface energy, γ^{TOT} , of a nonmetallic material is composed of London dispersive component, γ^{LW} , and acid/base component, γ^{AB} . Moreover, acid/base component, γ^{AB} , consists of electron acceptor, γ^{A} , and electron donor components, γ^{B} , as given in the following equations [99, 100]:

$$\gamma_i^{\text{TOT}} = \gamma_i^{\text{LW}} + \gamma_i^{\text{AB}} \quad (2.1)$$

$$\gamma_i^{\text{AB}} = 2 (\gamma_i^{\text{A}} \gamma_i^{\text{B}})^{1/2} \quad (2.2)$$

A characteristic property of acid and base components of surface energy is their nonadditivity. If one of phases has only acid or base component, then this component does not contribute to the total surface energy of the same phase. However, it can interact with the complementary component of other phase. For a bipolar liquid (L) contacting with the solid (S), total surface energy and its components such as γ^{LW} ,

γ^{AB} , γ^A and γ^B , can be calculated with ‘Young Equation’ given below by using contact angles of probe liquids measured on the sample surfaces [100-102].

$$(1 + \cos \theta_L) \gamma_L^{TOT} = 2 [(\gamma_L^{LW} \gamma_S^{LW})^{1/2} + (\gamma_L^A \gamma_S^B)^{1/2} + (\gamma_L^B \gamma_S^A)^{1/2}] \quad (2.3)$$

In addition, surface energy of polymeric materials depends on temperature and it can be calculated theoretically at any temperature by using Equations 2.4 and 2.5 [126].

$$-d\gamma/dT = (11/9) (\gamma_0/T_c) (1 - T/T_c)^{2/9} \quad (2.4)$$

$$\gamma = \gamma_0 (1 - T/T_c)^{11/9} \quad (2.5)$$

where γ_0 is the surface tension at 0 K, T_c is the critical temperature and T is the temperature of polymer in K [126]. If there are large differences in surface energies of composite constituents, desirable properties cannot be obtained from this composite. The affinity between used filler and polymer needs to be increased to obtain a well-integrated structure by improving surface properties of filler. Mostly, functional groups are added on the filler surfaces to improve the wetting property and dispersibility of the filler in the matrix, and to enhance adhesion between the composite constituents [103].

2.1.4.2 Interfacial Strength and Selective Localization of Filler

Interfacial tension between any two phases can be estimated using the harmonic mean equation [105-107]:

$$\gamma_{12} = \gamma_1 + \gamma_2 - 4 [(\gamma_1^{LW} \gamma_2^{LW}) / (\gamma_1^{LW} + \gamma_2^{LW}) + (\gamma_1^{AB} \gamma_2^{AB}) / (\gamma_1^{AB} + \gamma_2^{AB})] \quad (2.6)$$

where γ_i is total surface energy, γ_i^{LW} is London dispersive component of total surface energy and γ_i^{AB} is acid/base component of total surface energy [105-107].

Fillers such as carbon particles can be preferentially located in one phase of two immiscible polymers, at which it has the lowest interfacial energy. Using interfacial tension values of blend phases, selective localization of filler in polymer blend can be estimated using the wetting coefficient, W_a , [105-107]:

$$W_a = (\gamma_{2\text{-filler}} - \gamma_{1\text{-filler}}) / \gamma_{12} \quad (2.7)$$

where $\gamma_{1\text{-filler}}$, $\gamma_{2\text{-filler}}$ are the interfacial tension between the filler and polymer phases 1 and 2, respectively, γ_{12} is the interfacial tension between two phases. If W_a is greater than 1, the filler is located within phase 1. If W_a is less than -1, the filler is located within phase 2. If W_a is between -1 and 1, then the filler is distributed at the interface [105-107].

2.1.4.3 Doping

Semiconductors are usually doped by n-type and p-type of atoms, which place in the lattice structure of semiconductor by the covalent bonding (Figure 2.19). N-type dopant atom has five valence electrons and the extra electron is not needed in the band structure of dopant atom. Hence, the ionization energy required to set this electron free is very small when compared with the energy required to break a covalent bond. Therefore, at room temperature, this free electron can become a conduction electron. P-type dopant atom has only three valence electrons, and when this atom is inserted into a semiconductor, it has one electron less than necessary for the band. This vacancy is a place into which an electron can move. When an electron of a neighbor atom moves into this place, it leaves a new vacant space in the valence band. In the case of p-type doping, current conduction is realized with electrons of conduction band and holes of valence band [78].

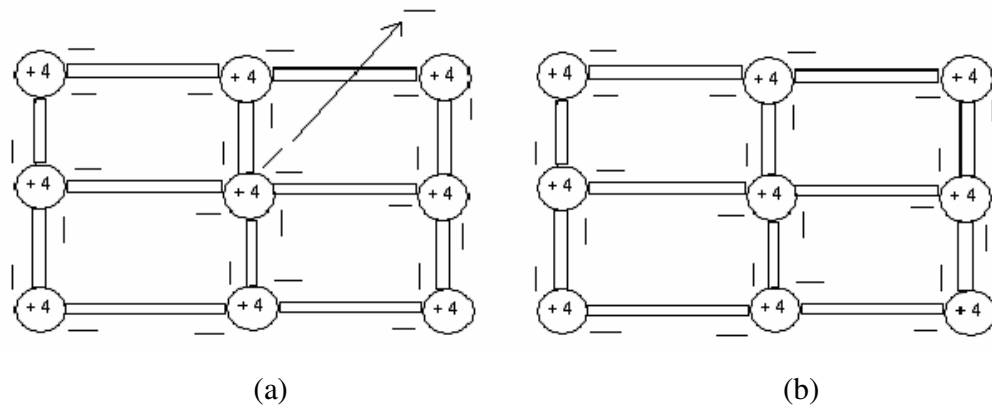


Figure 2.19 Bonding structures of (a) n-type dopant atom and (b) p-type dopant atom [78]

N-type dopant atoms are called as donor atoms. Addition of each n-type dopant atom to the crystal gives rise to a new isolated level, known as donor level, just below the conduction band (Figure 2.20). Because of small gap between the conduction band E_c , and the donor level, E_d , nearly all the donor atoms will have lost their electrons to the conduction band at room temperature. Each p-type atom, called as acceptor atom, introduced an additional isolated level just above the valence band (Figure 2.20). Because of small gap between the acceptor level, E_a , and the valence band, E_v , all the acceptor levels are filled with electrons, leaving an equal number of positive holes in the valence band. The conductivity depends on the number of charge carriers. Free electrons in conduction band and the holes in the valence band contribute to these charge carriers [104].

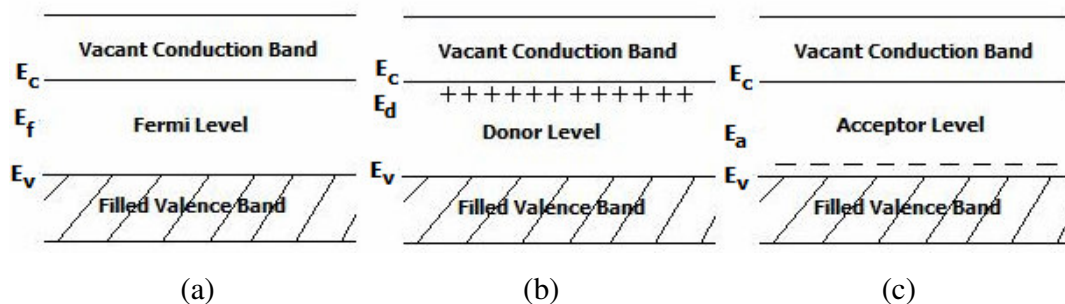


Figure 2.20 Energy band scheme for (a) intrinsic semiconductor, (b) n-type semiconductor and (c) p-type semiconductor [78]

2.2 Experimental Techniques for Material Characterization

2.2.1 Solution and Melt Viscosity, and Average Molecular Weights

Molecular chains of polymers produced by industrial polymerization processes can vary in dimensions and they need to be characterized in terms of average molecular weights, which can be obtained directly or indirectly from measurements of some physical properties of polymer [3, 93]. In the direct case, measured quantities are theoretically related to the average molecular weight. But, in the indirect case, a quantity is measured and related to molecular weight. End group analysis and colligative property measurements are among direct measurement methods. Solution viscosity, indirect measurement method, can be used to determine molecular weight of polymer [3]. Viscosity average molecular weight can be calculated using Mark-Houwink-Sakurada (MHS) relation:

$$[\eta] = k M_v^\alpha \quad (2.8)$$

where k and α are material dependent parameters, and η is the intrinsic viscosity [108]. Viscosities required for molecular weight calculation are usually measured in glass capillary viscometers such as Ostwald and Ubbelohde (Figure 2.21). Polymer solution is introduced through the filling tube and forced from the bulb through the capillary to the reservoir. The time required for polymer solution to pass through two timing lines is a measure for viscosity [3].

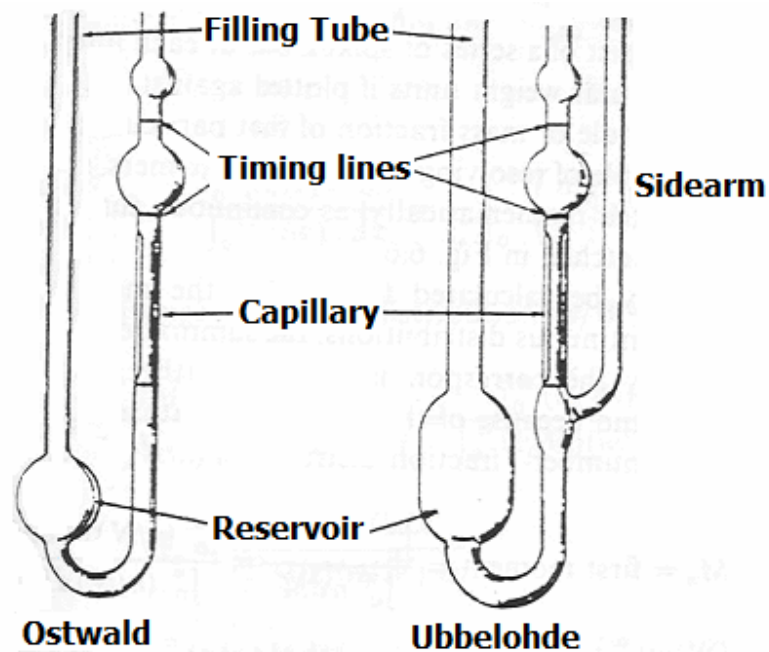


Figure 2.21 Two common types of capillary viscometers, Ostwald and Ubbelohde [3]

Melt flow index is another parameter in industry to characterize a polymer melt in terms of quality control. Polymer sample is heated in the barrel of an extrusion

plastometer and extruded from a short cylindrical die using a piston actuated by a weight. The melt flow index (MFI) of a polymer is the weight of the polymer in grams extruded during the 10-minute test period [108].

2.2.2 Electrical Conductivity

Semiconductor obeys Ohm's law at moderate voltages and the relationship between the terminal current and voltage is linear. The magnitude of the current depends on two factors, the densities of the free carriers and their speed. Since the number of carriers is assumed to be independent of the electric field, with respect to Ohm's law, the average speed of the two types of carriers is proportional to the field [77]. Electrons are continuously in motion. If a constant force is applied on these electrons, they will be accelerated. Any type of irregularities in metals and semiconductors lead to resist the flow of current [78]. Resistivity is defined as the resistance presented to the flow of current between opposite faces of a unit cube of the material [77].

Electrical conductivity of a semiconductor material can be determined using two point probe and four point probe methods. Two point probe technique appears to be easier to apply. However, the result of two point probe technique is complicated. This method measures total resistance between two probes. These resistances are the probe resistance R_p , the contact resistance R_c between the metal probe and the material surface, the spreading resistance under each probe R_{sp} and the material resistance R_s (Figure 2.22). The spreading resistance results from current transportation between the metal probe and the material. R_c and R_{sp} cannot be measured separately. Hence, exact resistivity cannot be extracted from the total resistance. Only R_p can be determined by contacting these two metal probes [109].

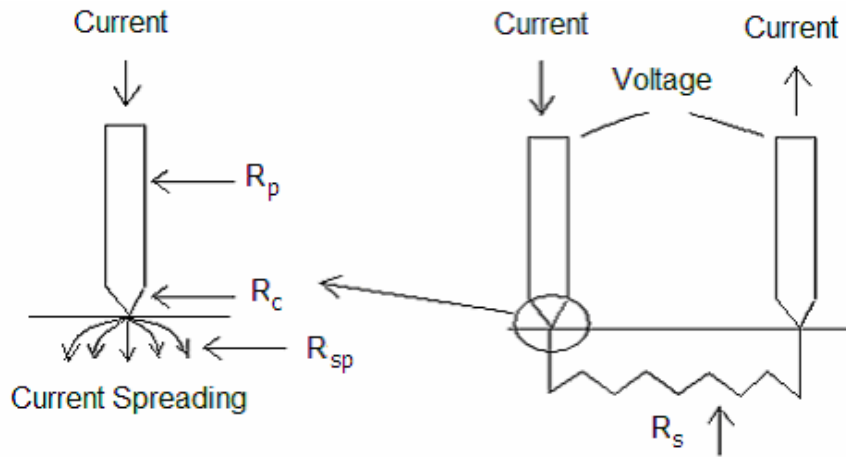


Figure 2.22 Resistance components of two point probe technique

The volume resistivity ρ with two point probe method is calculated from the relationship:

$$\rho = [(V) / (I)] \times [(S) / (L)] \quad (2.9)$$

in which V is the voltage drop, I is the current, L is the length and S is the cross sectional area of the sample.

The four point probe technique is the most common method for measuring the resistivity of the semiconductor material. The four point probe technique has an advantage over two point probe method. Two probes carry current and other two probes measure the voltage (Figure 2.23). Current carrying probes of four point probe technique have also contact and spreading resistance. However, voltage is measured with a potentiometer, which draws no current or with a high impedance voltmeter, which draws very little current. Hence, R_c , R_p , R_{sp} can be neglected owing to small voltage drop accompanying with small current flow [109].

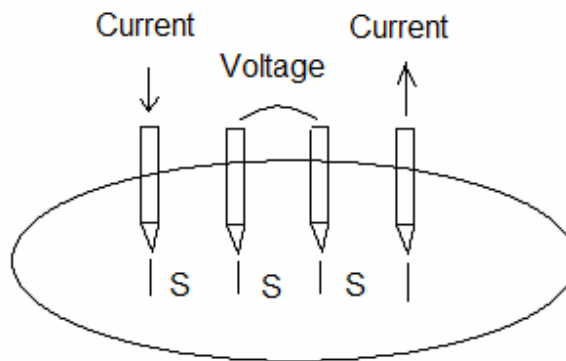


Figure 2.23 Four point probe head

For an arbitrarily shaped sample, the resistivity ρ is given by,

$$\rho = (2 \times \Pi \times S \times F) \times (V / I) \quad (2.10)$$

S is the distance between probes. In addition, F is a correction factor and it depends on the sample geometry. For very thin samples, satisfying the conditions for F to be approximately unity, the volume resistivity ρ is calculated from the following relationship:

$$\rho = (\Pi \times t) / (\ln 2) \times (V / I) = (4,532 \times t) \times (V / I) \quad (2.11)$$

in which V is the voltage drop, I is the current, t is the thickness of the sample [109].

2.2.3 Mechanical Properties

2.2.3.1 Tensile Test

Tensile test is a static test at which the deformation rate is steady in time [37]. Dumbbell test specimens are required for tensile testing. The specimen (Figure 2.24) is composed of a straight zone of uniform cross section (L_0), over which the deformation and corresponding stress are uniform, and two end tabs of larger cross-section, over which the test specimen is held. Polymeric materials with a uniform thickness (T_0) are held between clamps of the testing machine and pulled at a constant rate of elongation.

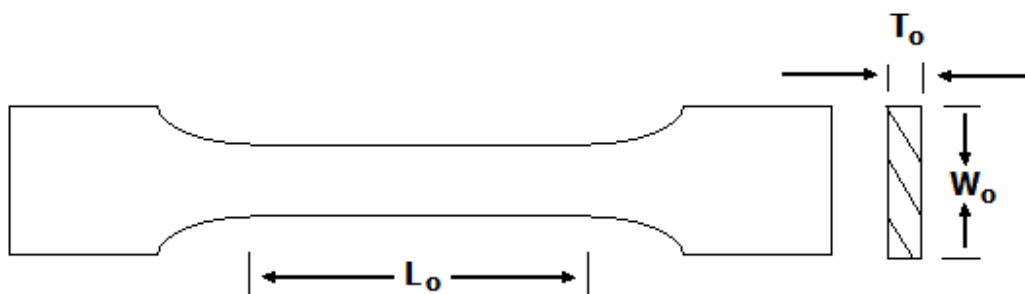


Figure 2.24 Illustration of a typical dumbbell test specimen [37]

According to the type of polymeric material, the strain rate must be specified. The temperature and the strain rate affect the tensile behavior of the polymeric material. As indicated in Figure 2.25, tensile modulus, tensile stress, elongation at break values can be determined using a full stress-strain curve of the tensile test. Yield

stress is the maximum stress point where the polymeric material will fully recover to its original shape. Ultimate stress is a point on the stress/strain curve at which the polymeric material fails. The initial slope of the stress/strain curve is called as initial modulus. In addition, secant modulus is the slope of the line joining the origin and the specified point on the stress/strain curve [95].

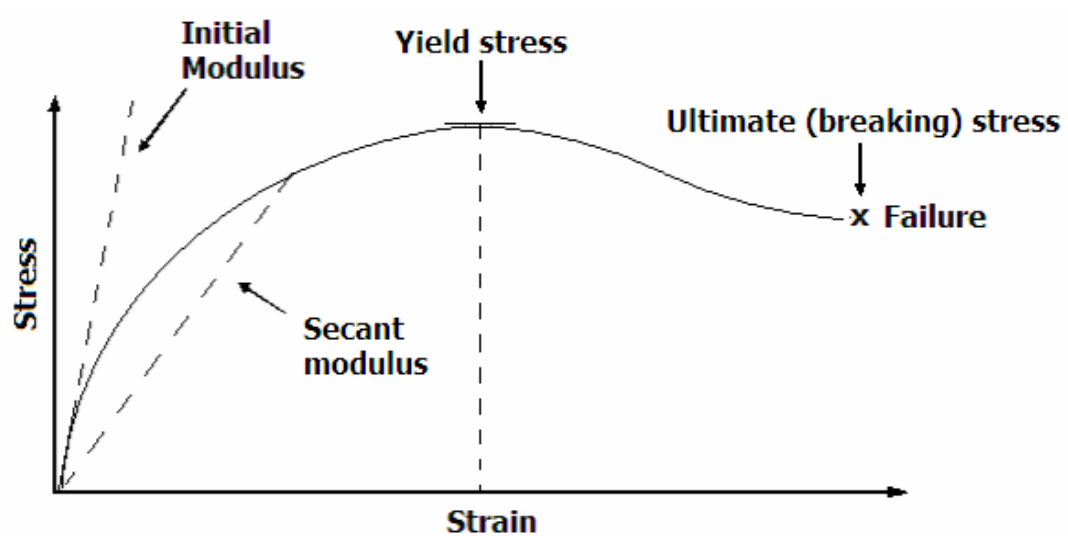


Figure 2.25 Idealized stress-strain curve for a polymer undergoing ductile failure [37]

2.2.3.2 Impact Test

Impact test has been developed for the purpose of assessing the fracture resistance of plastics for situations where a component may be subjected to rapid strokes [93]. It measures the energy expended up to failure under conditions of rapid loading [37].

Impact tests are divided into two main classes, pendulum test and falling weight test [93]. Izod and Charpy tests are two widely used pendulum tests. In the Charpy test, the test specimen is laid horizontally over two supports and struck in a three-point bending mode [95]. A hammerlike weight strikes the specimen and the energy-to-break is determined from the loss in the kinetic energy of the hammer [37]. The impact strength is quoted as energy per unit cross-section for Charpy test (J/m^2) [95]. According to impact test result, it can be understood whether a plastic material has sufficient energy-absorbing property to be useful for a particular application [37].

2.2.4 Scanning Electron Microscopy (SEM) and Transmission Electron Microscopy (TEM)

Resolution of microstructured or nanostructured composite morphology can be achieved using electron microscopes, scanning electron microscope and transmission electron microscope [85, 94]. Electrons are used as the probing medium in SEM. A fine beam of electrons is scanned across the surface of an opaque specimen, which has been coated with a conducting film. Secondary electrons, backscattered electrons and x-ray photons emitted are collected and used to obtain a three-dimensional image of the specimen in a television tube [85]. SEM provides better resolution than conventional microscopy. It can reveal surfaces down to 5 nm under suitable operational conditions [110]. Transmission electron microscopy is another imaging method at which a beam of electrons is transmitted through a sample, and then an image is formed, magnified and directed on a screen [111]. TEM provides higher resolution of a microstructural image compared to SEM. The samples of TEM have to be less than 100 nm in thickness to transmit the electrons of microscope through the sample, which limits TEM application. Hence, ultramicrotomy method is used to prepare thin samples, transparent to the electron beam [94, 110].

2.2.5 Electron Spectroscopy for Chemical Analysis (ESCA)

Electron spectroscopy for chemical analysis, also known as x-ray photoelectron spectroscopy (XPS), uses x-ray photons as the probing species, causing the ejection of core electrons from atoms in the material. Only, electrons from the first few atomic layers are able to escape from the surface to the collector due to the short mean free path for the core electrons. Hence, ESCA is a surface sensitive method. Furthermore, unique binding energies are associated with the molecular environment of each core electron; that is, the molecular structure where each electron comes from can be determined. In ESCA, counting techniques are quantitative and surface concentrations can be accurately determined [110].

2.2.6 X-ray Diffraction (XRD)

X-ray diffraction is a widely used technique for researching orderly arrangements of atoms and molecules [85]. Information about the crystalline and amorphous phases of polymeric materials can also be obtained using x-ray diffraction method. When a beam of X-rays, high energy photons, is focused on a sample, electrons are absorbed or transmitted or scattered, resulting in a scattering pattern. This pattern is function of scattering angle, 2θ . By using the scattering pattern, the positions of atoms in the polymer can be determined. There are two types of scattering patterns, wide-angle x-ray scattering and small-angle x-ray scattering. The former is used to investigate small scale structures below 10 \AA and the latter is used to study large-scale morphological structures from 10 to 10^4 \AA [37].

Additionally, x-ray diffraction can be used to determine detail microstructure of carbon like crystalline filler in polymer composites. Interlayer spacing between graphene layers of carbon black (d_{002}) can be calculated using the Bragg equation:

$$n \lambda = 2 d_{002} \sin \theta \quad (2.12)$$

where n is equal to one for monochromatic radiation, λ is wavelength of radiation, d_{002} is interlayer spacing between graphene layers and θ is diffraction angle of beam of radiation corresponding with Bragg's maximum [112, 113]. In addition, crystalline size along the c -axis (L_c) of carbon black can be calculated using the Scherrer equation:

$$L_c = K \lambda / (B \cos \theta) \quad (2.13)$$

in which K is Scherrer constant, equal to 0.89, L_c is crystalline size along the c -axis of carbon black, λ is wavelength of radiation, θ is diffraction angle of beam of radiation corresponding with Bragg's maximum, B is widening of diffraction line measured in the middle of its maximum intensity [101, 112, 113].

2.2.7 Microwave Properties

2.2.7.1 Electromagnetic Interference (EMI) Shielding Effectiveness (SE)

The performance of an instrument may be disturbed or degraded by an electromagnetic disturbance, which may be in the form of electromagnetic noise or an unwanted signal or a change in the propagation medium itself. The phenomenon of the degradation in the performance of an instrument by an electromagnetic disturbance is called as electromagnetic interference (EMI) [22, 114]. Radars, communication equipment, television, radio broadcast and various electronic devices can be shown as examples for strong electromagnetic signal radiating systems and also the sources of electromagnetic interference, which can hinder satisfactory operation of an instrument when the intensity of the electromagnetic interference will be out of tolerable limit. Several methods, grounding, shielding, bonding and filtering, are tried to reduce possible effects of EMI. Grounding is the method, which

provides a low resistance path between electronic device and the earth to bypass fault current or EMI signals. Electrical bonding is a method, in which electronic compounds of a device are electrically connected with a low impedance conductor. Filtering is a mitigation method to suppress undesired conducted EMI [22].

Shielding is another method to prevent the emissions of the electronic devices from radiating outside their boundaries, which is done to prevent them from causing interference with other electronic devices. Another aim of shielding is to prevent radiated emissions external to the product from coupling to the electronics of devices, which results in interference in the instrument (Figure 2.26) [23].

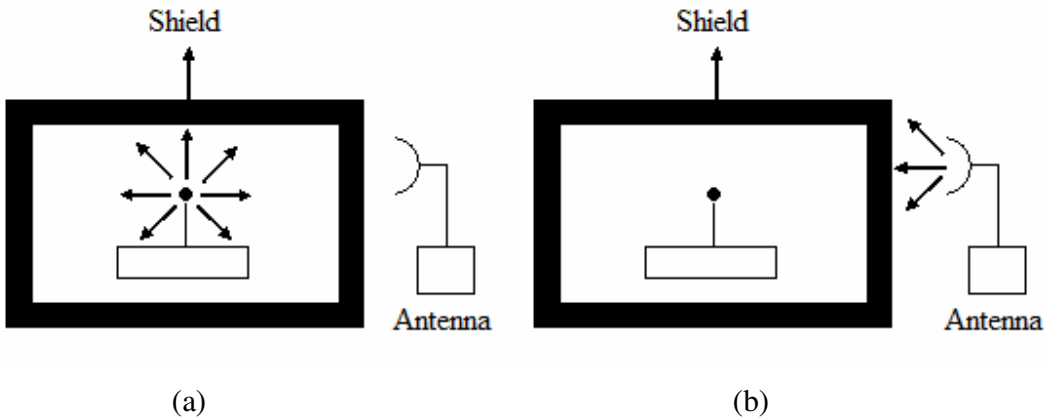


Figure 2.26 Illustration of a shield enclosure (a) to contain radiated emissions and (b) to exclude radiated emissions

A shield is a barrier to the transmission of electromagnetic fields and shielding effectiveness can be defined as the ratio of electromagnetic power incident on the

shielding sample (P_i) to electromagnetic power transmitted through the shielding sample (P_t) [22, 23].

$$SE \text{ (dB)} = 10 \log_{10} (P_i / P_t) \quad (2.14)$$

Shielding effectiveness (SE) values, obtained using insertion loss values, are given in the unit of decibel (dB). A shielding effectiveness of 10 dB means that incident electromagnetic radiation is reduced by a factor of 10 as it penetrates the shield [23].

Two mechanisms dominate in terms of EMI shielding, which are reflection loss and absorption loss. Some parts of electromagnetic waves are reflected from the shielding surfaces. Mobile charges, which are electrons and holes, are responsible for reflection mechanism by interacting with electromagnetic waves. In addition, some parts of waves are absorbed in the shielding material. In order to absorb electromagnetic waves, shield should possess electric and magnetic dipoles. An increase in conductivity and thickness of shielding material results in a parallel increase in absorption loss. Moreover, absorption mechanism dominates with increasing the frequency of electromagnetic wave, whereas the reflection loss decreases with ascending frequency [22, 115]. Besides absorption and reflection mechanisms, there are multiple reflections between interfaces of the shields. Multiple reflection mechanism can be taken into account when absorption mechanism is not effective. As a result, the sum of the reflection loss R (dB), absorption loss A (dB) and internal reflection losses IR (dB) constitute EMI shielding effectiveness SE (dB) [22].

$$SE \text{ (dB)} = R \text{ (dB)} + A \text{ (dB)} + IR \text{ (dB)} \quad (2.15)$$

2.2.7.2 Dielectric Constant

Under external electric field, mobile charge carriers of a material are pushed in opposite direction and the distorted charge distribution forms its own electric field, opposing the external field [28, 29]. Dielectric constant is defined to be the ratio of the applied field to the field inside the material [116]. Externally applied electric field leads to displacement of positive and negative charges of the material, which leads to the polarization within the material. Polarization process can be categorized as rapidly forming and slowly forming polarization. Rapidly forming polarization takes place due to displacement of electrons in the atoms relative to the positive nuclei. Displacement of atom relative to one another in the molecule results in relatively slow polarization. The time required for dipole or orientation polarization process depends on resistance of the material [117].

Polymer having polar group in its structure, can show orientation polarization, which contributes to the dielectric constant. Under an external electric field, there will be a change in the orientation of polar segments without changing in the orientation of whole macromolecule [117]. In composite system, interfacial polarization takes place if composite constituents have different dielectric constant and conductivity values. At interfacial polarization, mobile charges accumulate at the interfaces in the composite. This accumulation process takes place slowly so that it can be observed at very low frequencies. If one of the composite constituents is highly conductive, then the polarization process can be observed even at high frequencies [117]. If the conductive material possesses enough amounts of mobile charges then net electric field inside the composite material can be zero. A field can exist just at the surface but it cannot penetrate into the interior of the material. Electric field penetration depth depends on conductivity of the material, that is, amount of mobile charges of the material [118].

2.2.8 Fourier Transform Infrared (FTIR) Spectroscopy

There are several analytical methods to identify polymer microstructure and Fourier transform infrared (FTIR) spectroscopy is the most widely used method to characterize the polymer [37]. At FTIR spectroscopy, spectra are collected based on measurements of a radiation source [119]. Several chemical groups of polymer can be identified by the presence of a single absorption band. The local chemical environment, especially intra molecular and intermolecular bonding, determines the location of the absorption band of chemical groups. Besides, the presence of stereoisomerism and the degree of crystallinity affect the exact locations of absorbance peak maxima [37].

2.2.9 Electrochemical Capacitance Performances

Capacitors can be thought of as devices for accumulating or isolating electrostatic charge. A capacitor consisting of two parallel conducting plates of area A and separated by a distance d will produce a charge Q on each plate given by CV , where C is the capacitance in farads, when a voltage difference V will be applied with a battery across the capacitor. When a material is inserted between the conducting plates, the electric field polarizes the material, which results in internal electric field, opposing the applied electric field and compensating the charge on the conducting plates (Figure 2.27). More charge flows from the battery, and the same voltage V will now produce an increased charge Q on each plate, an increased capacitance and corresponding increase in stored energy, E . The capacitance is given by

$$C = Q/V = \epsilon_0 \epsilon_r A/d \quad (2.16)$$

where ϵ_0 is the dielectric constant of free space, ϵ_r is the dielectric constant of the material filling the space between the plates. Stored energy is given by

$$E = CV^2/2 \quad (2.17)$$

According to Equation 2.16, the capacitance and the charge amount of a capacitor depend on the surface area of the conductors, the distance between these plates and the dielectric constant of the material separating conductors. Charging the capacitor is similar to stretching a spring, storing potential energy. Under direct voltage to the conductors of capacitors, potential energy will be stored, which is released when the conductors are turned into short-circuit condition [120, 121].

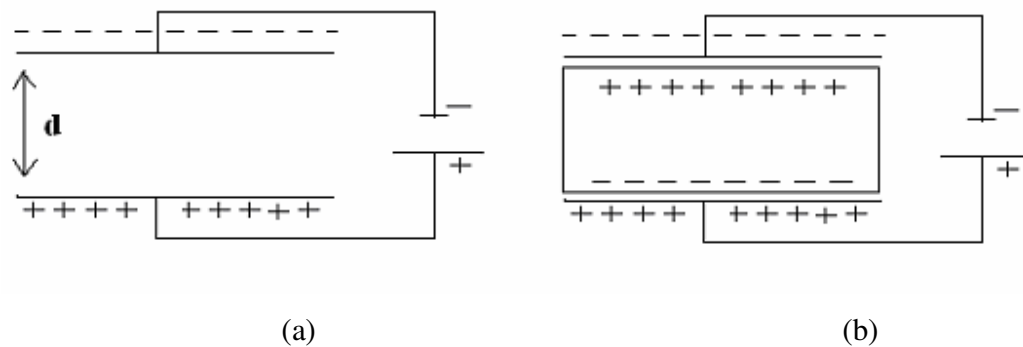


Figure 2.27 Polarization of conventional capacitor (a) without a dielectric material and (b) with a dielectric material

There are many types of capacitors each of which is usually named after its dielectric material. Electrolytic, mica, ceramics, plastics, air, certain gases and even a vacuum can be shown as example for capacitor types. The best capacitor for application is the one which offers the optimum combination of properties [120, 121].

Electrochemical capacitors store energy by utilizing double layer and pseudocapacity type processes [53]. When a potential difference occurs between two electrodes, a following charge separation of ions and electrons take place at the interface between the electrode material and the electrolyte, resulting in the double-layer capacitance, which depends directly on the applied potential (Figure 2.28) [52, 63]. The electrode surface area, double layer thickness, known as Helmholtz thickness, and dielectric property of the electrolyte; that is, ionic conductivity will determine the double layer capacitance. Besides, the thickness of the double layer depends on the ion size and concentration of the electrolyte. This type of capacitors needs porous electrodes with large surface area to provide better capacitive performances [122]. Charge-discharge processes are mainly electrostatic; that is, it includes only the separation of ions and electrons. Hence, charge-discharge processes of double-layer capacitors are reversible, which provides thousands of cycles with the double-layer capacitor without a distinctive loss in its performance [52, 63].

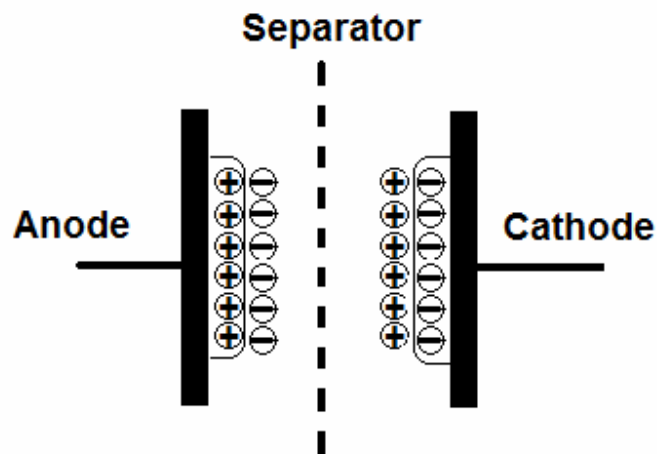


Figure 2.28 Polarization of electrochemical capacitor

On the other hand, charge-discharge processes of pseudocapacitor take place through redox reactions, which include electron transfer across the electrode and electrolyte interface. Capacitance is the change in the amount of charge with a change in potential [52, 63]. Hence, redox reactions, which give rise to pseudocapacitance, contribute to energy storage as double layer processes do. Pseudocapacitance processes take place in a shorter time scale due to high accessibility of electrode surfaces when compared with bulk processes and result in high power density. Pseudocapacitance processes are reversible; that is, these processes do not bring any morphological changes on the electrodes. A liquid electrolyte can access even to the micropores of a porous electrode up to 10 nm. Hence, to achieve high performance as a pseudocapacitor, the electrode material should have a high surface area with porous morphology [53].

Batteries and fuel cells, energy storage devices, have lower power densities than that of conventional capacitors, which have very low energy density. Electrochemical capacitors illustrate better performance in terms of energy density when compared with conventional capacitors and better performance in terms of power density compared to batteries. In addition, these capacitors possess a much longer cycle life than that of batteries [53, 122]. However, energy density of electrochemical capacitors is lower than that of these devices [53].

Capacitance performances of electrochemical capacitors can be investigated by cyclic voltammetry, charge-discharge test and ac impedance analysis.

2.2.9.1 Cyclic Voltammetry

Cyclic voltammetry (CV) is a kind of potentiodynamic electrochemical measurement. In a cyclic voltammetry experiment, a voltage is applied to a working electrode in an ionic solution. The cyclic voltammogram is obtained using the current flowing at the working electrode versus the applied voltage. Cyclic

voltammetry measurements give valuable information about the electrochemical capacitance performances of electrode systems [123]. Capacitance of an electrochemical capacitor can be calculated using the following relationship:

$$C = i / s \quad (2.18)$$

where i is the capacitive current and s is the sweep rate [52].

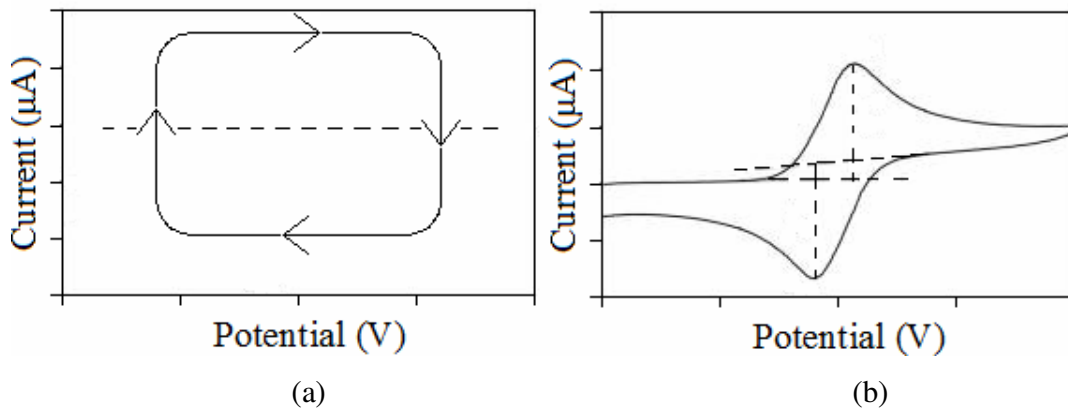


Figure 2.29 Cyclic voltammogram of (a) an ideal double layer capacitor and (b) a pseudocapacitor

An ideal double layer capacitor leads to a cyclic voltammogram in rectangular shape, shown in Figure 2.29 (a). The energy storage process is directly electrostatic and the resulting current is independent on potential. Upon reversal of the potential sweep, the sign of current is changed right away. However, cyclic voltammetry curve of electrochemical capacitor deviates from the rectangular shape with pseudocapacitance (Figure 2.29 (b)). Reversible redox peaks are added on CV curves

with faradaic reactions and the resulting current is dependent on potential. Charging with redox reactions is kinetically slow when compared with the electrostatic charging, resulting in a delay of potential during reversing the potential sweep [124].

The inner integrated area of cyclic voltammetry curve (current x voltage) gives the power density, which will be lower if the equivalent series resistance (ESR) is higher. An ideal rectangular shape in cyclic voltammetry curve can be thought as small ESR value in the electrode. ESR values can be compared from the differences in the slopes of voltage versus current plots [54].

2.2.9.2 Charge-Discharge Test

Galvanostatic charge-discharge test is another measurement technique to investigate capacitance performances of electrochemical capacitors. In this test, potential-time response of electrode cell systems is studied at a constant charge and discharge rates. For an ideal electrochemical capacitor, potential-time response of charge process is mirror image of its corresponding discharge counterpart (Figure 2.30) [72].

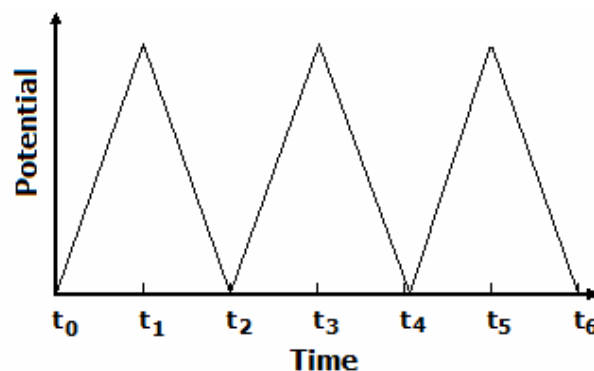


Figure 2.30 Galvanostatic charge-discharge plot of an ideal electrochemical capacitor

Capacitance, C , in farads can be calculated from the charge-discharge plot by using the following relationship:

$$C = I / (dV/dt) \quad (2.19)$$

where I is the discharge current in amperes and dV/dt is the slope in volt per second. The specific capacitance, C_s , can be calculated by using the following relationship:

$$C_s = C / m \quad (2.20)$$

where m is the mass of active electrode material in gram [65].

2.2.9.3 AC Impedance Analysis

The ratio of phasor voltage across a capacitor to the phasor current through the capacitor is called the capacitance, which can be calculated from the imaginary part of the complex impedance plot according to the relationship:

$$C = -1 / [\omega \text{Im}(Z)] \quad (2.21)$$

where C is the capacitance in farads, $\text{Im}(Z)$ is the imaginary component of complex impedance and ω is the angular frequency [122, 125]. The impedance of a capacitor is inversely proportional to the frequency; that is, the capacitive reactance, equal to $(\omega C)^{-1}$, approaches zero at high-frequency alternating current and the capacitive reactance increases and approaches to an open circuit condition at very low-frequency alternating current [125].

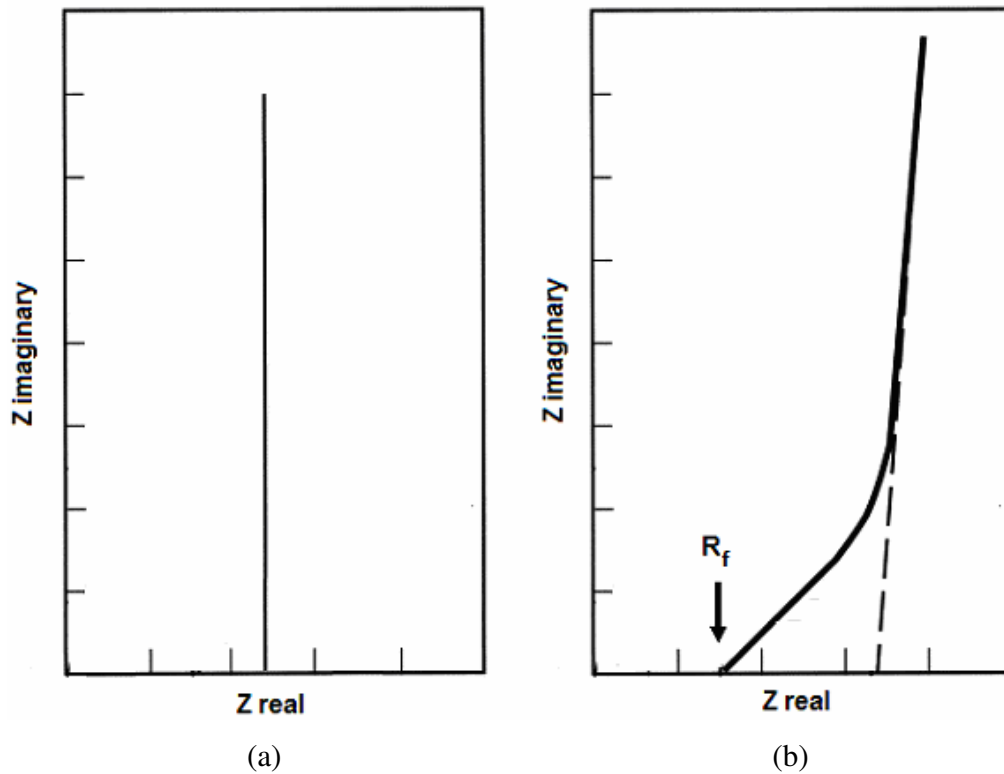


Figure 2.31 Impedance plots of (a) an ideal capacitor and (b) a real electrochemical capacitor [122]

The ideal electrochemical capacitor results in a straight line along the imaginary axis of impedance plot, given in Figure 2.31 (a). However, real capacitors give rise to a line with a finite slope due to the diffusive resistivity of electrolyte ions within the pores of the electrode active layer (Figure 2.31 (b)). On the other hand, the complex-plane impedance plot can be used to compare electrical resistance of different electrode materials when the electrolyte resistance is held constant. A change in R_f (Figure 2.31 (b)), which is the high-frequency real impedance component, indicates a change in electrode resistance [54].

CHAPTER 3

EXPERIMENTAL

Experimental part of this dissertation is separated into five sections. In the first section, the materials and methods used to prepare nylon 6/carbon black composites are described. In the second section, the materials used and the experimental procedure of surface treatment of filler to prepare LDPE/carbon black, nylon 6/carbon black and PET/carbon black systems are given. Then, the materials utilized and the experimental procedure of grinding to prepare PP/PET and PP/PET/CNT systems are described. Thereafter, the methods used to characterize all conductive polymer composites, prepared in the first three sections, are given. Finally, the materials and the methods utilized to prepare and characterize polyaniline/carbon nanotubes composites are expressed.

3.1 Preparation of Nylon 6/Carbon Black Composites

Two different techniques, in-situ polymerization and melt-mixing, were used to prepare nylon 6/carbon black composites. The details about the materials and the processing methods to prepare nylon 6/carbon composites are mentioned in this section. The methods used to characterize these composites are mentioned in the fourth section.

3.1.1 Materials

Chemicals used for ring opening polymerization of nylon 6 are given in Table 3.1. In-situ polymerization method was used to synthesize nylon 6 in the presence of carbon black particles, delivered by Turkish Petroleum Refinery. In addition, commercial grade nylon 6 pellets supplied by Tekno Polimer Ltd. was used as matrix material in melt mixing method. Table 3.2 summarizes properties of commercial grade nylon 6 and carbon black, respectively.

Table 3.1 Chemicals for ring opening polymerization of nylon 6

	Chemical	Company
Monomer	Caprolactam	Fluka Chemika (21500)
Initiator	Sodium Hydride 60% suspension in oil	Riedel-de Haen (62863)
Activator	N-acetylcaprolactam	Fluka Chemika (00981)
Shielding material	Polyethylene glycol 600	Fluka Chemika (87333)
Solvent of nylon 6	Formic acid 98-100 %	Merck (100263)

Table 3.2 Properties of commercial grade nylon 6 and carbon black

Material	Trade name & Supplier	Specifications
Nylon 6	Domamid 27; Tekno Polimer Ltd.	Melt flow index (2.16 kg; 235 °C): 30-35 g/10 min. Density: 1.14 g/cm ³
Carbon black (CB)	ISAF N-220; TUPRAS (Turkish Petroleum Refinery)	Iodine Number: 119 mg/g Dibutylphthalate Abs.: 114.2 ml/100 g

3.1.2 Composite Preparation Techniques

Masterbatch composites were prepared by in-situ polymerization method in the presence of 16 wt. % carbon black. To synthesize nylon 6, 250 g of caprolactam monomer was melted in a glass reactor, which was placed in jacketed heater, under nitrogen atmosphere at 70 °C. 48 g carbon black, dried at 100 °C for 24 hours, was stirred with molten caprolactam for 4 hours at the same temperature and at a speed of 260 rpm. After 4 hours mixing, the glass reactor was heated at 235 °C. In addition, 2.5 ml of N-acetylcaprolactam as an activator, and 0.4 g of polyethylene glycol, using to shield sodium ion of initiator, were loaded into the reaction medium. Then 0.4 g of sodium hydride as an initiator was added. The polymerization reaction ended up within 1-2 minutes. The experimental setup of nylon 6 synthesis is illustrated in Figure 3.1. Masterbatch composites, synthesized by in-situ polymerization method, were diluted with commercial grade nylon 6 in a co-rotating twin screw extruder (Thermo PRISM TSE-16-TC) (Figure 3.2) to obtain 1, 3, 6, 10 and 12 wt. % carbon black containing composites. The extrusion processes were carried out in the temperature profile of 220-230-235-240-245 °C and at a screw speed of 80 rpm. This procedure was called as method A.

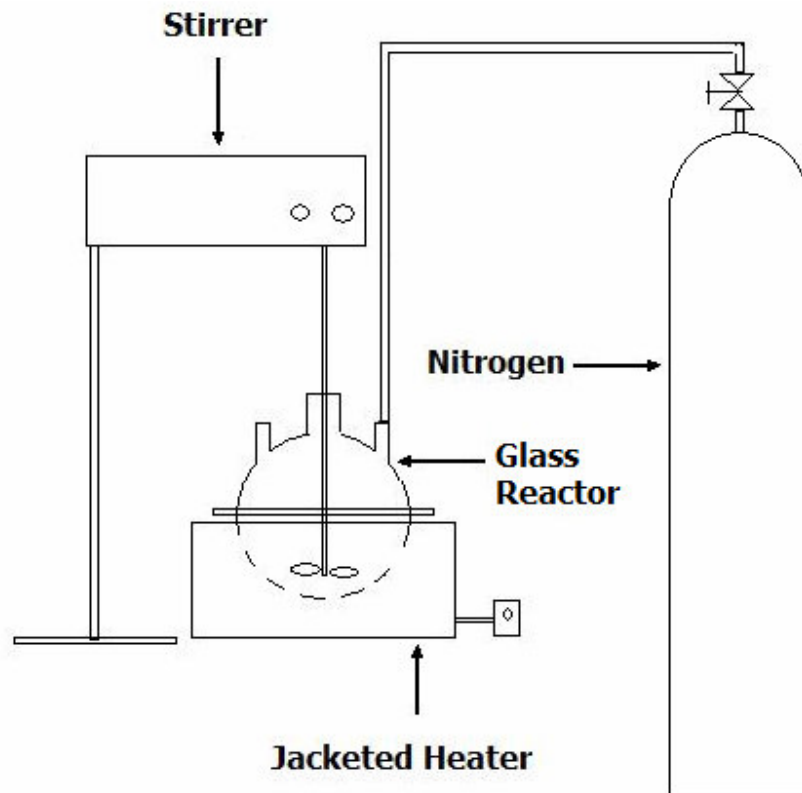


Figure 3.1 Experimental setup of nylon 6 synthesis

As an alternative composite preparation technique, melt mixing method was applied to prepare composites from commercial grade nylon 6 and carbon black. Prior to extrusion, nylon 6 pellets were dried in a vacuum oven for 24 hours at 90 °C. Melt mixing of nylon 6/carbon black was performed using the same extruder at the same process condition. In this method, commercial nylon 6 pellets were fed from the main feeder and carbon black particles were fed from the side feeder to provide identical compositions of method A. This technique was called as method B.



Figure 3.2 A photograph of the co-rotating twin screw extruder

Extruded composite pellets of both methods were molded both in compression molding (Figure 3.3) and injection molding devices (Figure 3.4) for sample preparation. These samples were used in the characterization experiments. Compression molded samples were used to determine electrical conductivity, while injection molded samples were used in mechanical tests and morphology analyses. Compression molding process was performed at 235 °C. First, pellets were heated for 1.5 minutes under 50 bar gauge pressure and then they were compressed for 1 minute under 150 bar gauge pressure. Afterwards, the molded samples were quenched to room temperature by water. A laboratory scale injection molding machine (Microinjector, Daca Instruments) was used to prepare test specimens at barrel temperature of 235 °C and mold temperature of 40 °C.

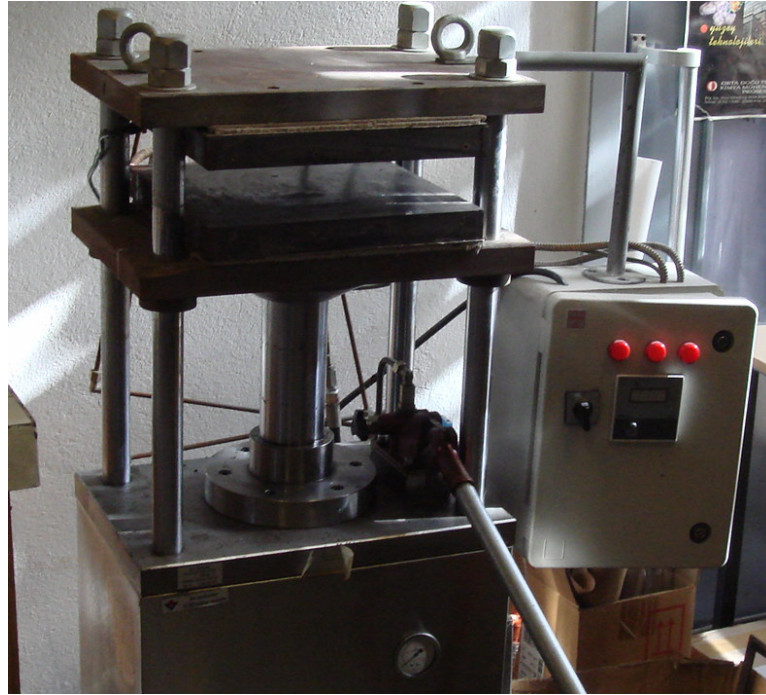


Figure 3.3 A photograph of the compression molding device



Figure 3.4 A photograph of the injection molding device (Daca Instruments)

3.2 Effect of Surface Treatment of Filler on LDPE/Carbon Black, Nylon 6/Carbon Black and PET/Carbon Black Composites

Surface treatment was applied to carbon black particles and then treated filler was compounded with LDPE, nylon 6 and PET matrices, respectively. The materials used and experimental procedures followed to treat carbon black surfaces and to prepare composites including treated conductive filler are mentioned in this section. Besides, the methods used to characterize composites, prepared in this section, are expressed in the fourth section.

3.2.1 Materials

Low-density polyethylene (LDPE), nylon 6 and poly(ethylene terephthalate) (PET) were selected as three different matrix materials. In addition, carbon black (CB) was used as conductive filler. 3-Aminopropyltriethoxysilane (APS) and formamide, whose chemical structures are shown in Figure 3.5, were utilized as surface treatment agents for carbon black. Physical properties of all materials are given in Table 3.3.

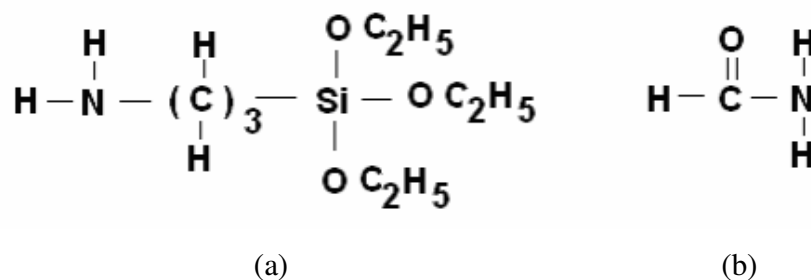


Figure 3.5 Chemical structures of surface treatment agents (a) 3-Aminopropyltriethoxysilane (APS) and (b) formamide

Table 3.3 Physical properties of materials

Material	Trade name & Supplier	Specifications
Low-density polyethylene (LDPE)	Petilen G03-5; PETKİM (Turkish Petroleum Product Producer)	Melt flow index (2.16 kg; 190 °C): 0.2 – 0.4 g/10 min. Density: 0.922 g/cm ³
Nylon 6	Domamid 27; Tekno Polimer Ltd.	Melt flow index (2.16 kg; 235 °C): 30-35 g/10 min. Density: 1.14 g/cm ³
Poly(ethylene terephthalate) (PET)	Melinar; Advansa	Upper working temp.: 115-170 °C Heat deflection temp. (1.8 MPa): 80 °C Density: 1.3-1.4 g/cm ³
Carbon black (CB)	ISAF N-220; TUPRAS (Turkish Petroleum Refinery)	Iodine Number: 119 mg/g Dibutylphthalate Abs.: 114.2 ml/100 g
3-Aminopropyl triethoxysilane (APS)	DYNASYLAN AMEO; Cam Elyaf Sanayi A.S.	Density (20 °C): 0.95 g/cm ³ Flash point: 93 °C
Formamide	Formamide; Merck	Density (20 °C): 1.13 g/cm ³ Flash point: 175 °C

3.2.2 Surface Treatment of Carbon Black

In order to modify surface chemistry of carbon black by chemical treatment, 1 wt. % APS and 1 wt. % formamide solutions were prepared by diluting 3-

Aminopropyltriethoxysilane and formamide, respectively, with distilled water. Besides 1 wt. % formamide solution, 2 and 3 wt. % formamide solutions were also prepared. Diluted solutions were mixed with untreated carbon black (UCB) particles. These mixtures were stirred for 10 minutes at room temperature in a beaker. Then, they were filtered to isolate treated carbon black particles. Afterwards, wet particles were dried at 100 °C for 24 hours. APS1-CB was the code used to identify carbon black treated with 1 wt. % 3-Aminopropyltriethoxysilane solution. In addition, FA1-CB, FA2-CB and FA3-CB were the codes used to identify carbon black treated with 1, 2 and 3 wt. % formamide solutions, respectively.

3.2.3 Composite Preparation

Prior to extrusion processes, nylon 6 pellets and PET pellets were dried in a vacuum oven for 24 hours at 90 °C and for 12 hours at 80 °C, respectively. LDPE and nylon 6 were compounded separately with APS1-CB and FA1-CB, while PET was compounded separately with FA1-CB, FA2-CB and FA3-CB in the twin screw extruder (Thermo PRISM TSE-16-TC) to obtain 1, 2, 4, 6 and 8 wt. % of CB containing composites. For comparison purposes, LDPE, nylon 6 and PET, respectively, were compounded with untreated carbon black. Extrusion process condition of LDPE/carbon black, nylon 6/carbon black and PET/carbon black systems is given in Table 3.4.

Table 3.4 Extrusion process condition of LDPE/carbon black, nylon 6/carbon black and PET/carbon black composites

Composite system	Temperature profile (°C)	Screw speed (rpm)
LDPE/CB	170-210-210-210-220	300
Nylon 6/CB	220-230-235-240-245	80
PET/CB	230-255-260-265-270	80

In order to determine electrical resistivity of the composites, test samples of LDPE/CB, nylon 6/CB and PET/CB systems were prepared by compression molding device. The detail of compression molding processes is given in Table 3.5. After molding, samples were quenched to room temperature by tap water. A laboratory scale injection molding instrument (DSM Micro 10 cc Injection Molding Machine), illustrated in Figure 3.6, was used to prepare test specimens of surface energy, tensile and microwave properties measurements. At the injection molding process of LDPE based composites, barrel and mold temperatures were 210 °C and 30 °C, respectively and during the injection molding process of nylon 6 based composites, barrel and mold temperatures were 240 °C and 35 °C, respectively. The injection molding process of PET based composites was performed at 285 °C barrel temperature and 30 °C mold temperature.

Table 3.5 Compression molding process condition of LDPE/carbon black, nylon 6/carbon black and PET/carbon black composites

Composite system	Preheating temperature, pressure and time			Molding temperature, pressure and time		
	Temperature (°C)	Pressure (bars)	Time (min.)	Temperature (°C)	Pressure (bars)	Time (min.)
LDPE/CB	210 °C	50 bars	1.5 min.	210 °C	150 bars	2 min.
Nylon 6/CB	240 °C	50 bars	1.5 min.	240 °C	150 bars	1 min.
PET/CB	285 °C	50 bars	1.5 min.	285 °C	150 bars	1 min.

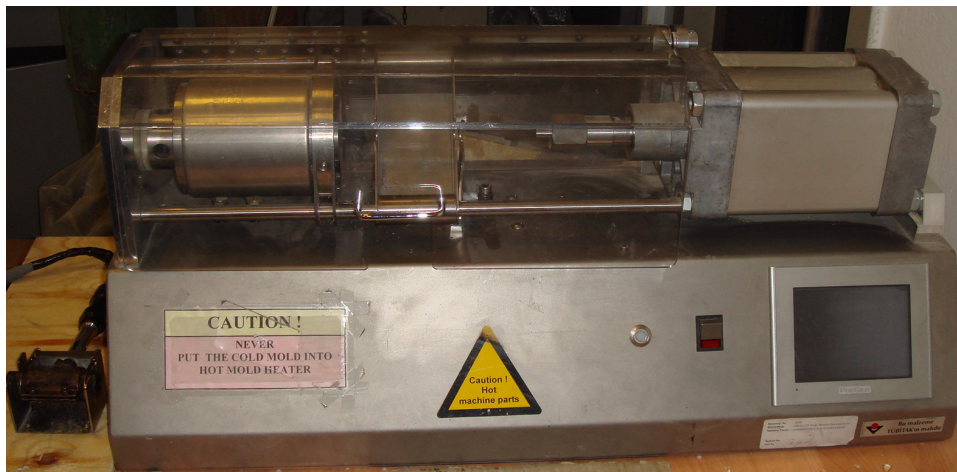


Figure 3.6 A photograph of the laboratory scale injection molding instrument (DSM Micro 10 cc Injection Molding Machine)

3.3 Effect of Grinding on PP/PET and PP/PET/CNT Systems

Grinding, a type of solid-state processing technique, was applied to PP/PET and PP/PET/CNT systems, prepared by melt-mixing method. The materials used and

experimental procedures followed to prepare conventional and ground PP/PET and PP/PET/CNT systems are given in this section. The methods used to characterize prepared composites and blends are described in the fourth section.

3.3.1 Materials

Poly(ethylene terephthalate) (PET) and polypropylene (PP) were used to prepare blend systems. Besides, carbon nanotubes (CNT) were added to these systems to obtain conductive polymer composites. In this study, carbon nanotubes were used as conductive filler, since nanoparticles with high aspect ratio were favorable compared to carbon black in terms of electrical conductivity. Table 3.6 summarizes properties of PET, PP and carbon nanotubes, respectively.

Table 3.6 Physical properties of materials

Material	Trade name & Supplier	Specifications
Poly(ethylene terephthalate) (PET)	Melinar; Advansa	Upper working temp.: 115-170 °C Heat deflection temp. (1.8 MPa): 80 °C Density: 1.3-1.4 g/cm ³
Polypropylene (PP)	PETOPLEN MH418; PETKIM	Melt flow index (2.16 kg; 230 °C): 4-6 g/10 min. Density: 0.91 g/cm ³
Carbon nanotubes (CNT)	Nanocyl 7000; Nanocyl	Average diameter: 10 nm Length: 0.1-10 micron

3.3.2 Blend and Composite Preparation and Grinding

Prior to melt compounding, PET pellets were dried in a vacuum oven for 12 hours at 80 °C and PP pellets were dried in a vacuum oven for 4 hours at 60 °C. PP/PET/CNT systems were prepared by using the twin screw extruder (Thermo PRISM TSE-16-TC). PP and PET pellets were mixed in solid form and fed into the extruder through the main feeder. In addition, carbon nanotubes were fed into the extruder through the side feeder to obtain conductive composite systems with the compositions of 90/10/1, 80/20/1, 70/30/1, 60/40/1, 40/60/1, 20/80/1 (PP/PET/CNT). Same blend compositions were also prepared in the absence of carbon nanotubes to observe the effect of carbon nanotubes on the blend systems. Besides PP/PET/CNT systems containing 1 wt. % carbon nanotubes, conductive filler content of the composite system, 70/30/1 (PP/PET/CNT), was changed to the compositions: 70/30/0.25, 70/30/0.5/, 70/30/2, 70/30/4 (PP/PET/CNT), respectively. The extrusion processes of PP/PET and PP/PET/CNT systems were experimented in the temperature profile of 260-260-260-260-260 °C with a screw speed of 200 rpm. After melt compounding, certain amounts of blend and composite pellets were exposed to grinding process to decrease domain size of PP and PET phases. Each system was ground using a Wiley mill intermediate model grinder (Arthur H. Thomas Co., Philadelphia, PA) at room temperature for 30 minutes and pellets were turned into powder after grinding. A photograph of this grinder is shown in Figure 3.7.



Figure 3.7 A photograph of the Wiley mill intermediate model grinder

In order to determine electrical resistivity of conductive composite systems, test samples of conventional PP/PET/CNT and ground PP/PET/CNT were prepared by compression molding device at 280 °C. To investigate possible effects of high temperature processing on composite microstructure, ground PP/PET/CNT pellets were molded at 230 and 280 °C, respectively. PP/PET/CNT pellets were heated for 0.5 minute under 50 bar gauge pressure and then they were heated for 2.5 minutes under 150 bar gauge pressure. Finally, compression molded samples were quenched to room temperature by water. Test samples required for mechanical property characterization were prepared using the laboratory scale injection molding instrument (DSM Micro 10 cc Injection Molding Machine). At the injection molding process of PP/PET and PP/PET/CNT systems, barrel and mold temperatures were 280 °C and 30 °C, respectively. Besides, tensile test samples of ground PP/PET/CNT systems were prepared at two different temperatures, 230 and 280 °C, to study

possible effects of high temperature processing on composite microstructure. PET does not melt at 230 °C and reduced domain structures of this phase should not change during molding processes at this temperature.

3.4 Characterization of Conductive Polymer Composites and Blends

The methods used to characterize nylon 6/carbon black composites, prepared by in-situ polymerization and melt-mixing methods, are intrinsic viscosity measurement, melt flow index test, electrical conductivity measurement, tensile and impact tests, scanning electron microscopy and transmission electron microscopy. Electron spectroscopy for chemical analysis is the method utilized to characterize surface treated carbon black. Contact angle measurement, x-ray analysis, electrical conductivity measurement and tensile test are the methods used to characterize LDPE/carbon black and nylon 6/carbon black composites, including treated carbon black. In addition, electrical conductivity measurement, electromagnetic interference shielding effectiveness analysis and dielectric constant measurement are the techniques utilized to characterize PET/carbon black composites, containing treated carbon black. The methods used to characterize conventional and ground PP/PET and PP/PET/CNT systems are contact angle measurement, electrical conductivity measurement, tensile and impact tests, scanning electron microscopy.

3.4.1 Intrinsic Viscosity Measurement

Solution viscosity measurement was used to compare molecular weight of synthesized and commercial grade nylon 6. The intrinsic viscosities of these matrices were determined using Ubbelohde viscometer. Nylon 6/carbon black composite, which was dissolved in formic acid, was centrifuged for one hour at 2300 rpm by using CS Model International Centrifuge in order to separate nylon 6 from carbon black to determine the intrinsic viscosity of synthesized nylon 6. 85 % formic acid was used as solvent for nylon 6 at a constant temperature of 25 °C, which was

provided with water bath. The polymer solutions flowed through a capillary and these flow times were used to calculate the intrinsic viscosity $[\eta]$. Then, these data were used to calculate viscosity average molecular weight (M_v) using Mark-Houwink-Sakurada (MHS) equation. MHS constants, K and a , are 22.6×10^{-5} and 0.82, respectively. These constants are relevant to nylon 6 in 85 % formic acid at 25 °C [126].

3.4.2 Melt Flow Index Test

Melt viscosities of synthesized and commercial grade nylon 6 were compared by melt flow index (MFI) measurements, which were performed by Omega model melt flow indexer according to ASTM D 1238 standard. Pure nylon 6 and nylon 6/carbon black composites prepared by method A and B were tested at 235 °C under 2.16 kg load.

3.4.3 Electrical Conductivity Characterization

Electrical conductivity measurement was the common characterization technique in this dissertation. The electrical resistivities of compression molded composites were examined by two point probe method with a constant current source (Keithley 2400). For better electrical contact in two point probe method, copper wires were placed into the compression molded composites during sample preparation. Conductivity measurement was performed by contacting probes with these copper wires. All measurements were done at room temperature and the average of six measurements was taken into account for each composition. Measurements of volume electrical resistance higher than 10^{10} ohm exhibited high deviations from average values, which reduced the reliability of high resistance measurements. Therefore, the electrical resistivity of neat nylon 6 was taken from the literature as 10^{15} ohm.cm [16].

3.4.4 Mechanical Property Characterization

Tensile and impact tests were used to characterize nylon 6/carbon black composites, prepared by in-situ polymerization and melt-compounding methods. Additionally, tensile test was utilized in the study, effect of surface treatment of carbon black on electrical conductivity of LDPE and nylon 6 composites. Effect of grinding on PP/PET and PP/PET/CNT systems were also studied in terms of mechanical properties by tensile and impact tests.

3.4.4.1 Tensile test

As explained before, this dissertation is composed of four different studies, all of which aimed to improve electrical conductivity of conductive polymer composites. These studies are separate and independent from each other. There is not any relation between these studies in terms of mechanical properties; that is, mechanical properties of composites, prepared in the course of these four different studies, were not compared with each other in the content of this thesis. Taking into account this situation, two different tensile testing instruments and standards were utilized to characterize tensile properties of conductive polymer composites. In detail, the tensile properties of nylon 6/carbon black composites prepared by method A and B were measured using a Lloyd 30K universal tensile testing instrument according to ASTM D 638 standard. In the surface treatment study, the tensile properties of LDPE/carbon black and nylon 6/carbon black composites containing 2 wt. % of untreated and treated carbon black, respectively, were measured using the same tensile testing instrument according to ISO 527-2 5A standard. Furthermore, in the grinding study, the tensile properties of PP/PET and PP/PET/CNT systems were measured using another tensile testing instrument (Shimadzu Autograph AG-100 KNIS MS) according to ISO 527-2 5A standard. Five specimens of each composition were tested and average of these five test results were illustrated in graphics with their standard deviations. Injection molded specimen of ASTM D 638 standard had a

thickness of 2.1 mm and width of 7.5 mm. Specimen gauge length was 80 mm. According to the gauge length and a strain rate of 0.1 min^{-1} , the crosshead speed of testing instrument was selected as 8 mm/min. In addition, injection molded specimen of ISO 527-2 5A standard had a thickness of 2 mm and width of 4 mm with a gauge length of 20 mm. According to the gauge length and a strain rate of 0.1 min^{-1} , the crosshead speed of testing instrument was selected as 2 mm/min.

3.4.4.2 Impact Test

Charpy impact strength of nylon 6/carbon black composites prepared by method A and method B was measured by a pendulum impact tester (Coesfeld Material Test). Besides, in the grinding study, charpy impact strength of PP/PET and PP/PET/CNT systems was measured by an other pendulum impact tester (Ceast Resil Impactor 6967) according to ASTM D 5942 standard.

3.4.5 Morphology Analysis

Scanning electron microscopy (SEM) and transmission electron microscopy (TEM) were performed to characterize morphologies of conductive polymer composites. Both SEM and TEM were used to visualize morphological structure of nylon 6/carbon black composite, prepared by in-situ polymerization and melt-compounding methods, respectively. In addition, SEM was used in the surface treatment study to observe effects of formamide treatment on carbon black structure in PET composite and in the grinding study to reveal the morphological differences between ground and conventional PP/PET/CNT systems.

3.4.5.1 Scanning Electron Microscopy (SEM)

Fractured surfaces of impact specimens of nylon 6/carbon black composites prepared by method A and method B, respectively, PET based composites containing 6 wt. %

of untreated and treated carbon black, respectively, and PP/PET/CNT systems were analyzed by using Scanning Electron Microscope (JEOL JSM-6400). Prior to SEM, a thin coating of gold was deposited on the sample surface to prevent the accumulation of static electric field during imaging. In order to increase carbon black resolution in SEM micrographs, injection molded specimens of PET based composites were fractured and stained with nitric acid for 3 hours at room temperature. Besides, prior to morphological analysis, conventional and ground PP/PET/CNT systems were exposed to chemical etching with trifluoroacetic acid for 6 hours to separate PET phase of composite systems.

3.4.5.2 Transmission Electron Microscopy (TEM)

Impact specimens of nylon 6/carbon black composites prepared by method A and method B were also analyzed by using Transmission Electron Microscope (Philips CM200 TEM). Samples were trimmed parallel to the molding direction and sections with a thickness of 70 nm were obtained at -100° C. TEM images were taken at an acceleration voltage of 120 kV.

3.4.6 Electron Spectroscopy for Chemical Analysis

Electron spectroscopy for chemical analysis (ESCA) was performed to investigate surface chemistry of untreated carbon black, UCB, and treated carbon black, APS1-CB, FA1-CB, FA2-CB and FA3-CB. Specs model spectrometer equipped with aluminum radiation at 1 W was used to obtain ESCA spectra of carbon black. The high resolution spectra of oxygen (O_{1s} peak) and of nitrogen (N_{1s} peak) were recorded with a pass energy of 48 eV at a vacuum level lower than 10^{-5} Pa. A non-linear background was removed from the spectra and XPSPeak 41, which is a curve fitting program, was used to fit the high resolution spectra of oxygen and nitrogen.

3.4.7 Contact Angle Measurement

Contact angle measurements were performed to investigate surface energy of untreated carbon black, UCB, and treated carbon black, APS1-CB, FA1-CB. In addition, contact angle measurements were carried out to obtain information about surface energy of PP, PET and carbon nanotubes, used to determine selective localization of carbon nanotubes in PP/PET systems. Diiodomethane (DIM), ethylene glycol (EG) and formamide were utilized as probe liquids during contact angle measurements. DIM was selected to calculate London dispersive component of surface energy, γ^{LW} . Meanwhile, EG and formamide were used to calculate acid/base component of surface energy, γ^{AB} . Surface free energy components of probe liquids are given in Table 3.7.

Table 3.7 Surface energy components of probe liquids, (mN/m) [127]

Liquid	γ_L^{TOT}	γ_L^{LW}	γ_L^{AB}	γ_L^A	γ_L^B
DIM	50.80	50.80	-	-	-
EG	48.00	29.00	19.00	3.00	30.10
Formamide	58.00	39.00	19.00	2.30	39.60

According to Sessile drop method, contact angles of probe liquids on injection molded samples of PP and PET were used to calculate surface energy [102]. On the other hand, carbon black and carbon nanotubes were pressed as discs under 150 bar gauge pressure and contact angles of probe liquids were determined from these pressed surfaces [101, 128, 129]. Three different contact angle measurements were

performed for each probe liquid and average of them was used to calculate surface energy components.

Surface energies of PET and PP were also calculated theoretically using Equations 2.4 and 2.5. For most polymers, T_c is about 1000 K. $-d\gamma/dT$ of PET and PP is equal to 0.065 mN/m.K and 0.056 mN/m.K, respectively. In addition, $\gamma_i^{AB}/\gamma_i^{Total}$ of PET and PP is equal to 0.221 and 0, respectively [126].

3.4.8 X-Ray Analysis

X-ray analysis was used to study the effect of surface treatment on the structural properties of carbon black in polymer matrix. X-ray diffraction (XRD) patterns of LDPE and nylon 6 composites containing 2 wt. % of untreated and treated carbon black, respectively, were obtained with a 100 kV Philips twin tube X-ray diffractometer (PW/1050) providing $CuK\alpha$ radiation ($\lambda=0.15418$ nm) at 40 kV and 40 mA. XRD patterns were attained at a scan speed of 1 °/min from 5° to 45°.

3.4.9 Microwave Property Characterization

Both electromagnetic interference (EMI) shielding effectiveness analysis and dielectric constant measurement were performed to study the application potential of PET/UCB, PET/FA1-CB, PET/FA2-CB and PET/FA3-CB composites as EMI shielding and dielectric material. Test samples were prepared using the injection molding device according to the procedure explained in section 3.2.3.

3.4.9.1 EMI Shielding Effectiveness Analysis

EMI shielding effectiveness of PET based composites containing 4, 6 and 8 wt. % untreated and treated carbon black were tested with a HP 8720D Hewlett Packard Network Analyzer and a waveguide having dimensions of 2.286 cm x 1.016 cm

operating in the X-band range (8 - 12 GHz). In order to prevent radiation leakage during absorption loss, return loss (reflection loss) and insertion loss measurements, test samples were fitted precisely to the shape of waveguide. The thickness of test samples was 4 mm. Prior to measurements, network analyzer was calibrated according to X-band range. The incident, reflected and transmitted waves were measured in the absence of samples, which were taken as reference data, and in the presence of the test samples. Absorption loss, return loss and insertion loss data were obtained in decibels (dB). During absorption loss measurements, a conductor was placed behind the samples. Hence, radiation, which was not absorbed in the sample, could be returned. Return loss and insertion loss measurement were conducted in air medium.

3.4.9.2 Dielectric Constant Measurement

Dielectric constant of PET based composites including 4, 6 and 8 wt. % untreated and treated carbon black was measured with a setup, illustrated in Figure 3.8. This setup includes a Microwave source (FMI 449x), a VSWR (Voltage Standing Wave Ratio) meter (Narda Microwave Corporation-Model 441F), determining the ratio of the maximum standing wave amplitude to the minimum standing wave value, a slotted line, which is a coaxial line with a slot at which a probe can measure varying electric field strength, an isolator, using to protect the source, and a sliding short, at which the sample is placed.

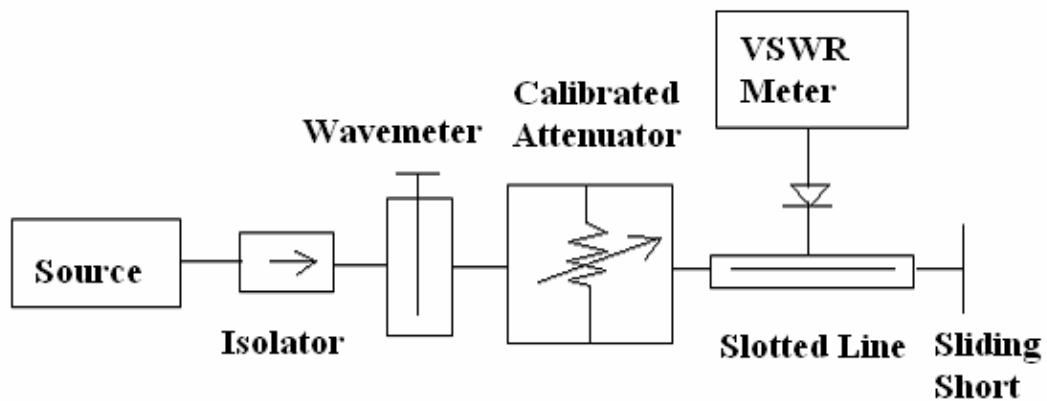


Figure 3.8 Experiment setup of dielectric constant measurement

Test samples of EMI shielding effectiveness analysis were used to determine dielectric constant values of composites at 8.5 and 10 GHz, respectively. The measurement method is to insert the dielectric sample at the end of a short circuited waveguide. In order to calculate dielectric constant, voltage standing wave pattern without the test sample was measured. When the test sample was inserted, the position of voltage minimum shifted by a distance of L . By measuring L , dielectric constant, ϵ_r , was calculated from the following relationships:

$$\lambda_0 = \frac{c}{f_0} \quad (3.1)$$

$$\frac{1}{\lambda_g^2} = \frac{1}{\lambda_0^2} - \frac{1}{(2a)^2} \quad (3.2)$$

$$\frac{\tan\left(2\pi\frac{d}{\lambda_{g\epsilon}}\right)}{\left(2\pi\frac{d}{\lambda_{g\epsilon}}\right)} = \frac{\lambda_g}{2\pi d} \tan\left(2\pi\frac{(L+d)}{\lambda_g}\right) \quad (3.3)$$

$$\frac{1}{\lambda_{g\epsilon}^2} = \frac{\epsilon_r}{\lambda_o^2} - \frac{1}{(2a)^2} \quad (3.4)$$

in which c is speed of light, f_o is the applied frequency, λ_g is the guided wavelength without the sample, a is equal to 2.286 cm (the larger dimension of the waveguide), d is the thickness of sample and $\lambda_{g\epsilon}$ is the guided wavelength in the sample filled region.

3.5 Electrochemical Capacitance Performances of Polyaniline/Carbon Nanotubes Composites and Polyaniline Films on Treated Current Collectors

Polyaniline/carbon nanotubes electrodes were prepared to study electrochemical capacitor application of conductive polymer composites. For this purpose, multi-walled carbon nanotubes were synthesized by chemical vapor deposition technique. Carbon nanotubes used in study was different from that of the grinding study. In-situ polymerization method was used to synthesize the conducting polymer in the presence of carbon nanotubes. Additionally, polyaniline film electrodes were prepared by depositing polyaniline solution on treated current collectors. In this section, the materials and methods used to prepare and characterize polyaniline/carbon nanotubes composites and polyaniline films on treated current collectors are expressed.

3.5.1 Materials

Chemicals used to synthesize polyaniline are given in Table 3.8. Additionally, chemicals used to treat the current collector and to coat it with polyaniline film are illustrated in Table 3.9.

Table 3.8 Chemicals used for polyaniline synthesis

Chemical	Company
Aniline hydrochloride	Alfa Aesar (A13024)
Ammonium peroxydisulfate	Alfa Aesar (54106)
Ethanol	Alfa Aesar (36642)
Acetone	Acros Organics (26831)
Hydrochloric acid	EMD Chemicals (HX0603)
Ammonium hydroxide	Fisher Chemicals (UN2672)

Table 3.9 Chemicals used to treat the current collector and to coat it with polyaniline film

Chemical	Company
Sulfuric acid	EMD Chemicals (SX1244)
Monosodium salt of 1,2-dihydroxyanthraquinone-3-sulphonic acid	Acros Organics (40048)
1-methyl-2-pyrrolidinone	Acros Organics (36845)

3.5.2 Growth of Carbon Nanotubes

The multi-walled carbon nanotubes (CNT) used for supercapacitor application were prepared by chemical vapor deposition (CVD) method according to the procedure applied in the laboratory of Prof. Ning Pan at UC Davis [61]. Carbon nanotubes were synthesized in a horizontal quartz tube in a furnace (Lindberg Blue M TF55035A-1) with 1 inch diameter and 12 inch heated lengths, operated by using programmable controller. Fe/Al₂O₃ catalyst powders were placed in a ceramic boat that was packed into the furnace subsequently (Figure 3.9) [61].

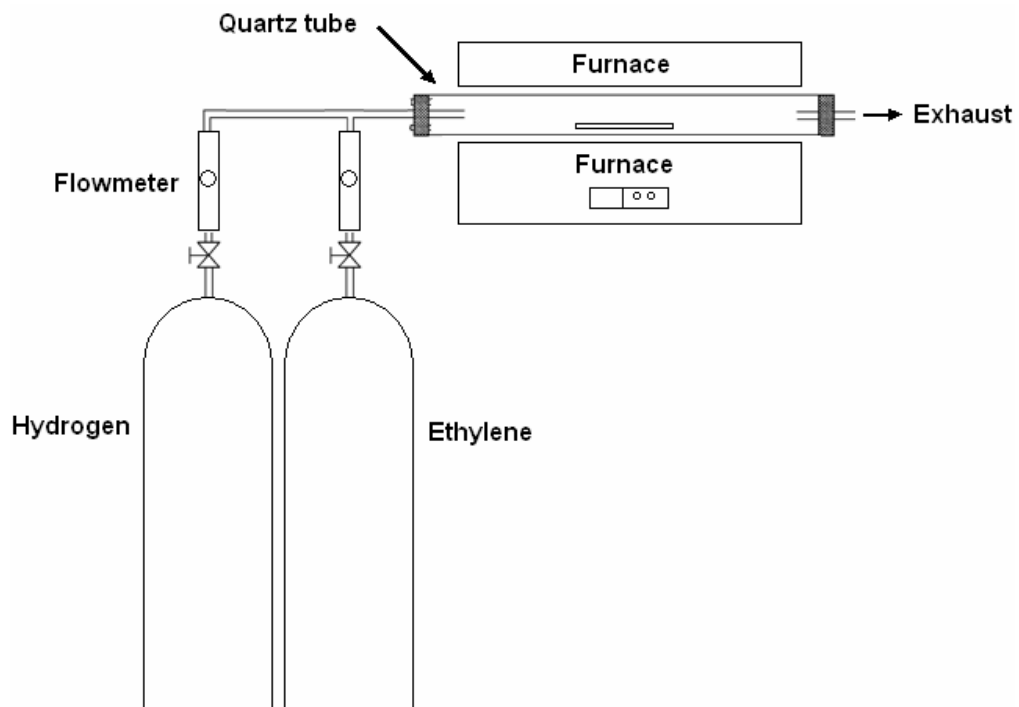


Figure 3.9 Schematic illustration of experimental setup for carbon nanotubes synthesis

Hydrogen was introduced into the furnace before heating to clean up the system. Then the furnace was heated up to 650 °C. When the furnace temperature became stable at 650 °C, a mixture of hydrogen and ethylene (1:2 volume ratio of hydrogen to ethylene) was fed into the furnace for 30 minutes. Operating gas flow rate of ethylene was 200 ml/min and its flow was stopped when the system started to cool. However, hydrogen flow was continued until the furnace was cooled to the room temperature [61].

In order to remove the catalyst powder, the samples were treated with hydrofluoric acid and hydrochloric acid solutions, separately. First carbon nanotubes were treated with dilute hydrofluoric acid solution for one day to remove Al₂O₃ from carbon nanotubes. Then, they were filtered under vacuum and rinsed with distilled water several times. After filtration, they were treated with hydrochloric acid solution for 3 hours to remove Fe catalyst from carbon nanotubes. Then, they were collected again with filtration under vacuum and rinsed with distilled water until the particles were neutralized. After washing with water, carbon nanotubes were rinsed with ethanol to extract water. Finally, the resultant nanotube particles, separated from catalyst particles, were dried at 60 °C overnight [61].

3.5.3 Synthesis of Polyaniline and Polyaniline/Carbon Nanotubes Composites

Composites of doped polyaniline (Pani) with multi-walled carbon nanotubes (CNT) were prepared by in-situ polymerization method. Polyaniline was synthesized in the presence of carbon nanotube particles by chemical oxidative polymerization. Aniline hydrochloride was dissolved in ethanol to provide 0.04 M solution and ammonium peroxydisulfate was similarly dissolved in distilled water to yield 0.05 M solution. Various weight ratios of nanotube particles were added in 0.04 M aniline hydrochloride solution and stirred for one hour [130, 131]. Carbon nanotubes are good electron acceptor and aniline is known as good electron donor. Aniline monomers and carbon nanotube particles might form charge transfer complex,

resulting in adsorption of aniline monomers on nanotubes [132]. The oxidant solution and monomer solution containing various portions of carbon nanotubes were mixed to start the polymerization. Aniline monomers adsorbed on nanotubes resulted in the formation of polyaniline. The reaction mixture was stirred for 24 hours at room temperature and a dark-green suspension formed at the end of this reaction period, which indicated the formation of emeraldine salt form of polyaniline on carbon nanotubes. Polyaniline coated nanotubes were filtered under vacuum and rinsed with 0.2 M hydrochloric acid solution to remove residual monomers and to provide a more uniform doping of polyaniline with chloride ions. Additionally, they were rinsed with acetone to remove oligomers and to prevent aggregation of polyaniline deposited nanotube particles during drying. Finally, they were dried at 60 °C for 24 hours [130, 131].

Pani/CNT composites, containing 10, 20, 40, 60 and 80 wt. % polyaniline, were prepared according to the procedure given above. For comparison purposes, polyaniline salt was synthesized in the absence of nanotube particles by applying the same procedure. The only difference was that aniline hydrochloride was dissolved in distilled water instead of ethanol. In addition, a portion of synthesized polyaniline in emeraldine salt form was converted to emeraldine base form. For this purpose, polyaniline powders were added to 1 M ammonium hydroxide solution and held for 24 hours in this medium for deprotonation. The color of deprotonated polyaniline suspension turned to blue from dark-green. Then, deprotonated powders were filtered under vacuum and rinsed with acetone before drying at 60 °C for 24 hours [130, 131].

3.5.4 Preparation of Polyaniline Films on Treated Current Collectors

Polyaniline base samples in varied amounts were dissolved in 10 ml of 1-methyl-2-pyrrolidinone (NMP) for 24 hours to obtain polyaniline base solutions with different concentrations. Besides, for the treatment purpose, nickel (Ni) foil current collectors

were immersed in 1 M H₂SO₄ solution for 5 minutes and then they were washed with acetone. Afterwards, nickel foils were immersed in an aqueous solution of monosodium salt of 1,2-dihydroxyanthraquinone-3-sulphonic acid (alizarin) (50 mg alizarin/100 ml distilled water) for 5 minutes. After washing with distilled water, nickel foils were left for drying at room temperature. Finally, electrodes were prepared by directly depositing 10 µl of each polyaniline base solution on alizarin treated nickel foils. They were allowed to dry at room temperature for 3 days. PA250, PA100, PA50, PA25, PA16.7 and PA6.7 were the codes used to identify electrode systems deposited with polyaniline base solutions, including 250, 100, 50, 25, 16.7 and 6.7 mg of polymer, respectively. For comparison purposes, one electrode pair was prepared by depositing polyaniline base solution, containing 25 mg of polymer, on untreated nickel foils. This electrode system was coded with NPA25.

3.5.5 Characterization of Polyaniline/Carbon Nanotubes and Polyaniline Films on Treated Current Collectors

3.5.5.1 Fourier Transform Infrared (FTIR) Spectroscopy

Fourier transform infrared (FTIR) spectroscopy was utilized to be aware of the interaction between carbon nanotubes and polyaniline. Nicolet 6700 (Thermo Electron Corporation) model spectrometer was used to record spectra of multi-walled carbon nanotubes, polyaniline and polyaniline coated carbon nanotubes. Samples were milled with potassium bromide to form a very fine powder. This powder was then pressed into a thin pellet. FTIR characterization was done in the frequency range from 4000 to 400 cm⁻¹ with a resolution of 2.0 cm⁻¹.

3.5.5.2 Electrochemical Capacitance Characterization

The electrochemical capacitance performances of polyaniline/carbon nanotubes composites and polyaniline films on treated nickel foils were evaluated using a two-electrode cell system. The electrodes of Pani/CNT systems were fabricated by mixing 80 wt. % active material, polyaniline/carbon nanotubes, and 20 wt. % poly(tetrafluoroethylene) (PTFE) as binder. They were pasted onto a nickel current collector (1 cm x 1 cm) using a conductive silver paste and pressed under 70 bar gauge pressure at 260 °C for 5 minutes. The test cell of electrochemical capacitors was fabricated using two prepared electrodes and a separator, glass fiber filter paper. The separator was immersed into 1 M NaNO₃ electrolyte and placed between these two electrodes.

The cyclic voltammetry, galvanostatic charge/discharge tests and electrochemical impedance analyses of all electrochemical capacitors were performed using a Potentiostat/Galvanostat (EG&G Princeton Applied Research, Model 263A). Cyclic voltammetry scans were recorded from 0 V to 0.9 V at a scan rate of 50 mV/s. Charge/discharge tests of Pani/CNT based electrode systems were performed at a discharge current of 1 mA. Besides, charge/discharge tests of Pani based electrode systems, prepared by deposition of polyaniline on treated nickel foils, were performed at a discharge current of 0.1 mA. Impedance analyses were performed using the EG&G 263A Potentiostat/Galvanostat with a frequency response detector in the frequency range from 50000 Hz to 0.05 Hz at an ac modulation of 10 mV.

3.5.5.3 Scanning Electron Microscopy (SEM)

SEM was performed to investigate morphologies of Pani/CNT composites. Powders of pure carbon nanotubes, composites containing 20, 40 and 60 wt. % polyaniline, respectively, pure polyaniline were analyzed by using Scanning Electron Microscope (Zeiss SUPRA 50 VP). Prior to SEM, a thin coating of gold was not deposited on the

samples since carbon nanotubes, composite and polyaniline powders were highly conductive to prevent the accumulation of static electric field during imaging.

CHAPTER 4

RESULTS AND DISCUSSION

Main goal of this thesis is to improve electrical property of conductive polymer composites. In the view of this purpose, different processing studies were performed and the results of these studies are expressed in four parts in this chapter. First part contains characterization test results of nylon 6/carbon black composites, prepared by in-situ polymerization and melt mixing methods, respectively. Then, effects of surface treatment of carbon black on electrical conductivity of LDPE and nylon 6 composites are discussed. Additionally, to reveal application potential of conductive polymer composites, EMI shielding effectiveness and dielectric property of PET composites containing treated carbon black are described. Thereafter, effects of grinding on electrical conductivity and mechanical properties of PP/PET/CNT systems are discussed. Final part includes characterization test results of polyaniline/carbon nanotubes composites and polyaniline films on treated current collectors as electrode material for application in electrochemical capacitors.

4.1 Preparation of Nylon 6/Carbon Black Composites

Electrical resistivity of composite depends on the processing technique used to combine conductive filler with polymer matrix. As an alternative to melt mixing method, in-situ polymerization technique can be utilized to enhance electrical conductivity of polymer composites by reducing average agglomerate size of conductive filler in matrix. In this part, the effects of in-situ polymerization and melt mixing techniques on electrical conductivity, mechanical properties and morphology

of nylon 6/carbon black composites are discussed and compared. Prior to electrical conductivity and mechanical properties characterization, solution and melt viscosities of the composites, prepared by both methods, are compared below.

4.1.1 Intrinsic Viscosity and Melt Flow Index Measurements

As stated before, method A and method B are the codes used to define the composite preparation techniques, which are in-situ polymerization and melt mixing, respectively. In order to compare method A with method B, synthesized nylon 6 has to be comparable with commercial grade nylon 6. The comparison is based on melt flow index and solution viscosity values of nylon 6. The intrinsic viscosity and viscosity average molecular weight values of synthesized nylon 6, synthesized and then centrifuged nylon 6 in the presence of 16 wt. % carbon black and commercial grade nylon 6 are given in Table 4.1. According to the results, viscosity average molecular weights of synthesized and commercial grade nylon 6 are nearly equal. High molecular weight in masterbatch composite, 65509 g/mol, reveals that nylon 6 with a molecular weight similar to commercial grade nylon 6, 64145 g/mol, is synthesized in the presence of 16 wt. % carbon black.

Table 4.1 Intrinsic viscosity $[\eta]$ and viscosity average molecular weight M_v

	$[\eta]$ (dl/g)	M_v (g/mol)
Nylon 6 synthesized	2.0088	65410
Nylon 6 synthesized in the presence of 16 wt.% filler (centrifuged)	2.0113	65509
Commercial grade nylon 6	1.9769	64145

Melt flow index (MFI) values of composites prepared by method A and B are given in Table 4.2. Both MFI values of masterbatch diluted composites and melt mixed composites fluctuate between 1 and 12 wt. % of carbon black. Their trends are similar. However, certain MFI values of masterbatch diluted composites are lower compared to melt mixed composites. Possible reason may be the morphological difference. As the carbon black agglomerate size decreases, filler-matrix interaction area increases, which may result in higher melt viscosity for masterbatch diluted composites up to 6 wt. % of carbon black composition in comparison to those prepared by method B.

Table 4.2 Melt Flow Index results of composites prepared by method A and B

Filler content	0 wt. %	1 wt. %	3 wt. %	6 wt. %	10 wt. %	12 wt. %
Method A (g/min)	3.01	3.42	3.33	3.61	3.24	2.56
Method B (g/min)	3.34	3.62	3.47	4.77	3.04	2.34

4.1.2 Electrical Conductivity Characterization

Carbon black tends to form agglomerates due to weak van der Waals forces among its particles and can preserve these structures into some extent even in polymer matrices [4]. Electrical conductivity in carbon black filled composites occurs by means of the transportation of electrons between these conductive agglomerates, which are separated from each other by polymer layers. Electrons may transfer through the insulating polymer layers by tunneling mechanism during conduction. These layers are the main reason for electrical resistance [2]. So, the distance

between the agglomerates should be as small as possible. Hence, a decrease in average agglomerate size also reduces the thickness of the insulating layer. It is aimed to decrease agglomerate size by in-situ polymerization method in this study. During the polymerization of nylon 6 in the presence of carbon black, filler particles act as catalyst due to their high surface area. Owing to the smaller size of caprolactam in comparison to that of nylon 6 polymer, the monomer can enter the pores of carbon black and polymerize there. As the chain length increases, agglomerates are broken into small pieces and they are separated from each other. Decreased particle size results in increased particle-particle interaction, which increases electron transfer probability between conductive agglomerates [11]. Consequently, lower electrical resistivity is provided by method A compared to method B at the same compositions (Figure 4.1).

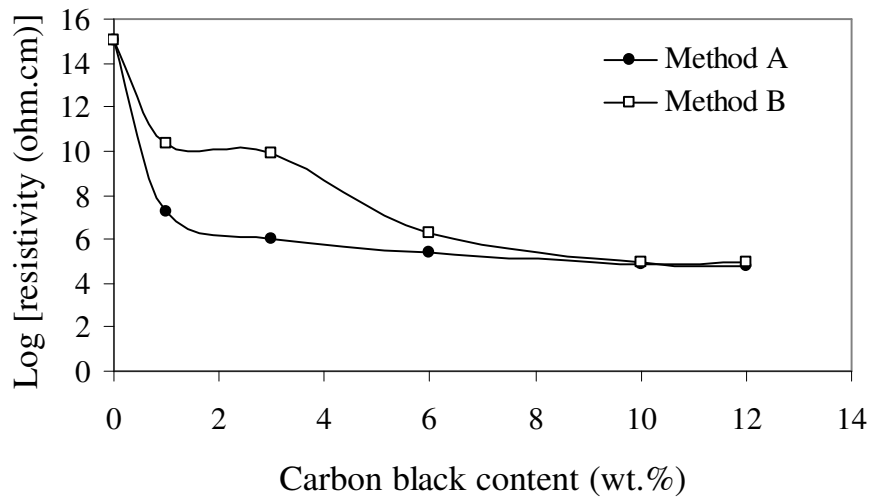


Figure 4.1 The electrical resistivity values of carbon black filled nylon 6 composites prepared by method A and method B

Due to low melt viscosity of nylon 6 (Table 4.2), carbon black agglomerates cannot be broken efficiently in melt mixing method. As a result of this inefficient mixing, low compositions of method B could not provide high conductivity when compared with method A. However, high loadings of both methods, 10 and 12 wt. % carbon black, have similar resistivity values. This improvement in electrical conductivity is the result of increased melt viscosity of composites (Table 4.2) prepared by method B, and also an increase in carbon black content decreases electrical resistivity by reducing the insulating polymer layer between agglomerates. The onset in electrical conductivity of composites, prepared by method A and method B, from insulator to semi conductor region is accomplished at around 1 and 6 wt. % of carbon black loading, respectively. In the literature, transition from insulator to semiconductor region of nylon 6 based composite, prepared by melt compounding method, is accomplished at around 10 wt. % of carbon black [7]. Additionally, nylon 6 composite, prepared by in-situ polymerization technique, reaches semiconductive level at 2 wt. % of graphite content according to the literature [16]. It is aimed to obtain semiconductive polymer composite at relatively low composition. Thus, method A is favorable compared to method B and other techniques applied in the literature in terms of electrical conductivity [7, 16].

4.1.3 Mechanical Property Characterization

As stated before, carbon black particles have a strong tendency to agglomerate and these structures should be broken as much as possible since they create weak points in polymer matrices and can easily break when stress is applied. A broken agglomerate then behaves as a strong stress concentrator, reducing the tensile strength of the composites [4]. Masterbatch preparation and dilution process of method A may prevent agglomeration into some extent, which results in an increase in the tensile strength at low compositions up to 6 wt. % compared to method B (Figure 4.2). Method A provides also lower electrical resistivity at low compositions. Improvement in tensile strength and electrical conductivity can be attributed to the

increase in interfacial area of particles at the same carbon black concentration. As the filler concentration increases, tensile strength of the composites prepared by method A decreases slightly; whereas, composites of method B show fluctuations in tensile strength values. Relatively high melt viscosity (Table 4.2) increase the shearing effect of rotating screws, which may lead to a decrease in agglomerate size of carbon black particles in 12 wt. % composite of method B when compared with other compositions of the same method. Hence melt mixed composites filled with 12 wt. % carbon black have higher tensile strength value (Figure 4.2). All composites of method B show high standard deviations from average tensile strength values. Large standard deviations may be the result of less homogeneous filler distribution. In contrast to method B, tensile strength values of method A show small deviations from the average values at the same compositions, which may be the evidence of more homogeneous distribution provided by method A.

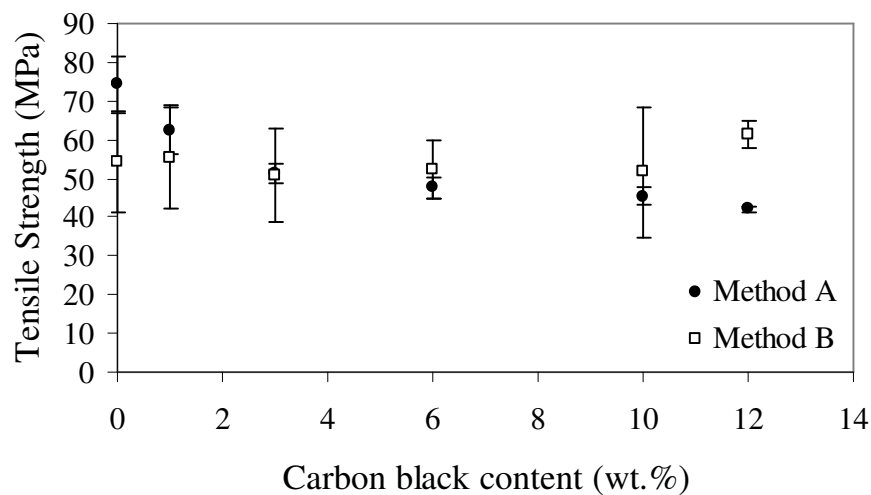


Figure 4.2 The tensile strength values of carbon black filled nylon 6 composites prepared by method A and method B

Even though particle agglomeration tends to reduce the tensile strength, the agglomerate may be strong enough to increase the initial modulus, since carbon black addition increases the modulus of prepared composites [4]. As the filler content increases, tensile modulus values of composites prepared by method A increase slightly; whereas, modulus values of composites prepared by method B increase sharply with filler contribution and decrease after 6 wt. % of carbon black composition (Figure 4.3). This difference in tensile modulus values of composites obtained by method A and method B may be the consequence of the difference in agglomerate size of carbon black. Below a critical size, filler may lose its effect on tensile modulus [4]. As it is observed from electrical resistivity results, method A provides a decrease in agglomerate size. As a result, tensile modulus does not change significantly due to small sizes of carbon black agglomerates in composites prepared by method A.

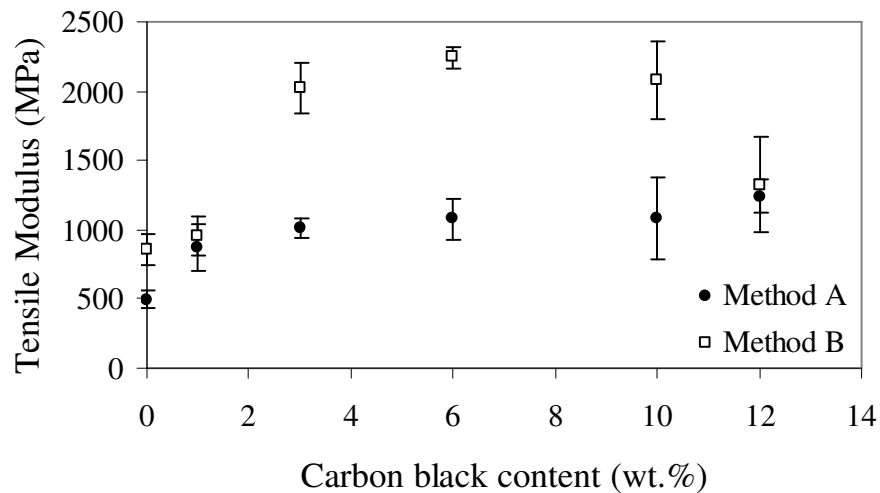


Figure 4.3 The tensile modulus values of carbon black filled nylon 6 composites prepared by method A and method B

Elongation at break values (Figure 4.4) of both methods decrease sharply with 1 wt. % filler content due to brittle character of carbon black agglomerates and do not change significantly upon further increase in filler composition. In addition, the values in both methods are close to each other except for 1 wt. % of carbon black composition. At 1 wt. % composition, test samples of method B elongate more compared to other filled composites. Besides, electrical conductivity in insulator range was obtained at this composition of method B, which is the consequence of incomplete carbon black network in the composite. Hence, incomplete filler network results in higher elongation at break value.

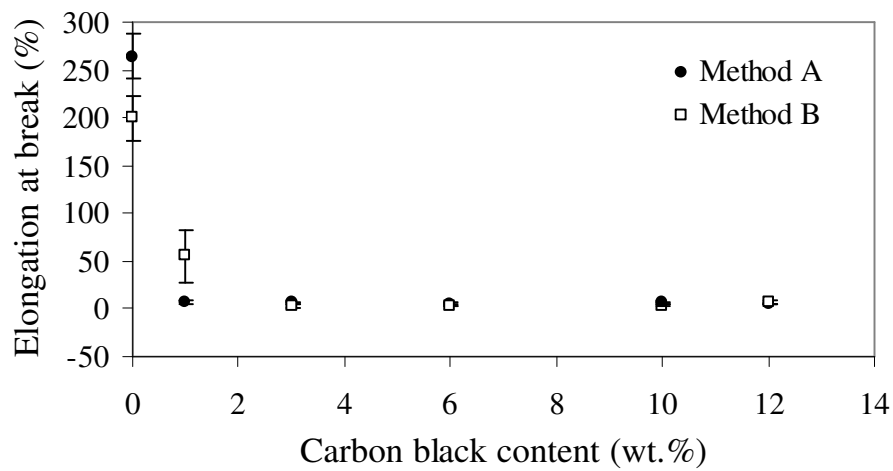


Figure 4.4 The elongation at break values of carbon black filled nylon 6 composites prepared by method A and method B

Impact samples of pure nylon 6 could not be broken with the available impact tester. The impact strength of the composites prepared by both methods decreases with filler contribution, excluding 10 and 12 wt. % compositions of method B. Low compositions of method A have higher impact strength values compared to method B (Figure 4.5), which may be the consequence of improved interfacial interaction between composite constituents since a decrease in agglomerate size enhances interfacial interaction between the polymer and the filler.

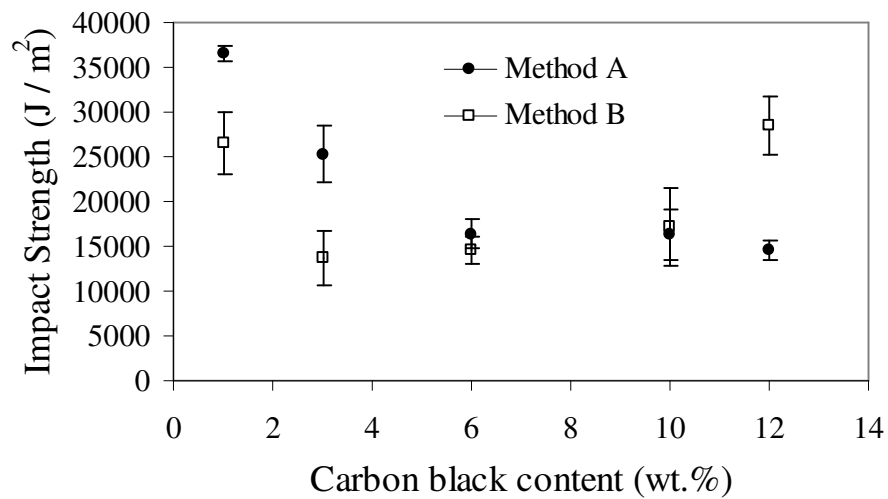


Figure 4.5 Charpy impact strength values of carbon black filled nylon 6 composites prepared by method A and method B

4.1.4 Morphology Analysis

Figure 4.6 shows SEM micrographs of impact fractured surfaces of the composites containing 6 wt. % carbon black for both method A and method B. Carbon black agglomerates could not be detected on SEM micrographs at high resolution around micron size. From these micrographs, it can be concluded that the carbon black agglomerates are under micron size for both composite preparation methods.

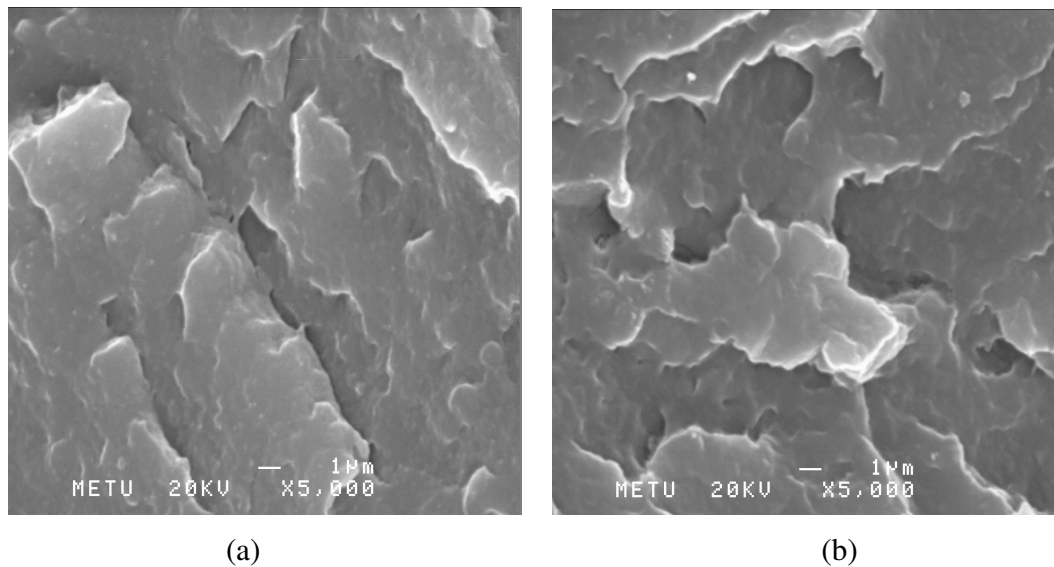


Figure 4.6 SEM micrographs of impact fractured samples containing 6 wt. % carbon black, (a) Method A (x5000) and (b) Method B (x5000)

Due to limited resolution of SEM, the size and dispersion of carbon black particles in the composites are investigated by TEM analyses. Figures 4.7 and 4.8 illustrate TEM micrographs of the composites prepared by method A and method B with 3 wt. %

carbon black. In Figures 4.7 (a) and 4.8 (a), a few small carbon black clusters are observed as less dense areas with the size smaller than 200 nm. In Figures 4.7 (b) and 4.8 (b), more dense areas and larger agglomerate sizes are recognizable for method B. Therefore, method A provides smaller and less dense agglomerates, which result from the entering of nylon 6 monomer into the pores of carbon black particles during polymerization reaction. As a result, lower electrical resistivity and improved tensile strength and impact strength were obtained for the composites prepared by in-situ polymerization method at lower concentration of carbon black.

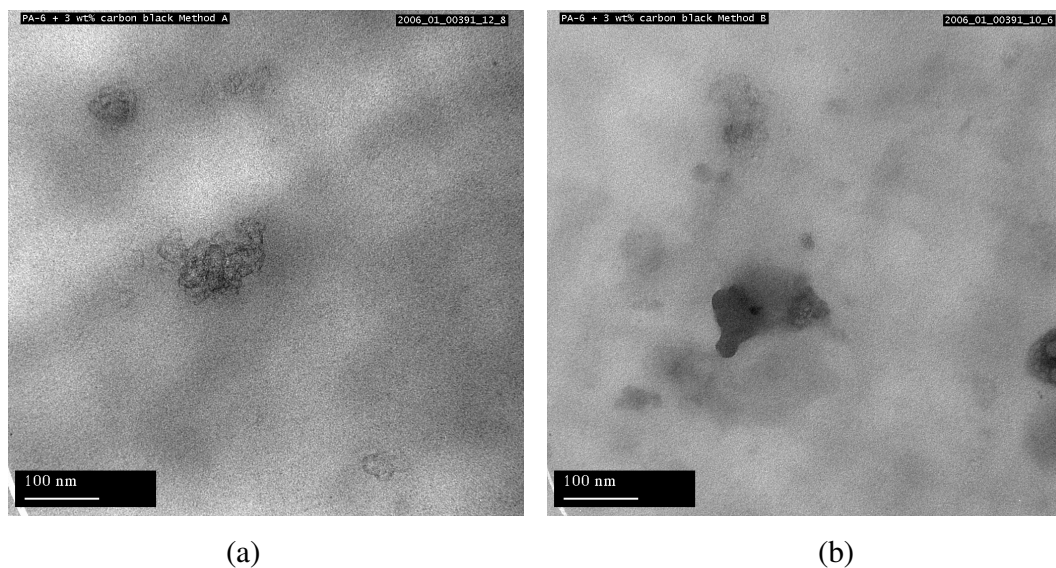


Figure 4.7 TEM micrographs of impact samples containing 3 wt. % of carbon black, (a) Method A and (b) Method B

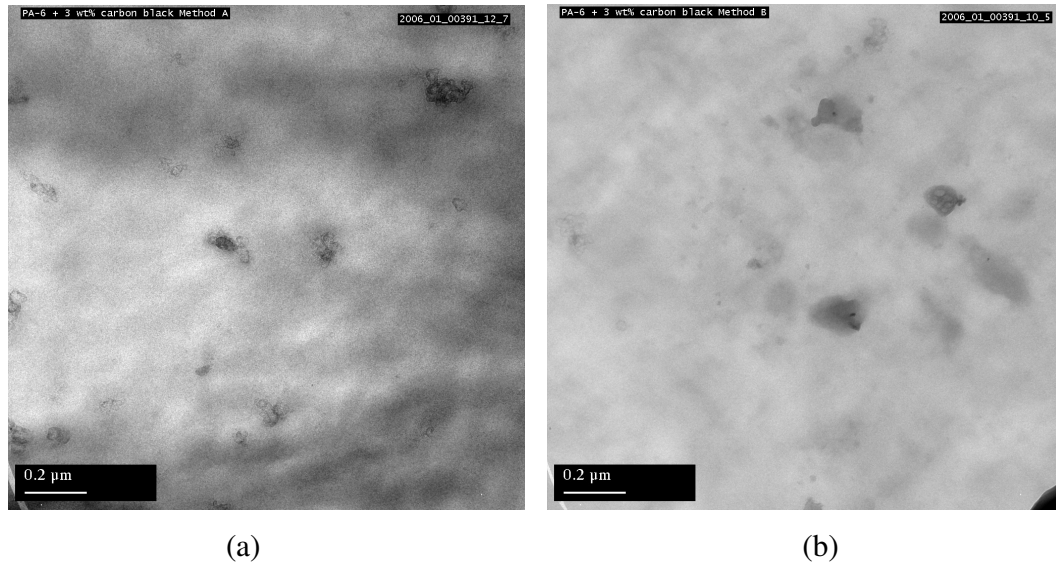


Figure 4.8 TEM micrographs of impact samples containing 3 wt. % of carbon black, (a) Method A and (b) Method B

4.2 Effect of Surface Treatment of Filler on LDPE/Carbon Black, Nylon 6/Carbon Black and PET/Carbon Black Composites

Electrical resistivity of polymer composites not only depends on the processing technique used to combine conductive filler with insulating matrix but also electrical conductivity of the filling material. That is, any attempt to increase electrical conductivity of the filling material decreases electrical resistivity of prepared composites. Hence, surface treatment can be applied to conductive filler to increase electrical conductivity of polymer composites. In this part, the effects of surface treatment of carbon black on electrical conductivity of LDPE and nylon 6 composites are discussed. Beside electrical conductivity, EMI shielding effectiveness and dielectric property of polymer composites can be enhanced using treated conductive filler. As an application, the effects of surface treatment of carbon black

on EMI shielding effectiveness and dielectric property of PET composites are also discussed in this part. Thus, the surface treatment study is separated into two subsections. In the first subsection, characterization test results of LDPE and nylon 6 composites are given. Characterization test results of PET composites are expressed in the second subsection. In fact, this part is studied to assess the properties of PET/treated carbon black systems for EMI shielding and dielectric material application. Before discussing the effects of surface treatment on composite systems, ESCA results of untreated and treated carbon black are expressed below.

4.2.1 Electron Spectroscopy for Chemical Analysis

The surface chemistry of untreated and treated carbon black was characterized by ESCA. According to O_{1s} spectrum of untreated carbon black (Figure 4.9), there are different kinds of oxygen functional groups on the surface of carbon black before surface treatment. O_{1s} spectrum of untreated carbon black is fitted to four peaks: a peak for C=O type oxygen at 531.6 eV, a peak for C-O type oxygen (C-OH, C-O-C) at 532.8 eV, a peak for -OH type of oxygen at 532 eV and a peak for adsorbed oxygen ($-O_2$) at the binding energy of 530.3 eV. In addition, N_{1s} spectrum of untreated carbon black, given in Figure 4.10, is fitted to three peaks: a peak for adsorbed nitrogen at 400 eV, a peak for NH_2 type of nitrogen, bonded to phenyl, at 399.2 eV and a peak for nitrogen, which is in conjugated structure of graphene, at 398.1 eV.

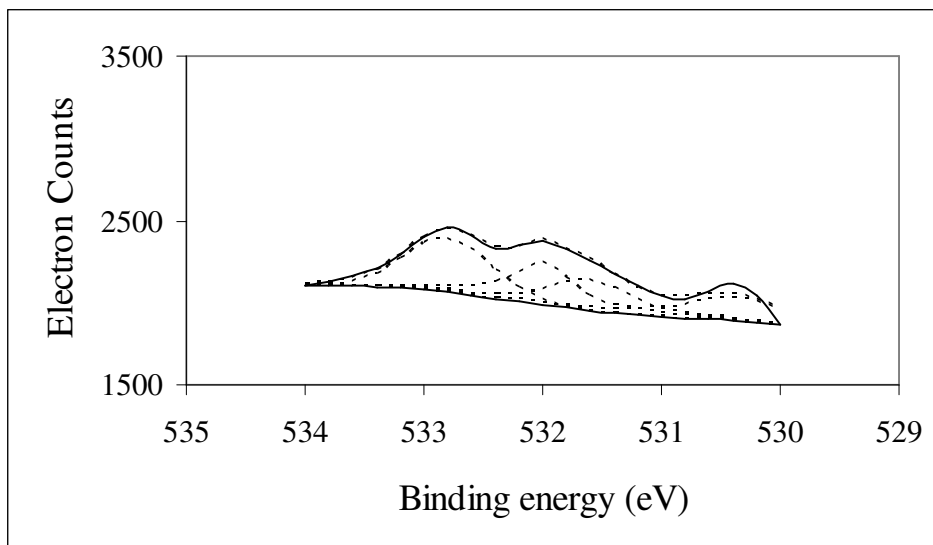


Figure 4.9 High resolution spectrum of oxygen (O_{1s}) of untreated carbon black (UCB)

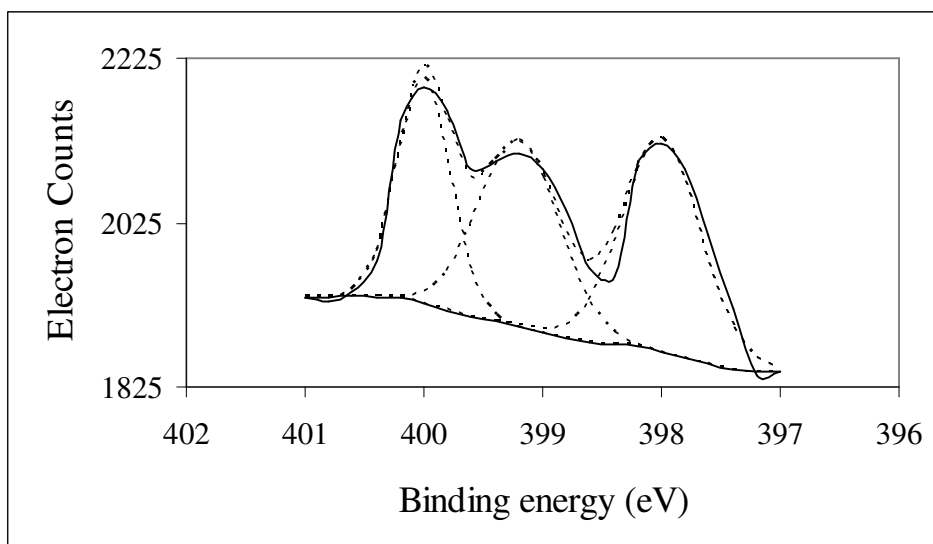


Figure 4.10 High resolution spectrum of nitrogen (N_{1s}) of untreated carbon black (UCB)

O_{1s} spectra of 1 wt. % APS solution treated carbon black and 1 wt. % formamide solution treated carbon black are fitted to two peaks (Figures 4.11 and 4.12): a peak for C=O type oxygen at 531.6 eV and a peak for C-O type oxygen (C-OH, C-O-C) at 532.8 eV. Besides, O_{1s} spectrum of 2 wt. % formamide solution treated carbon black is fitted to two peaks (Figure 4.13): a peak for C=O type oxygen at 531.3 eV and a peak for C-O type oxygen at 532.5 eV. Likewise, O_{1s} spectrum of 3 wt. % formamide solution treated carbon black is fitted to two peaks (Figure 4.14): a peak for C=O type oxygen at 531.2 eV and a peak for oxygen contaminated on carbon black at 532.2 eV. In general, O_{1s} spectra of all treated carbon black systems, APS1-CB, FA1-CB, FA2-CB and FA3-CB, are similar to each other.

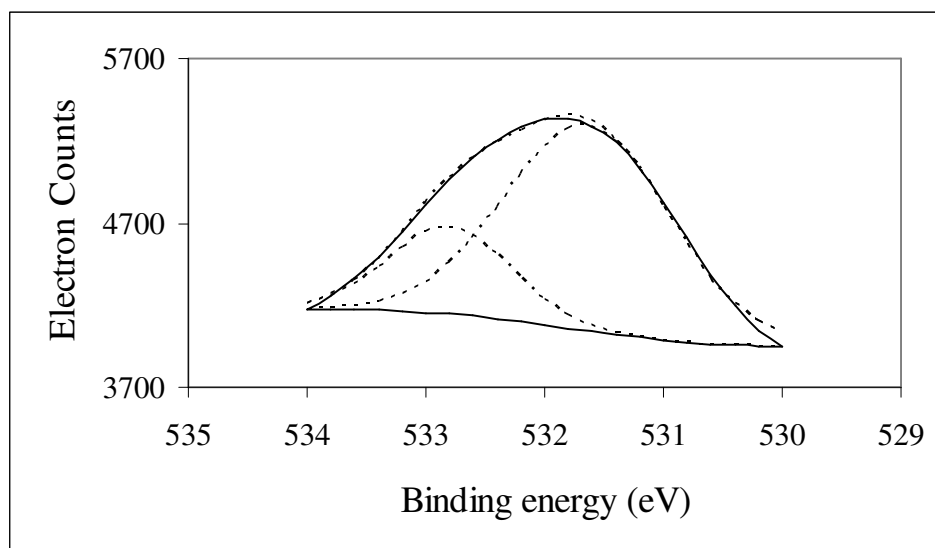


Figure 4.11 High resolution spectrum of oxygen (O_{1s}) of 1 wt. % APS solution treated carbon black (APS1-CB)

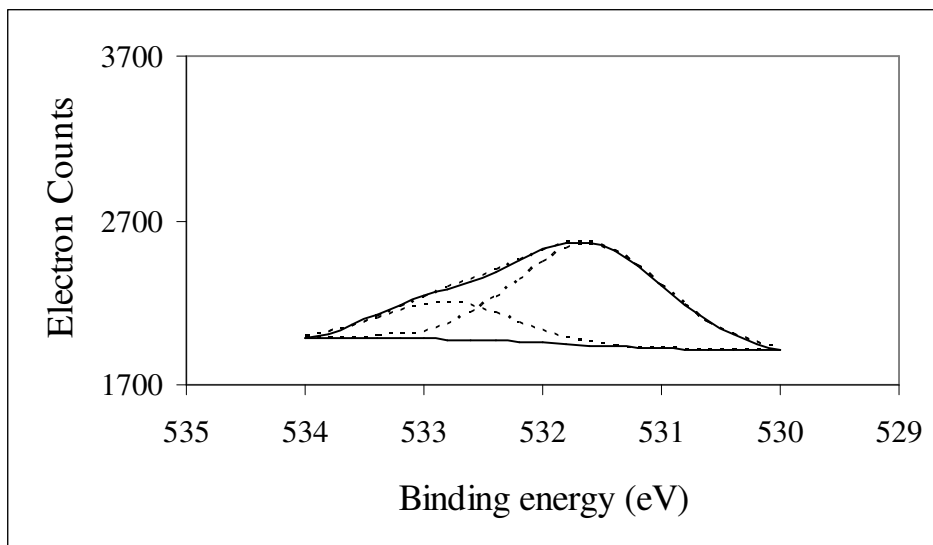


Figure 4.12 High resolution spectrum of oxygen (O_{1s}) of 1 wt. % formamide solution treated carbon black (FA1-CB)

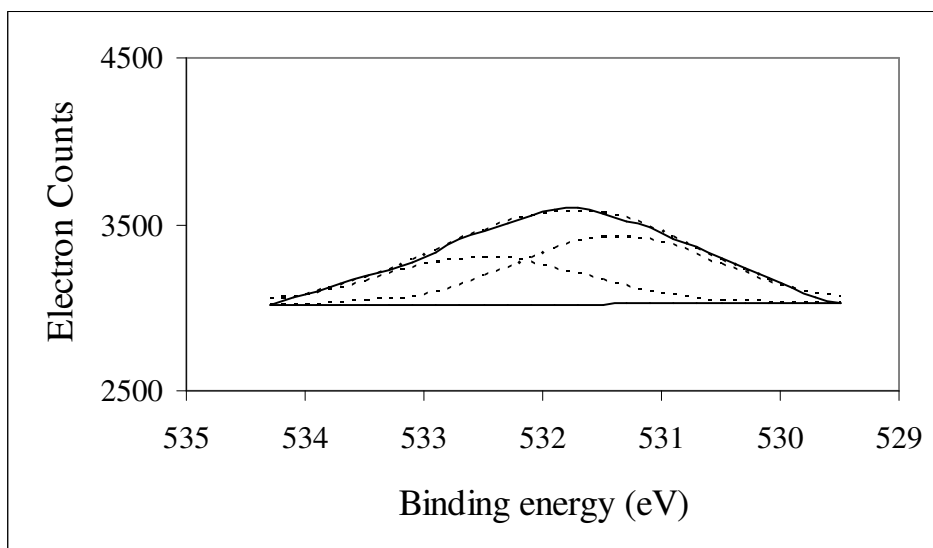


Figure 4.13 High resolution spectrum of oxygen (O_{1s}) of 2 wt. % formamide solution treated carbon black (FA2-CB)

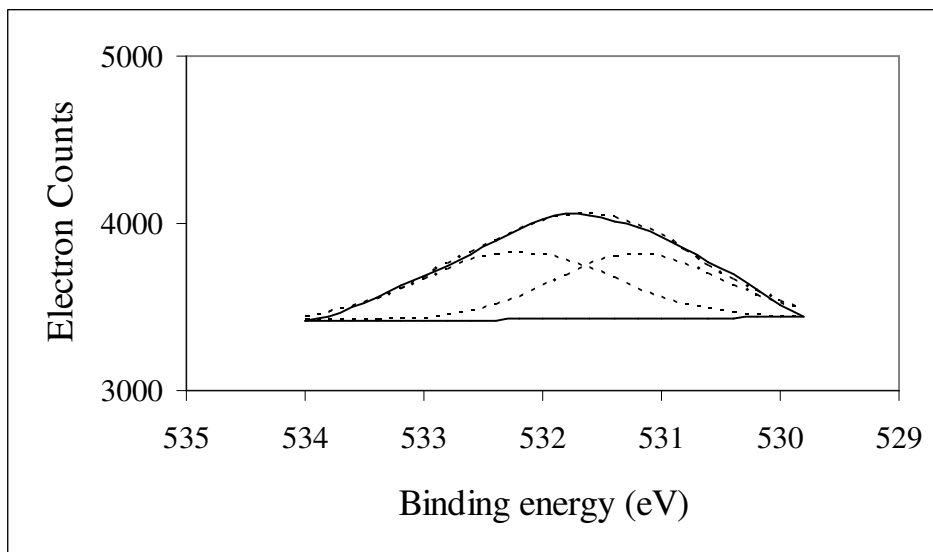


Figure 4.14 High resolution spectrum of oxygen (O_{1s}) of 3 wt. % formamide solution treated carbon black (FA3-CB)

Bulk structure of carbon black consists of highly conductive graphene layers [19] and the regular structure of these layers disappears at the surface of carbon black, resulting in active carbon sites, known as dangling bonds, and potential centers for possible chemical reaction, e.g. oxidation [133]. Hence, carbon black may have a large amount of these active carbon sites owing to its high surface area. High resolution spectra of oxygen (O_{1s}) of APS1-CB and FA1-CB, FA2-CB and FA3-CB reveal the same result that there is an increase in the intensity of peak for C=O type of oxygen (Figures 4.9-4.14) due to the oxidation of the active carbon sites during surface treatment of carbon black.

N_{1s} spectrum of APS1-CB is fitted to three peaks (Figure 4.15): a peak for -N type nitrogen at 397.7 eV, a peak for $-NH_2$ type nitrogen at 399.3 eV and a peak for $H_3N^+CHR_2COO^-$ type nitrogen at 400.9 eV. N_{1s} spectrum of FA1-CB is fitted to three

peaks (Figure 4.16): a peak for adsorbed nitrogen at 397 eV, a peak for -NH_3 type nitrogen at 398.6 eV and a peak for nitrogen (N-H or N-O) at 400.2 eV. Likewise, N_{1s} spectrum FA2-CB is fitted to three peaks (Figure 4.17): a peak for nitrogen of nitride at 397.7 eV, a peak for -NH_3 type nitrogen at 398.6 eV and a peak for nitrogen (N-H or N-O) at 400.2 eV. Besides, N_{1s} spectrum FA3-CB is fitted to four peaks (Figure 4.18): a peak for nitrogen atom bonded to N_2 at 396.5 eV, a peak for nitrogen of nitride at 397.7 eV, a peak for -NH_3 type nitrogen at 398.6 eV and a peak for NH_2 type nitrogen at 399.3 eV. Non-carbon atoms and carbon atoms aside from graphitic structure on carbon black surface affect electrical property of the conductive filler. Non-graphitic structures on the carbon black surface prevent current conduction by direct contact process [19]. Surface carboxyl groups create insulating oxide layer among carbon black particles. As a result of this, electrical resistivity of carbon black increases with an increase in surface carboxyl groups [18]. Although APS1-CB, FA1-CB, FA2-CB and FA3-CB possess larger amount of surface carboxyl groups when compared with untreated carbon black (Figures 4.11-4.14), treated carbon black improves electrical conductivity of composites much more than untreated carbon black does. The reason for this improvement is amine functional groups observed on treated carbon black surfaces [17, 20]. Amine type of functional group of APS and amide type of functional group of formamide react with carboxyl group of carbon black to obtain salt of $\text{R-NH}_3^+\text{-COO}^-$, where nitrogen atom is in quaternary structure (Figure 4.19) [134]. N_{1s} spectra of APS1-CB, FA1-CB, FA2-CB and FA3-CB confirm this reaction that there is a peak for $\text{H}_3\text{N}^+\text{CHRCOO}^-$ type nitrogen at 400.9 eV (Figure 4.15) and a peak for -NH_3^+ type nitrogen at 398.6 eV (Figures 4.16-4.18), respectively. Quaternary nitrogen, formed during surface treatment, is crucial in terms of doping mechanism, since nitrogen as n-type of dopant atom increases the electrical conductivity of carbon black by increasing the number of charge carriers [17, 20, 78].

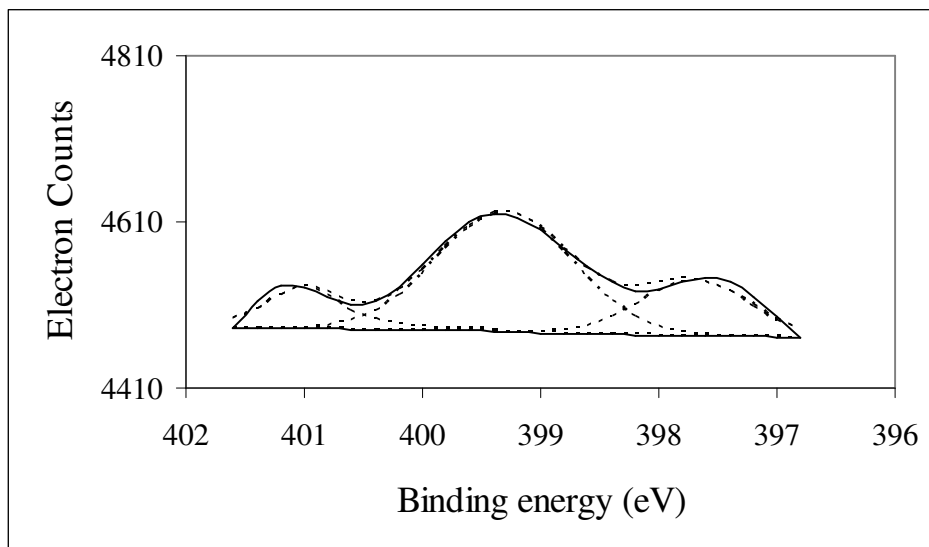


Figure 4.15 High resolution spectrum of nitrogen (N_{1s}) of 1 wt. % APS solution treated carbon black (APS1-CB)

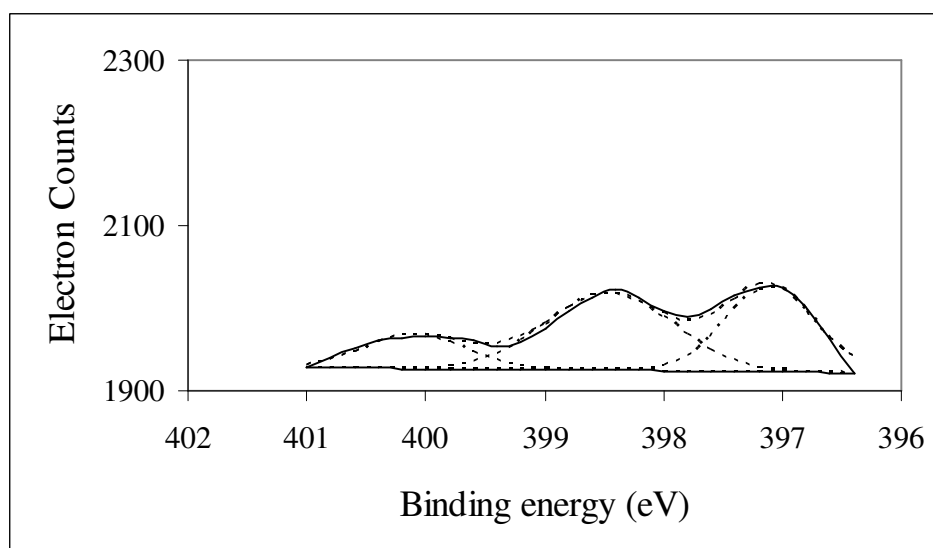


Figure 4.16 High resolution spectrum of nitrogen (N_{1s}) of 1 wt. % formamide solution treated carbon black (FA1-CB)

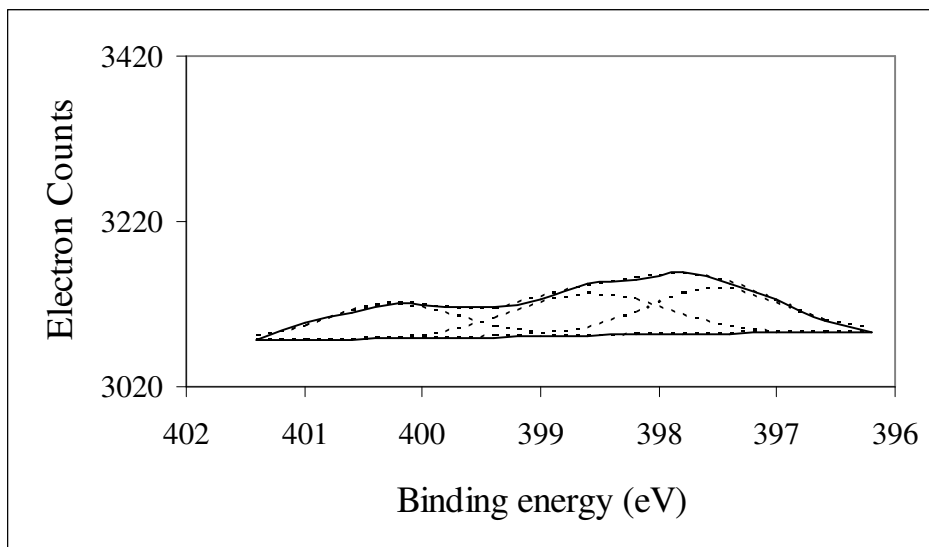


Figure 4.17 High resolution spectrum of nitrogen (N_{1s}) of 2 wt. % formamide solution treated carbon black (FA2-CB)

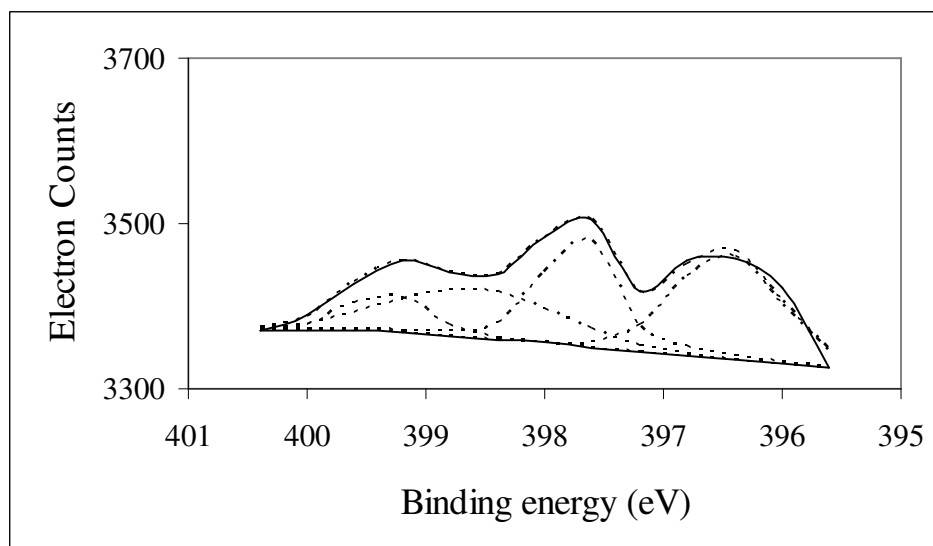


Figure 4.18 High resolution spectrum of nitrogen (N_{1s}) of 3 wt. % formamide solution treated carbon black (FA3-CB)

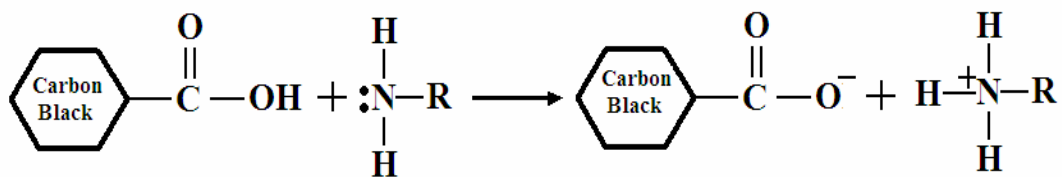


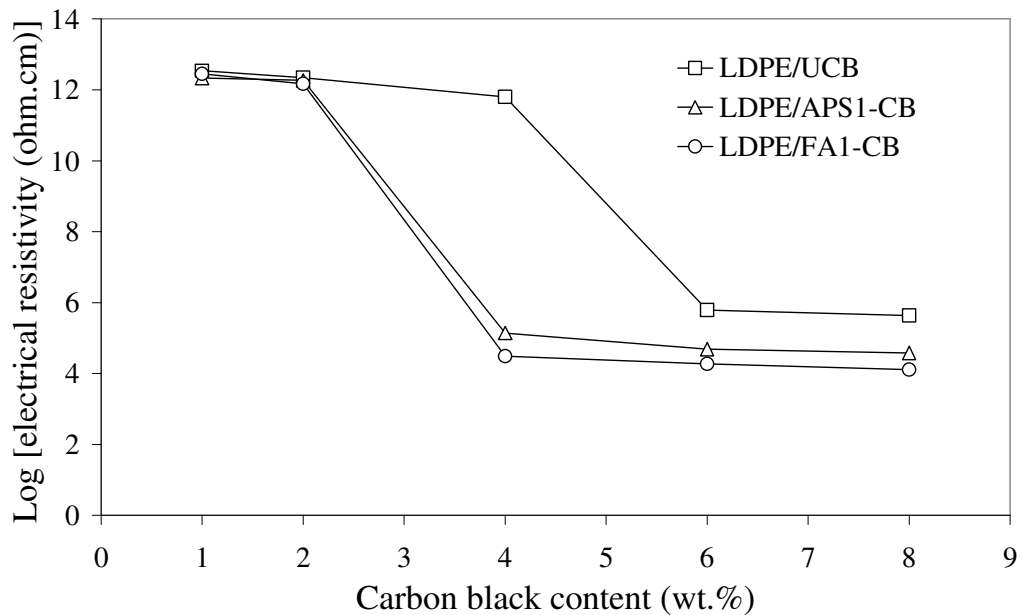
Figure 4.19 Doping mechanism of nitrogen atom during surface treatment of carbon black [134]

4.2.2 Effect of Surface Treatment of Filler on LDPE/Carbon Black and Nylon 6/Carbon Black

4.2.2.1 Electrical Conductivity Characterization

In the first subsection of the surface treatment study, carbon black was treated with 1 wt. % APS solution and 1 wt. % formamide solution, respectively and treated carbon black systems, APS1-CB and FA1-CB, were melt-mixed with LDPE and nylon 6, respectively. Nitrogen atoms of APS and formamide may act as dopant atoms following the reaction between nitrogen atoms of these surface modifiers and carboxyl groups of carbon black (Figure 4.19) and this doping reaction increases electrical conductivity of carbon black and its composites (Figures 4.20 (a) and 4.20 (b)). Thus, when compared to polymer/untreated CB system, lower electrical resistivity is obtained at each composition of LDPE/CB and nylon 6/CB systems, containing surface modified carbon black. In addition, APS and formamide types of surface treatments lower percolation threshold concentrations of LDPE/ carbon black and nylon 6/carbon black systems from 5 wt. % to 3 wt. % of filler content due to the improvement in electrical conductivity of treated carbon black. In the literature review, percolation threshold composition of high-density polyethylene/carbon black composite is shifted from 10 to 0.4 vol. % with APS type of surface treatment [17].

During surface treatment, at the same weight % of the surface modifiers, the number of molecules of formamide is higher than the number of molecules of APS owing to the lower molecular weight of formamide. In addition, formamide having small molecules can react with carbon black easily (Figure 4.19). When compared with APS, nitrogen atoms of formamide seem to be more effective as dopant since formamide treated carbon black improves electrical conductivity of LDPE and nylon 6 more than APS treated carbon black does (Figures 4.20 (a) and 4.20 (b)).



(a)

Figure 4.20 The electrical resistivity values of (a) LDPE based composites

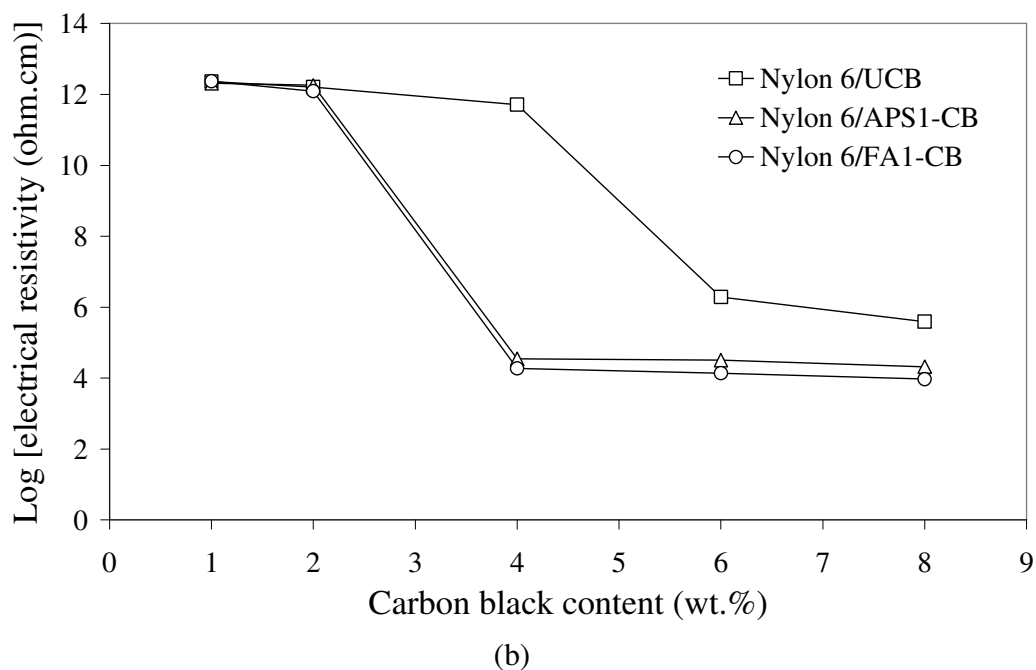


Figure 4.20 (Cont'd) The electrical resistivity values of (b) nylon 6 based composites

4.2.2.2 Surface Energy Analysis

According to the results of the surface energy analyses (Table 4.3), untreated carbon black has a lower surface energy compared to APS and formamide treated carbon black. With chemical treatment, surface chemistry of carbon black is altered by adding polar groups on the surface of conductive filler. Total surface energy, γ_s^{TOT} , of treated carbon black increases with a parallel increase in acid/base component of surface energy, γ_s^{AB} , and this increase may be an evidence for chemical modification of carbon black surfaces in addition to ESCA results. According to surface energy analyses, base component, γ_s^{B} , of total surface energy increases with surface modifications, which may be a result of added amide groups to carbon black surface (Table 4.3). In addition, acid component, γ_s^{A} , of total surface energy of treated

carbon black is higher with respect to untreated one owing to NH_3^+ structure formed following the reaction between surface modifiers and carbon black (Figure 4.19), which is an evidence for quaternary nitrogen structure on the surface of treated carbon black. On the other hand, the higher intensity of the peak for C=O type of oxygen for modified carbon black when compared with that of the untreated one (Figures 4.9 and 4.11-4.14) contributes to acid/base component of total surface energy of modified carbon black. Additionally, the London dispersive component, γ_s^{LW} , of modified carbon black particles increases, which may result from an increase in effective surface area since the particle size and effective surface area determine the London dispersive component [129, 136].

Table 4.3 Surface energy components of carbon black, (mJ/m^2)

Specimen	γ_s^{TOT}	γ_s^{LW}	γ_s^{AB}	γ_s^{A}	γ_s^{B}
UCB	42.46	35.17	7.29	1.07	12.45
APS1-CB	50.05	38.73	11.32	1.31	24.49
FA1-CB	54.79	40.41	14.38	1.96	26.38

4.2.2.3 X-Ray Diffraction Analysis

The effect of surface treatment on the structural properties of carbon black can be analyzed by x-ray diffraction, whose patterns are given in Figures A.1 and A.2. According to ESCA and surface energy analyses, 1 wt. % APS and formamide solutions change the surface chemistry of carbon black. One of the critical points in surface modification is to alter the chemical structure of the surface in order to obtain desired property without sacrificing the bulk properties of the materials. Carbon

black is composed of graphene layers, which are held together with weak van der Waals forces [4], and interlayer spacing between these layers (d_{002}) does not change significantly with the treatment due to the low concentration of APS and formamide solutions. Also, there is not a distinctive effect of chemical treatment on crystalline size along the c-axis (L_c) of carbon black (Table 4.4). As a result, the chemical treatment does not significantly change the bulk structure of carbon black.

Table 4.4 Structural properties of untreated, APS treated and formamide treated carbon black (CB) in nylon 6 and LDPE matrices

Material	2θ	B	d_{002} (Å)	L_c (Å)
2/98 (wt/wt) UCB/Nylon 6	23.11	5.31	3.848	0.264
2/98 (wt/wt) APS1-CB/Nylon 6	20.83	5.52	4.264	0.253
2/98 (wt/wt) FA1-CB/Nylon 6	21.17	5.5	4.197	0.254
2/98 (wt/wt) UCB/LDPE	21.38	0.65	4.156	2.148
2/98 (wt/wt) APS1-CB/LDPE	21.25	0.72	4.181	1.939
2/98 (wt/wt) FA1-CB/LDPE	21.27	0.61	4.177	2.289

4.2.2.4 Mechanical Property Characterization

Besides x-ray diffraction (XRD) analysis, tensile test results can be utilized to evaluate structural changes of the bulk material. Table 4.5 shows the tensile properties of the composites containing untreated and treated carbon black. Both tensile strength and modulus remain almost constant with APS or formamide treatment for both LDPE/CB and nylon 6/CB systems. As a result, it can be said that

both APS and formamide treatments do not significantly affect the bulk properties of these composites.

Table 4.5 Tensile properties of composites containing untreated and treated carbon black (CB) with (\pm) standard deviations

Material	Tensile Strength (MPa)	Tensile Modulus (MPa)
2/98 (wt/wt) UCB/Nylon 6	43.11 \pm 1.98	1277 \pm 65
2/98 (wt/wt) APS1-CB/Nylon 6	43.79 \pm 0.99	1483 \pm 46
2/98 (wt/wt) FA1-CB/Nylon 6	46.48 \pm 2.12	1485 \pm 95
2/98 (wt/wt) UCB/LDPE	24.68 \pm 3.66	272 \pm 29
2/98 (wt/wt) APS1-CB/LDPE	25.05 \pm 1.70	290 \pm 27
2/98 (wt/wt) FA1-CB/LDPE	27.42 \pm 2.47	273 \pm 8

4.2.3 Effect of Surface Treatment of Filler on PET/Carbon black (EMI shielding and Dielectric Material Applications of Conductive Polymer Composites)

EMI shielding effectiveness and dielectric property of conductive polymer composites depend on electrical conductivity of composite constituents. Hence, with surface treatment of carbon black, not only electrical conductivity, but also EMI shielding effectiveness and dielectric property of polymer composites can be improved. Furthermore, surface treatment may enhance application potential of conductive polymer composites as EMI shielding and dielectric material.

4.2.3.1 Electrical Conductivity Characterization

Due to the advantage of formamide as doping agent compared to APS, only formamide was selected as surface modifier of carbon black in the second subsection of the surface treatment study. In the first subsection, 1 wt. % formamide solution was applied to carbon black. In this part, three different formamide concentrations, 1, 2 and 3 wt. %, were used to modify the surface chemistry of carbon black. In addition, treated carbon black systems, FA1-CB, FA2-CB and FA3-CB, were compounded only with PET rather than LDPE and nylon 6 since PET/UCB system provides higher electrical conductivity than those of LDPE/UCB and nylon 6/UCB systems at the same composition (Figure 4.21).

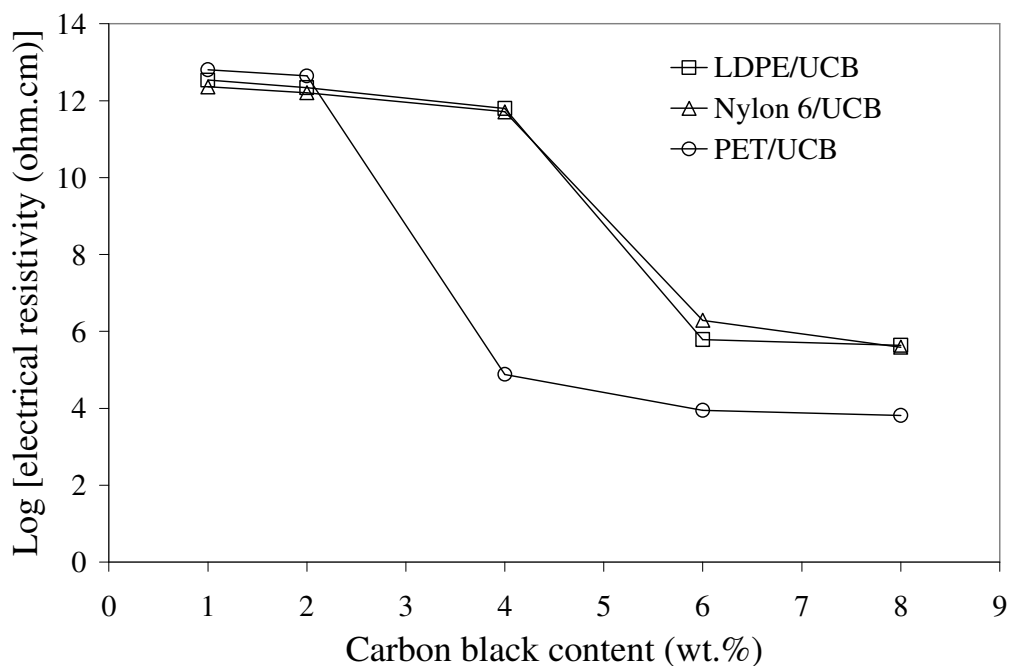


Figure 4.21 Comparison of the electrical resistivity values of LDPE, nylon 6 and PET based composites containing untreated carbon black

Treatments of formamide solutions with three different concentrations seem to be efficient in terms of their doping effects on electrical conductivity of carbon black since FA1-CB, FA2-CB and FA3-CB enhance electrical conductivity of PET composites more than UCB does (Figure 4.22). Formamide treatments reduce percolation threshold concentration from 3 to 1.5 wt. % of carbon black composition. In addition, lower electrical resistivity was obtained at each composition of PET composites containing treated carbon black when compared with the composites containing untreated carbon black.

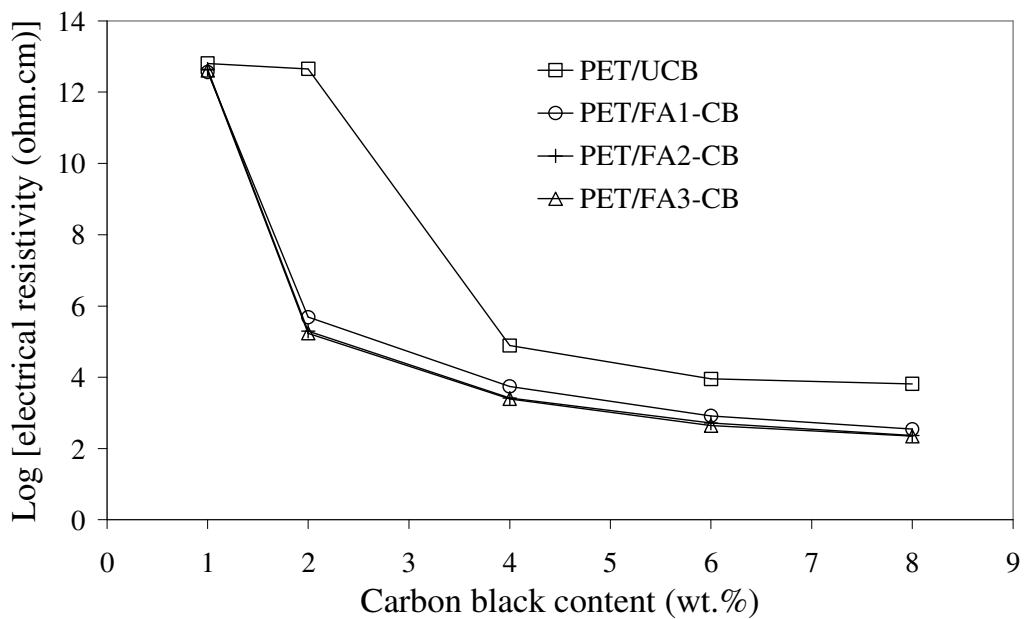


Figure 4.22 The electrical resistivity values of PET based composites

Electrical conductivities of PET/FA2-CB and PET/FA3-CB are higher than the electrical conductivity of FA1-CB/PET system. Besides, the change in formamide solution concentration from 2 to 3 wt. % leads to a small improvement in electrical conductivity of PET composites, which is difficult to figure out from the electrical resistivity graph in logarithmic scale (Figure 4.22). In both FA2-CB and FA3-CB filled PET composites, the resistivity levels off at around 200 ohm.cm for 8 wt. % carbon black content.

4.2.3.2 Microwave Property Characterization

Microwave properties of composites are directly proportional to electrical conductivity, and PET based composites provide higher electrical conductivity when compared with LDPE and nylon 6 based systems. Hence, only PET based composites were characterized in terms of microwave properties since EMI shielding and dielectric material applications require high electrical conductivity. Meanwhile, microwave properties of composites, including 4, 6 and 8 wt. % UCB, FA1-CB, FA2-CB and FA3-CB, respectively, were measured since these compositions exceed percolation threshold content among the composites studied (Figure 4.22).

4.2.3.2.1 EMI Shielding Effectiveness Analysis

Insertion loss values were used to determine EMI shielding effectiveness. Besides insertion loss, absorption loss and return loss measurements were performed. It is seen from Figure 4.23 that absorption loss changes between 0 and 4 dB for the different contents of UCB and FA1-CB particles which are incorporated to PET. Absorption loss behavior shows a similar trend with electrical conductivity of the shielding material in a way that absorption loss of composites increases with increasing filler content [22, 115]. Except for composite containing 8 wt. % FA1-CB, absorption loss is improved with increasing carbon black composition in the whole X-band range (Figure 4.23). In addition, absorption loss values approach to

each other at frequency close to 12 GHz. This implies that filling effect diminishes with increasing frequency of incident wave. Absorption loss of composite including 4 wt. % UCB is low compared to all other composites. Low conductivity value of this composite may be responsible for this result (Figure 4.22). Additionally, the dimensions of test samples are held to be the same since absorption loss depends on the thickness of the shielding material [22, 115]. Composites containing 8 wt. % UCB, FA1-CB, FA2-CB and FA3-CB have high electrical conductivity and may exhibit metallic character, since these composites may function mainly by reflection rather than absorption mechanism due to the free electrons in them [115]. Therefore, absorption loss values of all PET composites, with 8 wt. % carbon black, do not change significantly, which means that surface treatment of carbon black seems to be ineffective in terms of its doping effect on absorption loss of composites (Figure 4.24).

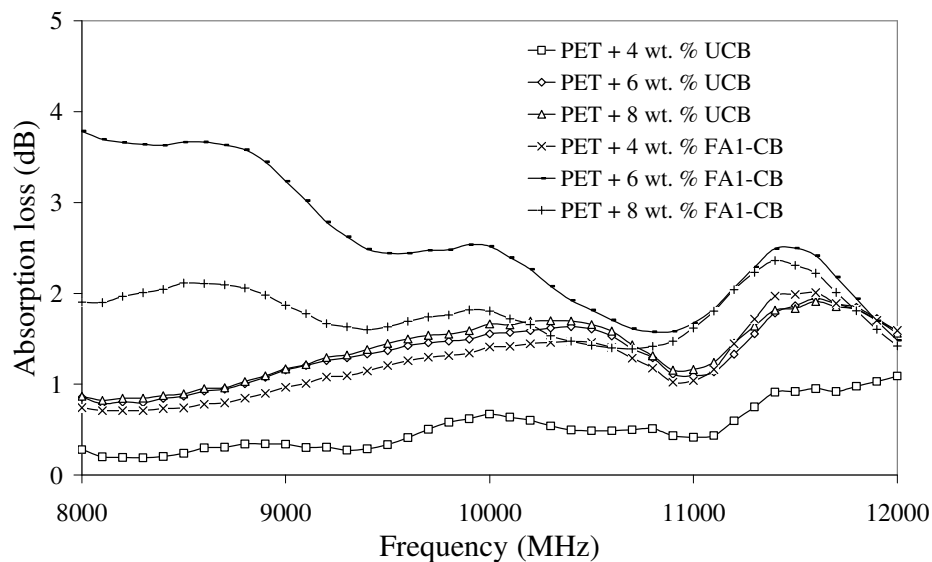


Figure 4.23 Variation of absorption loss of PET/UCB and PET/FA1-CB systems in X-band range

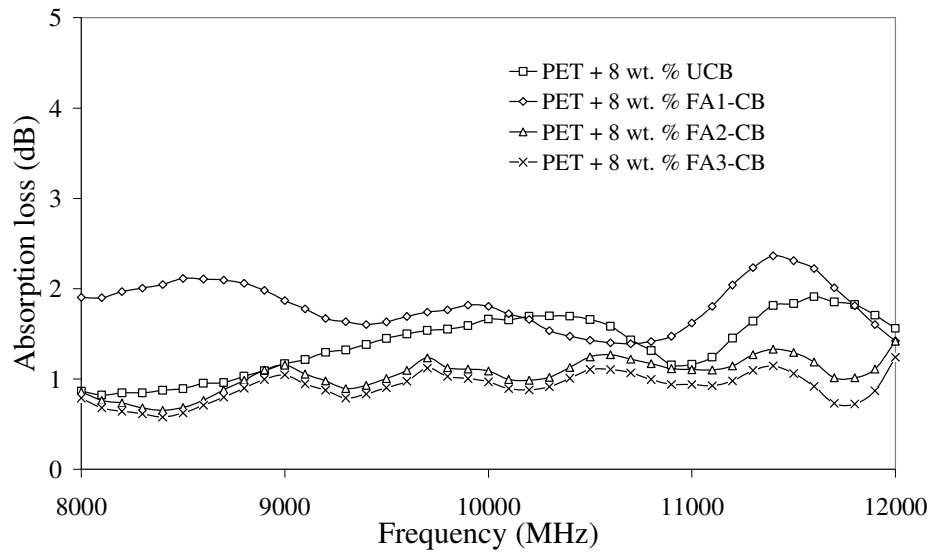


Figure 4.24 Variation of absorption loss of composites containing 8 wt. % UCB, FA1-CB, FA2-CB and FA3-CB, respectively, in X-band range

Return loss also has a direct relation with electrical conductivity of the shielding material. As electrical conductivity of the shielding material increases, reflection mechanism should be more effective. That is, return loss should diminish with increasing filler content [22, 24, 25, 115]. Figure 4.25 exhibits the effects of return loss for the different compositions of UCB and FA1-CB particles compounded with PET. As expected, the composite filled with 4 wt. % UCB has higher return loss value than the composites having 6 and 8 wt. % UCB. There is a small difference between return loss values of composites containing 6 and 8 wt. % UCB as they have similar electrical conductivity values (Figures 4.22 and 4.25). However, this trend cannot be seen by the composites filled with FA1-CB. Return loss depends not only on conductivity of composite, but also on the polymer viscosity, polarity of matrix, aspect ratio and distribution of conductive filler in matrix [24]. The uneven variation of return loss with frequency for FA1-CB/PET systems may be owing to random

distribution of carbon black in the matrix [24]. Consequently, relation of return loss with carbon black concentration in composites seems to be complicated. In other words, return loss might not change according to composite concentration variation [25, 26]. Return losses of composites including UCB and FA1-CB vary from 2 to 7 dB (Figure 4.25). Meanwhile, FA2-CB/PET and FA3-CB/PET systems exhibit lower electrical resistivity when compared with UCB/PET and FA1-CB/PET systems (Figure 4.22). Parallel to conductivity results, return loss values of PET composites having 8 wt. % carbon black decrease as formamide solution concentration changes from 1 to 2 and 3 wt. % (Figure 4.26).

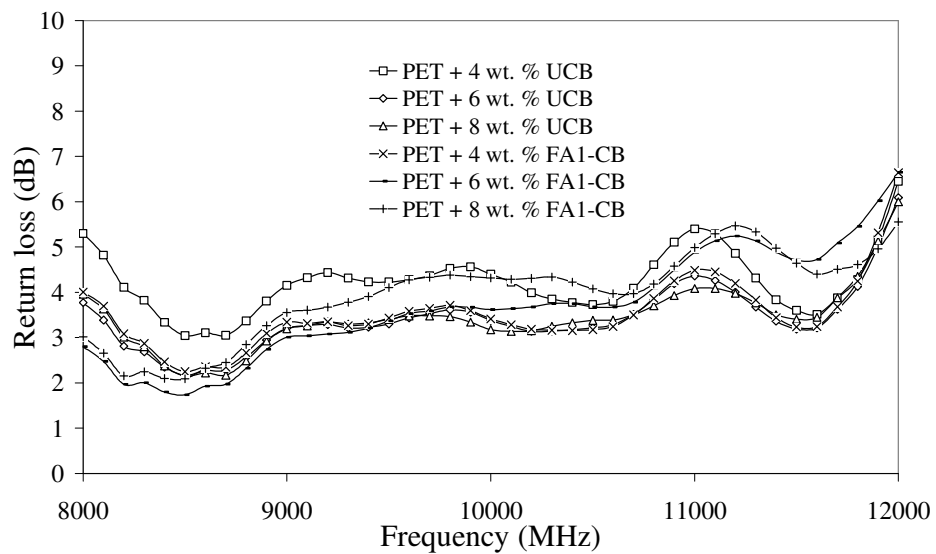


Figure 4.25 Variation of return loss of PET/UCB and PET/FA1-CB systems in X-band range

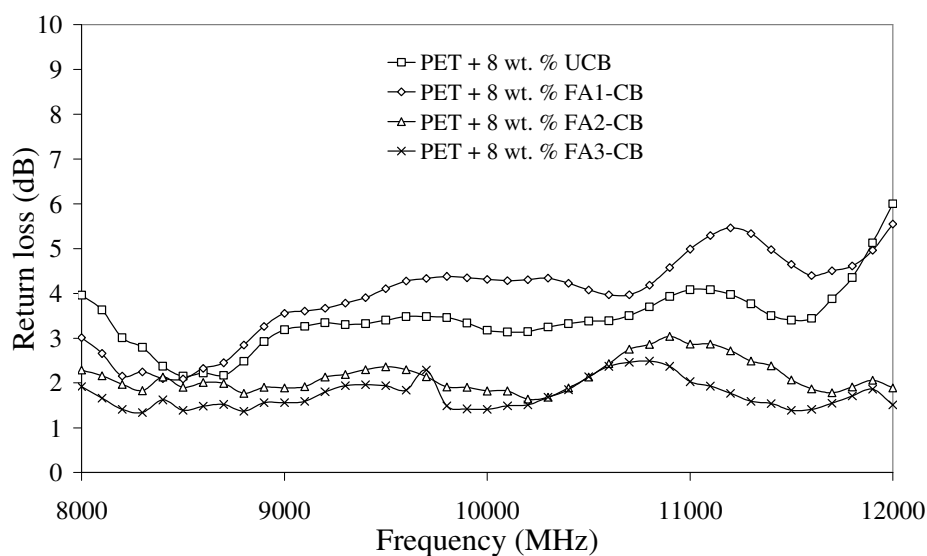


Figure 4.26 Variation of return loss of composites containing 8 wt. % UCB, FA1-CB, FA2-CB and FA3-CB, respectively, in X-band range

EMI shielding effectiveness (SE), which was obtained from insertion loss values, increases with increasing carbon black content of composites (Figure 4.27) and formamide solution concentration of surface modifier (Figures 4.28-4.30). As expected, EMI SE of composites improves with a parallel improvement in electrical conductivity (Figures 4.27-4.30). When compared with studies experimented in the literature, higher shielding effectiveness values are obtained at low conductive filler compositions [24, 25]. Especially, composites filled with 6 and 8 wt. % FA1-CB, FA2-CB and FA3-CB show higher EMI shielding effectiveness and 27 dB of EMI SE is obtained when 8 wt. % of FA3-CB was incorporated into PET (Figures 4.29 and 4.30), which reveals again the success in improving electrical conductivity of PET based composites containing formamide treated carbon black.

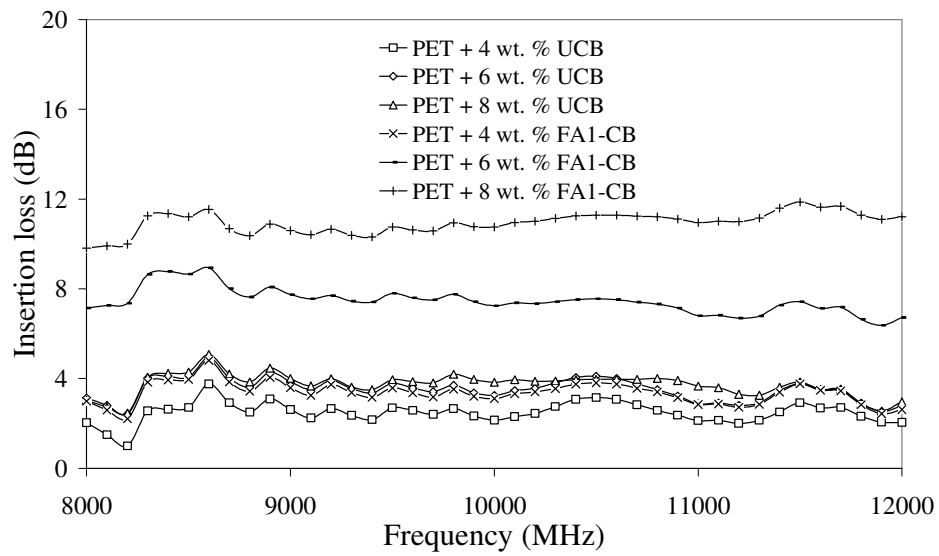


Figure 4.27 Variation of insertion loss of PET/UCB and PET/FA1-CB systems in X-band range

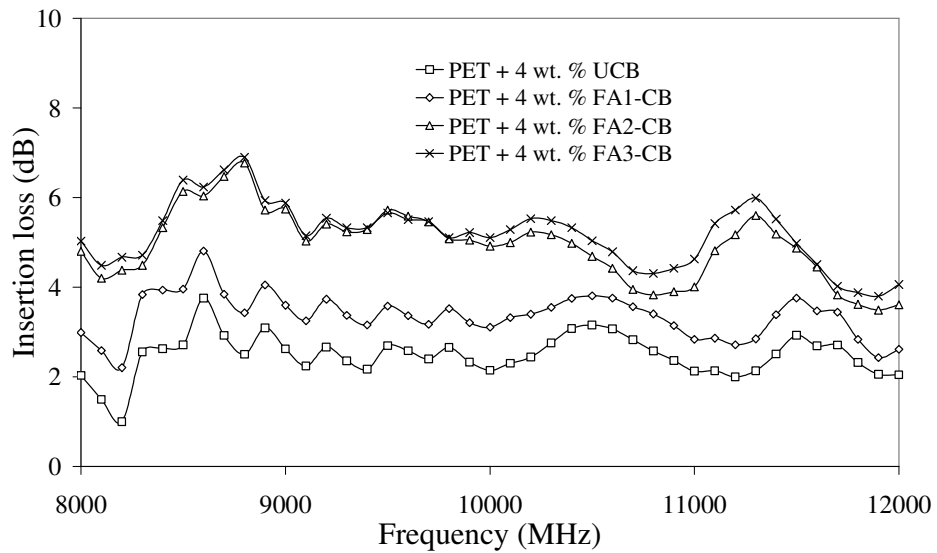


Figure 4.28 Variation of insertion loss of composites containing 4 wt. % UCB, FA1-CB, FA2-CB and FA3-CB, respectively, in X-band range

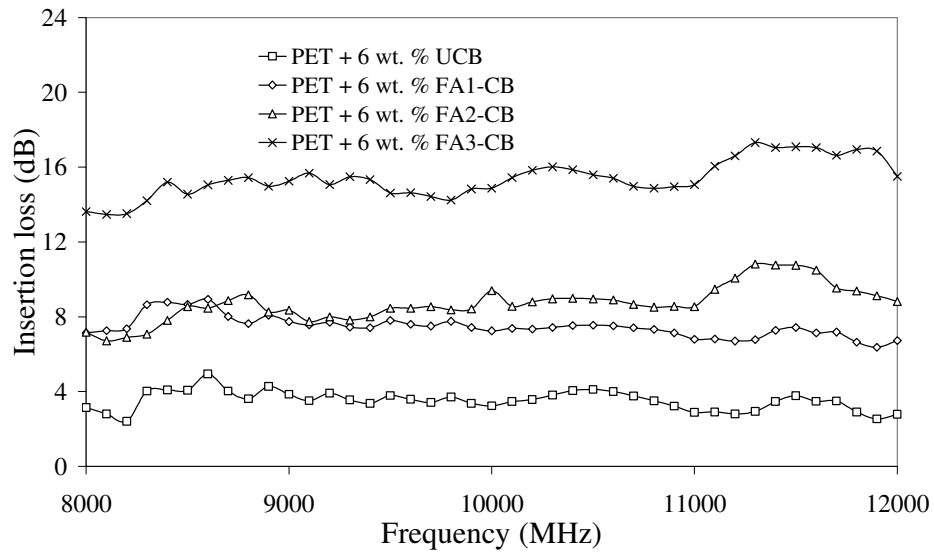


Figure 4.29 Variation of insertion loss of composites containing 6 wt. % UCB, FA1-CB, FA2-CB and FA3-CB, respectively, in X-band range

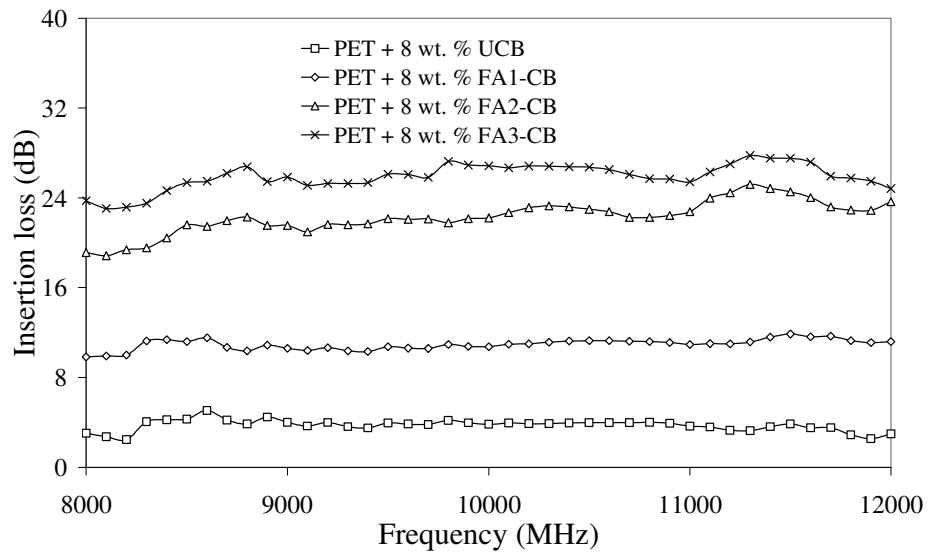


Figure 4.30 Variation of insertion loss of composites containing 8 wt. % UCB, FA1-CB, FA2-CB and FA3-CB, respectively, in X-band range

4.2.3.2.2 Dielectric Constant Measurement

Dielectric constant value depends on the number of mobile charge carriers [28] and chemical treatments were applied to carbon black to improve its electrical conductivity by increasing the number of mobile charge carriers [20]. The change in dielectric constant with the addition of both treated and untreated carbon black particles into PET at different filler compositions are shown in Figures 4.31 and 4.32. As expected, dielectric constant increases with increasing filler content from 4 to 8 wt. % and with increasing formamide solution concentration from 1 to 3 wt. %. Dielectric constant values of composites containing treated carbon black are higher than those of composites containing untreated carbon black at 8.5 and 10 GHz and composites containing FA3-CB exhibit the highest dielectric constant values at both frequencies (Figures 4.31 and 4.32). Although dielectric constant decreases exponentially with increasing frequency [33], dielectric values, obtained at 8.5 GHz frequency, are not so different from dielectric values measured at 10 GHz. Mobile charges form dipoles against incident electric field. Meanwhile, at high frequency, mobile charges do not have sufficient time to form dipoles and to absorb energy of incident electric field, which might result in low dielectric values [32]. In spite of this negative effect of microwave frequency measurement, relatively higher dielectric constant values were obtained at low carbon black compositions [35].

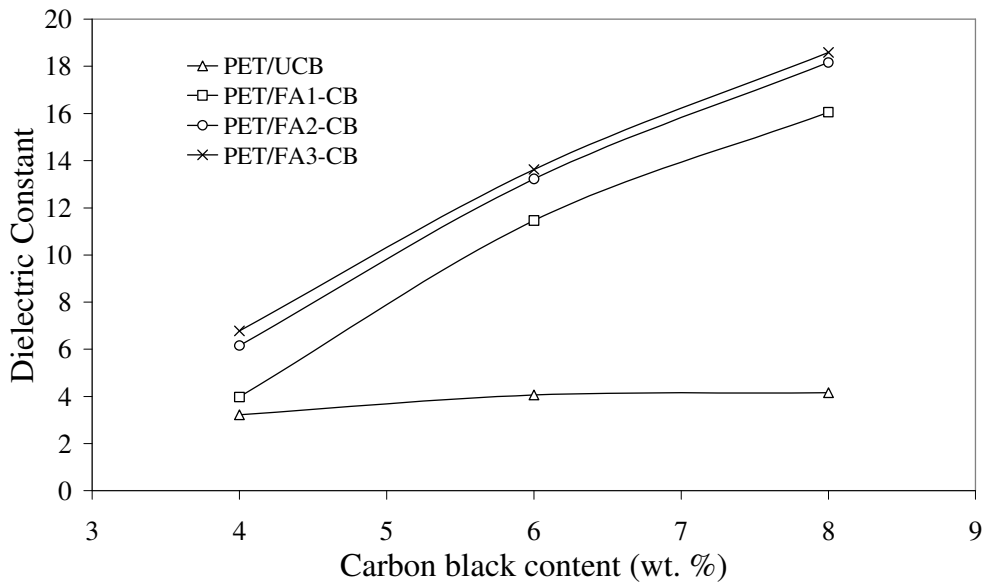


Figure 4.31 Dielectric constant values of PET based composites at 8.5 GHz

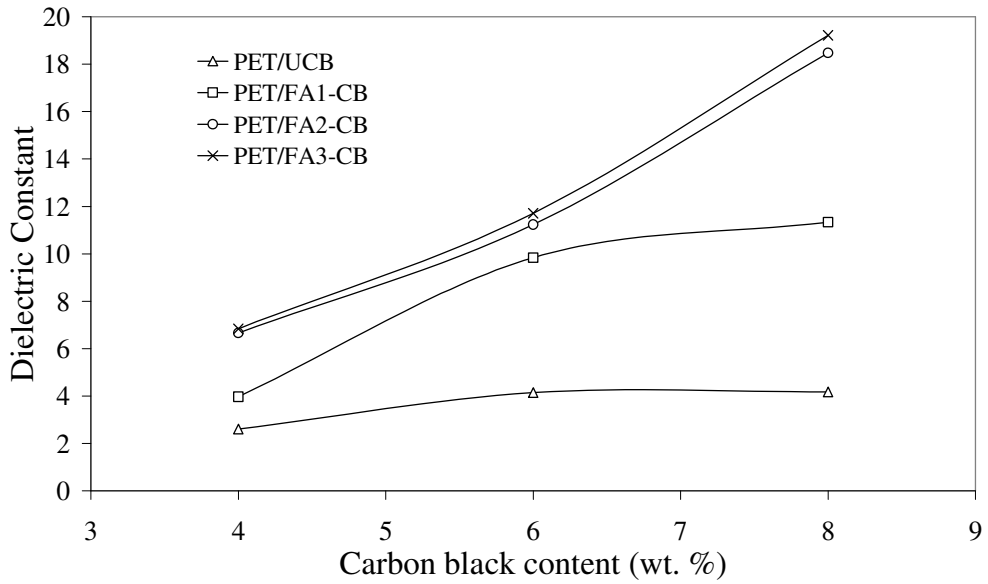


Figure 4.32 Dielectric constant values of PET based composites at 10 GHz

4.2.3.3 Morphology Analysis

Scanning electron microscopy was performed to compare the morphological differences in PET composites containing treated and untreated carbon black, respectively. In order to increase carbon black resolution in SEM micrographs, staining was applied to fractured test specimens of microwave measurements with nitric acid. SEM micrographs of the composites containing UCB and FA1-CB are not different from each other. Carbon black agglomerates can be seen in both micrographs (Figure 4.33). There is not any distinct change at submicron level in distribution and size between untreated carbon black and formamide treated carbon black. Hence, surface treatment may not significantly affect agglomerate size of carbon black and their distribution in the composites.

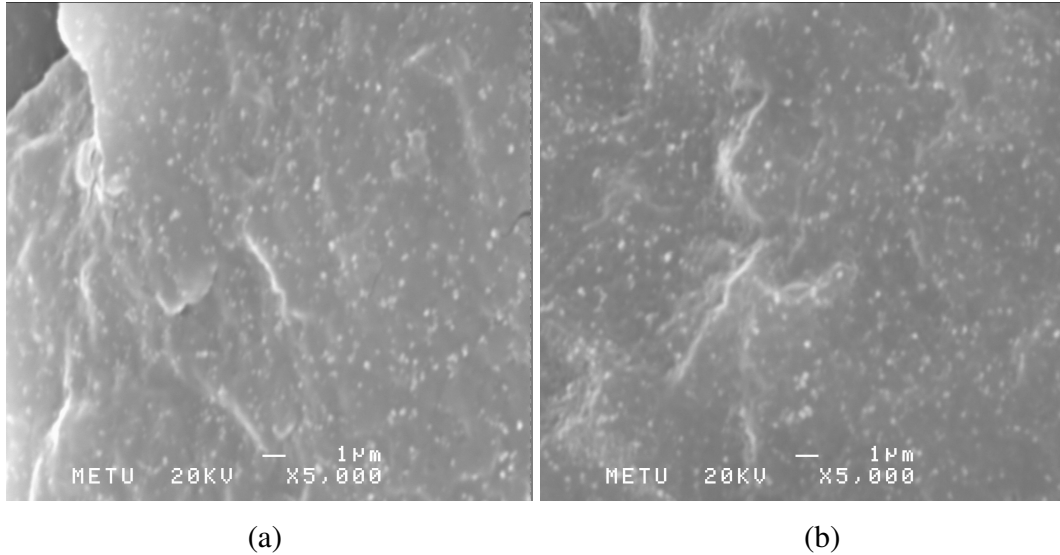


Figure 4.33 SEM micrographs of impact fractured samples of PET containing (a) 6 wt. % UCB (x5000) and (b) 6 wt. % FA1-CB (x5000)

On the other hand, PET and carbon black are compatible, and surface treatment of carbon black with formamide makes the filler more compatible with PET owing to the presence of more number of reactive groups on the surface of treated carbon black as observed in ESCA analyses (Figures 4.12 and 4.16). Thus, potential interactions between carbon black and PET upon formamide treatment can affect the electrical and microwave properties of the composites.

4.3 Effect of Grinding on PP/PET and PP/PET/CNT Systems

Another approach to increase electrical conductivity of conductive polymer composites is based on the selective localization of conductive filler in immiscible polymer blends. However, immiscible blend systems result in poor interphase adhesion and mechanical properties. By employing a type of solid-state processing technique, grinding, microstructured or nanostructured blend systems can be obtained, providing improvement in electrical conductivity and mechanical properties of conductive polymer composites composed of two immiscible phases. In this part of the thesis, the effects of grinding on electrical and mechanical properties of conventional PP/PET and PP/PET/CNT systems are discussed. The selective localization of carbon nanotubes in PP/PET systems can be determined using the results of surface energy analyses.

4.3.1 Surface Energy Analysis and Selective Localization of CNT

The surface energy components of PP, PET and carbon nanotubes are calculated using contact angle measurements at 20 °C and they are illustrated in Table 4.6.

Table 4.6 The surface energy components of PP, PET and CNT at 20 °C, (mJ/m²)

Specimen	γ_{sol}^{Tot}	γ_{sol}^{LW}	γ_{sol}^{AB}	γ_{sol}^A	γ_{sol}^B
PP	32.87	32.13	0.74	0.14	0.92
PET	36.96	29.06	7.9	4.73	3.30
CNT	46.14	35.67	10.47	2.17	12.62

Surface energy of polymer phases is effective in selective localization of filler in blend systems [105, 106]. In order to determine the selective localization of carbon nanotube particles in PP/PET blend systems, surface energy values of PP and PET at the extrusion process temperature, 260 °C, are essential and it is difficult to measure these values at this temperature with contact angle method. However, surface energies of molten PP and PET can be calculated theoretically using Equations 2.4 and 2.5. In order to observe reliability of surface energies calculated using theoretical equations, surface energies of PP and PET are also calculated for 20 °C using Equations 2.4 and 2.5 (Table 4.7).

Table 4.7 The surface energy components of PP and PET calculated using theoretical equations for 20 and 260 °C, (mJ/m²)

Specimen	γ_{sol}^{Tot}	γ_{sol}^{LW}	γ_{sol}^{AB}
PP (20 °C)	29.98	29.98	0
PET (20 °C)	34.80	27.11	7.69
PP (260 °C)	18.06	18.06	0
PET (260 °C)	20.96	16.33	4.63

Surface energies of PP and PET, measured at 20 °C with contact angle method, are quite close to the values calculated for 20 °C using theoretical equations (Tables 4.6 and 4.7). Hence, the reliability of the theoretical equations is checked and it is suitable to use surface energy values, calculated using Equations 2.4 and 2.5, to determine selective localization of nanotube particles in PP/PET systems. For this purpose, interfacial tension values, given in Table 4.8, are calculated using Equation 2.6 and utilized to calculate the wetting coefficient, W_a .

Table 4.8 The interfacial tension between PP/PET/CNT composite constituents, (mJ/m²)

γ_{PP-CNT} (260 °C)	16.24
$\gamma_{PET-CNT}$ (260 °C)	9.45
γ_{PP-PET} (260 °C)	4.72

The wetting coefficient, W_a , is calculated as 1.44 after substituting calculated interfacial energies into Equation 2.7. According to the wetting coefficient result, carbon nanotubes may prefer PET phase rather than PP phase in the blend.

4.3.2 Electrical Conductivity Characterization

Polypropylene based composite containing 1 wt. % carbon nanotubes is electrically insulating and it has an average electrical resistivity value of 10^{11} ohm.cm; whereas, PET based composite containing 1 wt. % carbon nanotubes is not electrically insulating and it has an average electrical resistivity value of 50 ohm.cm. Additionally, conventional PP/PET/CNT systems at low PET compositions illustrate

insulating resistivity values (Figure 4.34). These results support the same idea that carbon nanotubes are located at PET phase of PP/PET/CNT systems.

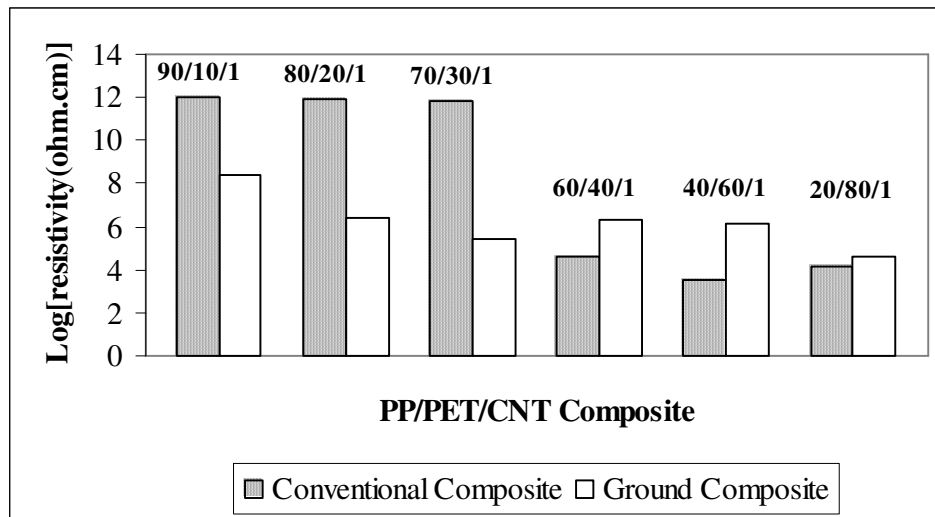


Figure 4.34 Electrical resistivity of conventional and ground PP/PET/CNT systems

Electrical conductivity of PP/PET/CNT systems strongly depends on the double percolation phenomenon [7, 136, 137]. The percolation of nanotube particles in PET phase, which is the first percolation threshold, is provided since electrical resistivity of PET based composite containing 1 wt. % carbon nanotubes is in semiconductive range. The continuity of PET phase in blend system, which is known as the second percolation, is significant on account of the formation of conductive pathways throughout the blend sample [136, 137]. Conventional composites containing 40, 60 and 80 wt. % PET are in semiconductive level. At these compositions, PET may provide the continuity in blend structure and also the second percolation. When PET

content in the blend is less than 40 wt. %, most of PET domains may disperse in PP phase and the conductive pathways throughout the blend sample cannot be formed, even if carbon nanotubes content in PET phase is above percolation threshold concentration. For the blend systems exposed to grinding, the second percolation threshold is shifted to lower PET content. Grinding is applied to decrease average domain size of phases. As the domain size decreases, probability of contact between domains of phases increases. With grinding, domain size of both PP and PET may be reduced since ground composites containing 10, 20 and 30 wt. % PET are in semiconductive level (Figure 4.34), which shows that PET domains with nanotube particles are in contact and charge transfer may be provided throughout the samples. Hence, grinding technique is successful to some extent since there is a huge difference between electrical resistivity values of conventional and ground composites up to 40 wt. % PET composition.

There is a reverse trend when PET content of composites is more than 40 wt. % (Figure 4.34). Conventional composites have lower electrical resistivity than those of ground systems at high PET compositions. The reason for this reverse trend may be the difference in domain size of composites. Starting with 40 wt. % composition, PET domains start to form the continuous structure in blend systems. As PET composition of blend increases, conductive networks are enhanced along PP/PET/CNT samples. With grinding, conductive networks may be destroyed. When PET is the continuous phase, grinding increases both the probability of contact of PET domains and the contact resistance between PET phases by decreasing the domain size.

4.3.2.1 High Temperature Processing of Ground PP/PET/CNT Systems

PP and PET phases are subjected to high compressive and shearing forces with grinding, which causes fragmentation and dispersion of micron sized domains [50]. Reduced polymer domains combine to form larger domains with a net reduction in

interfacial area during high temperature processing above melting points of polymers [50]. Compression and injection molding processes were also performed above melting temperatures of both PP and PET. Coalescence is the major drawback of high temperature processes since high temperature and long term processes enlarge the domains of phases [41, 42, 50]. Reduced domain structures of PP and PET phases might tend to coalesce during molding processes since electrical resistivity of ground composites, molded at 280 °C, is higher than that of ground composites, molded at 230 °C (Figure 4.35). Molding temperature of 280 °C, above the melting point of PET, is adequate to ruin microstructure of blends. However, the effect of high temperature processing on blend morphology should be limited, that is, reduced domain structures might not coalesce too much during molding processes since ground systems, containing less than 40 wt. % PET and molded at 280 °C, have electrical conductivity in semiconductive level (Figure 4.35).

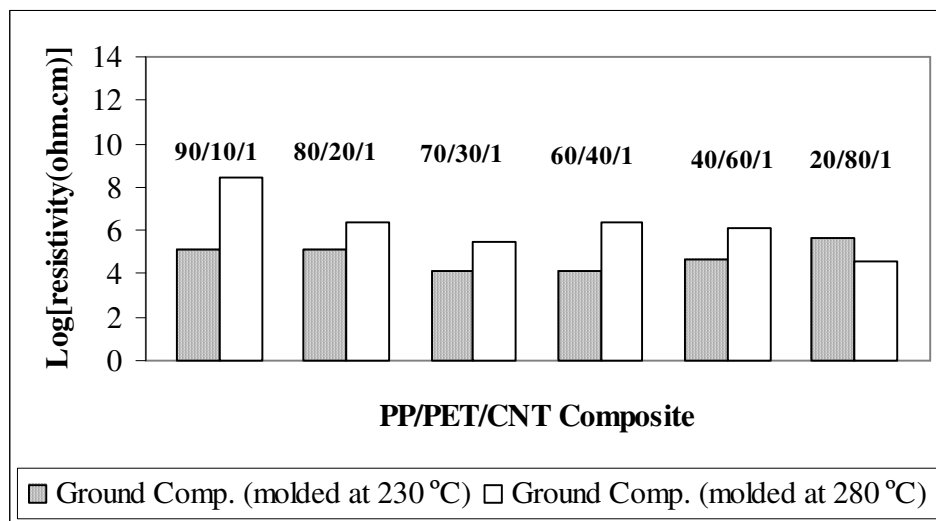


Figure 4.35 Electrical resistivity of ground PP/PET/CNT systems, prepared at 230 °C and 280 °C

4.3.2.2 Effect of Carbon Nanotubes Content on PP/PET/CNT System

An increase in carbon nanotube content of the conventional composite, containing 30 wt. % PET, does not change its electrical resistivity since carbon nanotube particles may localize selectively in PET phase of the blend and conductive PET phases do not provide the continuity at this composition of the conventional PP/PET/CNT system. On the other hand, the ground system provides the continuity at 30 wt. % PET composition and an increase in carbon nanotubes content enhances electrical conductivity of this ground composite (Figure 4.36).

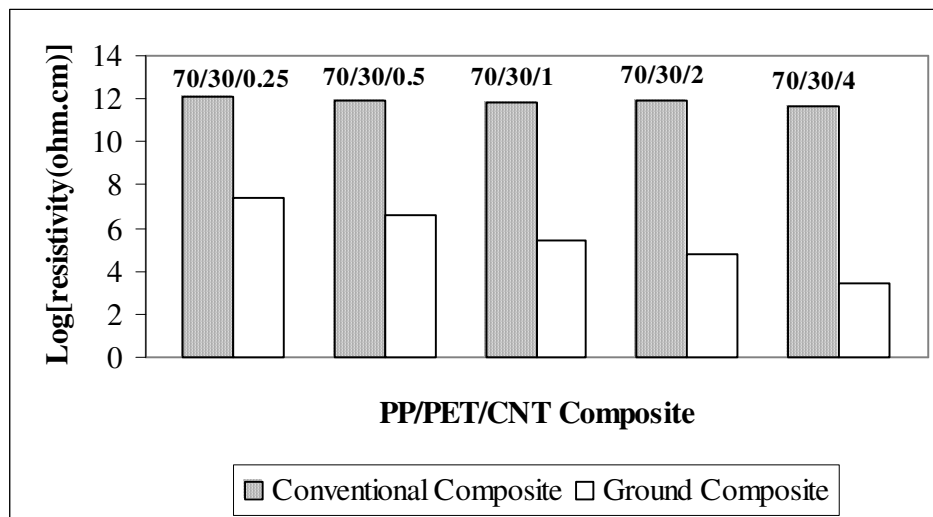


Figure 4.36 Electrical resistivity of conventional and ground PP/PET/CNT systems containing 30 wt. % PET and different amount of carbon nanotubes

4.3.3 Mechanical Property Characterization

PP/PET system, which is a physical blend, is thermodynamically immiscible. Hence, PET/PP blend system exhibits poor adhesion between phases and poor mechanical properties [138]. Reduced domain structure, attained by solid state processing, has a distinct effect on the mechanical properties of blend systems [44]. Ground blends have higher tensile strength values than conventional ones (Figure 4.37). With grinding, average domain size of PP and PET phases might be reduced, which results in enhanced tensile strength due to advanced interfacial interaction between phases [4].

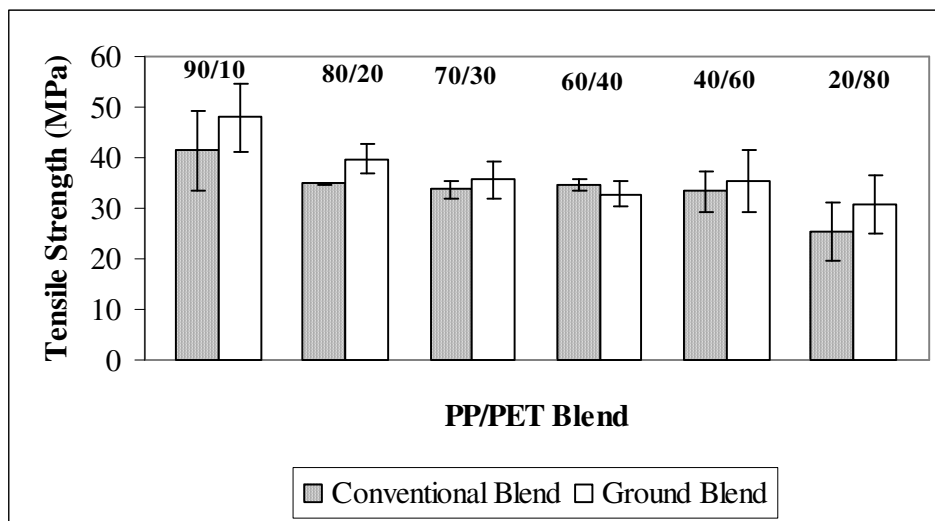


Figure 4.37 Tensile strength values of conventional and ground PP/PET systems without carbon nanotubes

Tensile strength value of neat PET is 46.3 MPa and tensile strength value of neat PP is 30.5 MPa. With increasing PET content of both blend systems, tensile strength decreases slowly (Figure 4.37). Blend systems containing less than 40 wt. % of PET have higher tensile strength values compared to neat PP, which may be due to reinforcing effect of PET phase in blend systems.

Tensile modulus values of neat PET and PP are 948 MPa and 511 MPa, respectively, and tensile modulus values of ground and conventional blend systems fluctuate between these values (Figure 4.38). They do not illustrate a distinct trend. Excluding 40 and 80 wt. % PET containing systems, ground blends have higher tensile modulus values compared to conventional blends.

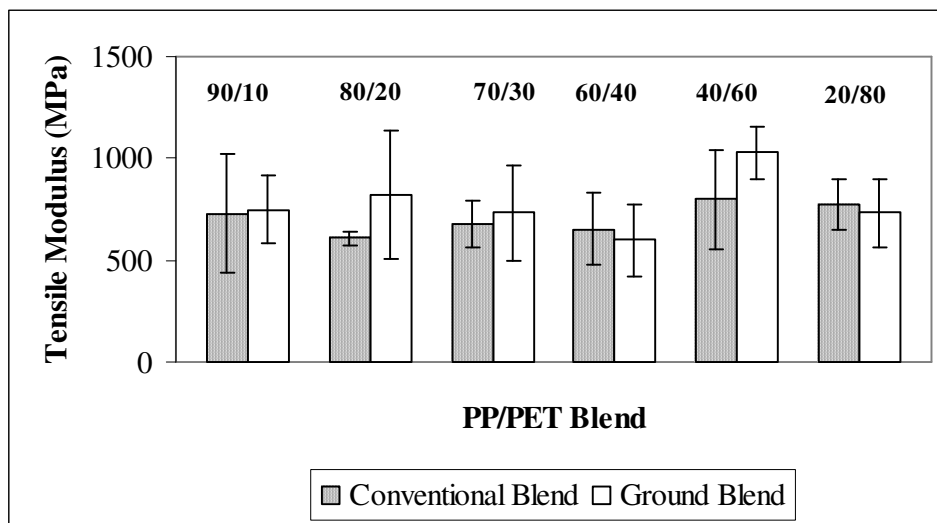


Figure 4.38 Tensile modulus values of conventional and ground PP/PET systems without carbon nanotubes

Tensile strength value of PET composite containing 1 wt. % carbon nanotubes is 21.9 MPa and tensile strength value of PP composite containing 1 wt. % carbon nanotubes is 31.5 MPa. When PET content of PP/PET/CNT systems increases, tensile strength of both ground and conventional composites diminishes slightly. As the domain size of blend phases decreases, tensile strength increases since interfacial area between phases increases and the probability of finding a large flaw, resulting stress concentration, in blend structure decreases [4]. Except for 60 wt. % PET containing system, ground composites provide higher tensile strength values when compared with conventional composites (Figure 4.39).

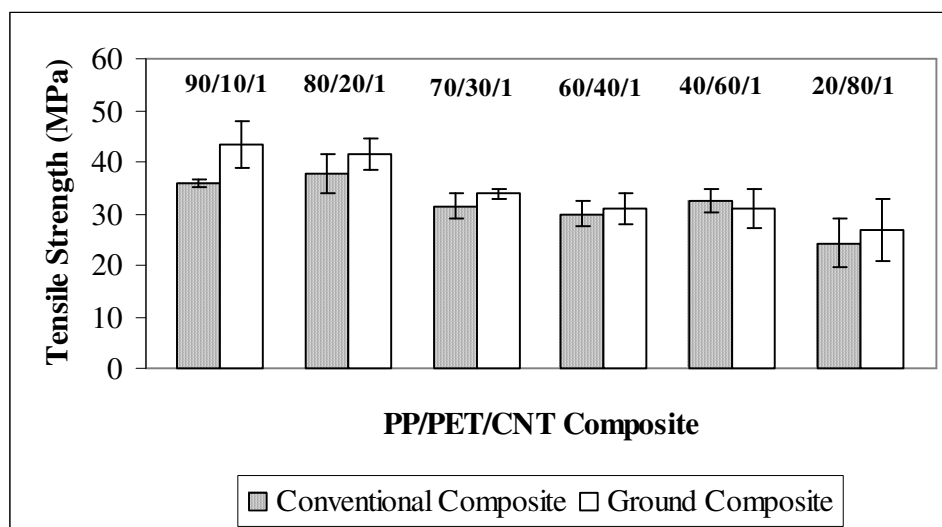


Figure 4.39 Tensile strength values of conventional and ground PP/PET/CNT systems

When PET content is 10 wt. %, tensile strength of ground PP/PET/CNT system is at 43.3 MPa, which is higher than that of PP composite including 1 wt. % nanotube particles. Reinforcing effect of PET phase may cause to this improvement in tensile strength. Besides, tensile strength value of conventional PP/PET/CNT system with 10 wt. % PET is 35.9 MPa. There is a distinct difference in tensile strength value at this composition when compared with other PP/PET/CNT systems. On the other hand, tensile strength values of blend systems decrease slightly with carbon nanotubes contribution (Figures 4.37 and 4.39).

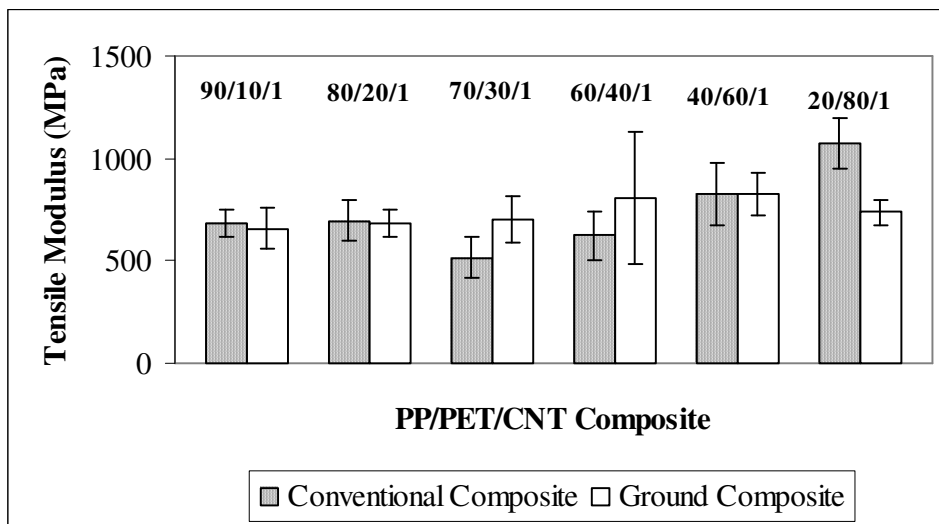


Figure 4.40 Tensile modulus values of conventional and ground PP/PET/CNT systems

Tensile modulus values of PET composite containing 1 wt. % carbon nanotubes and PP composite containing 1 wt. % carbon nanotubes are 910 MPa and 749 MPa,

respectively. Tensile modulus values of both conventional and ground composites fluctuate as PET content of PP/PET/CNT changes from 10 to 80 wt. % (Figure 4.40). Furthermore, carbon nanotubes do not have a distinctive effect on tensile modulus values of both composite systems (Figures 4.38 and 4.40). When PET content is more than 30 wt. %, tensile modulus values of both blend systems start to increase.

Excluding 20 wt. % PET composition, impact strength values of conventional and ground blend systems are close to each other. Contribution of PET phase decreases impact strength of both blend systems, since this phase of PP/PET system is highly crystalline and rigid (Figure 4.41). The impact strength increases as the domain size of phases decreases, which may be the reason for explicit difference in impact strength values of conventional and ground blend systems containing 20 wt. % PET.

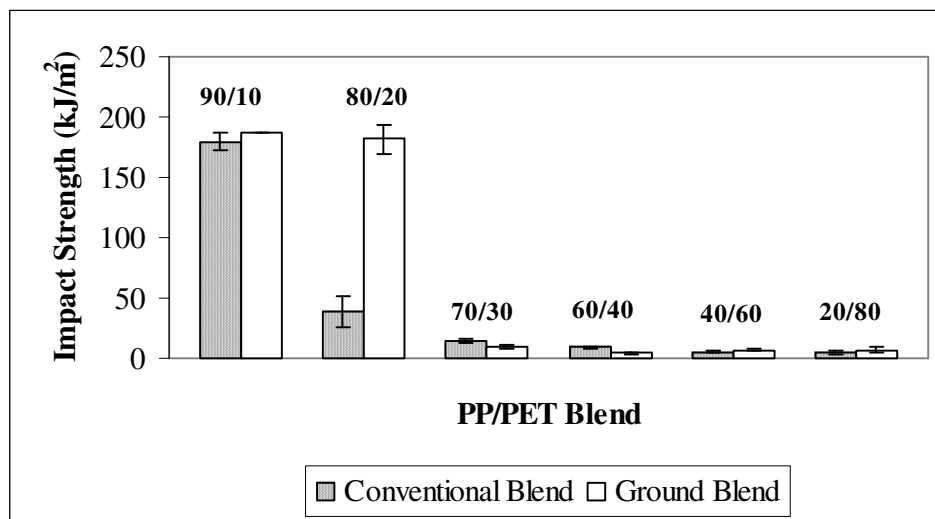


Figure 4.41 Impact strength values of conventional and ground PP/PET systems

On the other hand, impact strength behavior of composite systems does not change with carbon nanotubes contribution (Figures 4.41 and 4.42). Impact strength of both composite systems decreases with increasing PET composition. Low compositions of ground composites, containing 10 and 20 wt. % PET, have higher impact strength values compared to conventional composites.

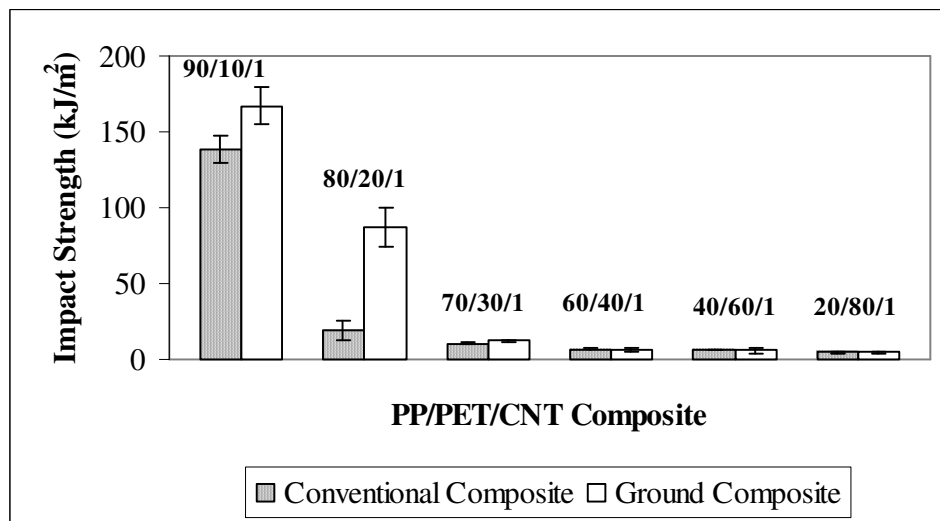


Figure 4.42 Impact strength values of conventional and ground PP/PET/CNT systems

4.3.3.1 High Temperature Processing of Ground PP/PET/CNT Systems

As stated previously, coalescence of reduced domains attained by grinding is the major drawback of long term and high temperature processing [41, 42, 50]. Most of ground composites prepared at 230 °C have slightly higher tensile strength values

than those of ground composites prepared at 280 °C. PET domains in ground systems might tend to get enlarged during molding processes at 280 °C, resulting in poor interfacial adhesion between blend phases and lower tensile strength values [4]. However, the difference in tensile strength values of ground systems prepared at 230 and 280 °C, respectively, is not so much (Figure 4.43), which may be due to short term molding processing.

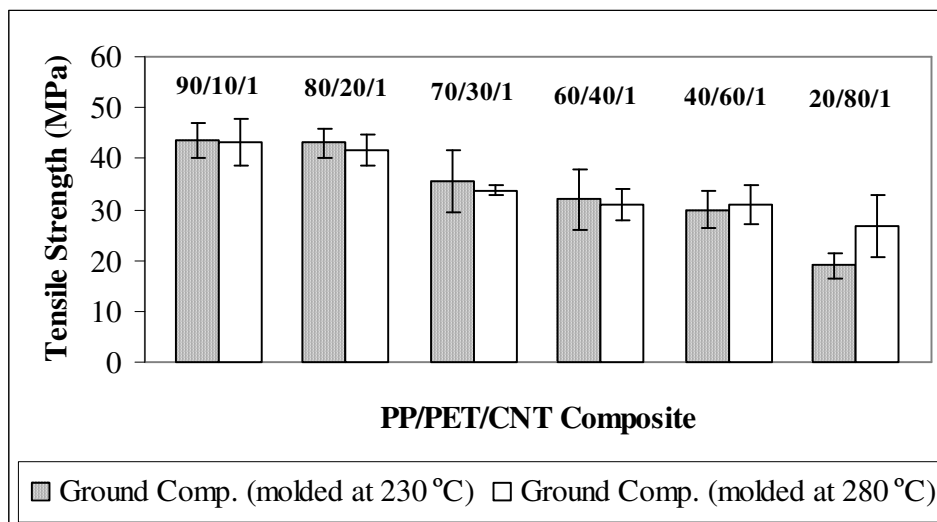


Figure 4.43 Tensile strength values of ground PP/PET/CNT systems, prepared at 230 °C and 280 °C

If the domain size of blend phases diminishes, tensile modulus increases [4]. Ground PP/PET/CNT systems molded at 230 °C may have smaller domain structures compared to ground systems molded at 280 °C since the systems prepared at 230 °C have higher tensile modulus values (Figure 4.44). The difference in tensile modulus

values of ground systems prepared at 230 and 280 °C, respectively, are much more than the difference observed in tensile strength results (Figures 4.43 and 4.44).

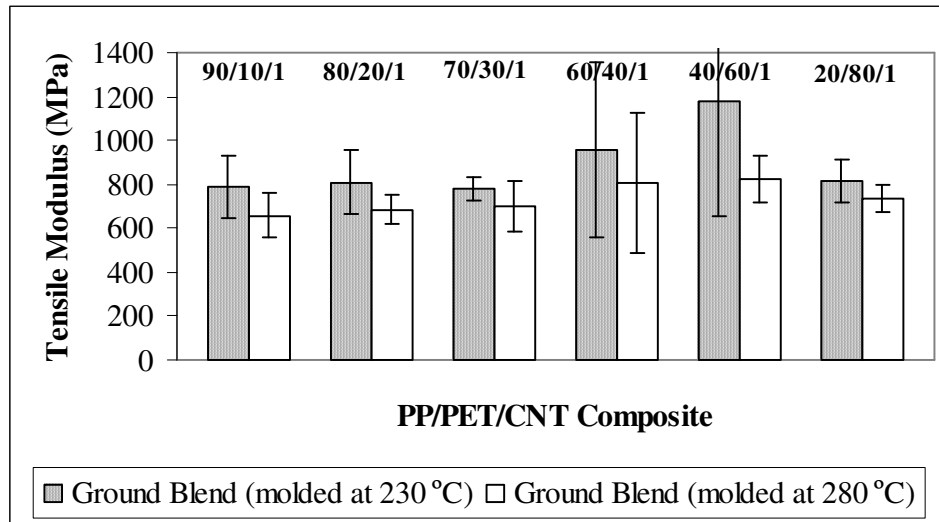


Figure 4.44 Tensile modulus values of ground PP/PET/CNT systems, prepared at 230 °C and 280 °C

4.3.3 Morphology Analysis

SEM micrographs reveal the difference in morphologies of ground and conventional composites (Figures 4.45-4.47). Average domain size of the minor phase, PET, in ground system of 10 wt. % composition is around 1 μm or smaller (Figure 4.45); whereas average domain size of PET in conventional composite is around 100 μm , two orders of magnitude larger than that obtained in the ground composite.

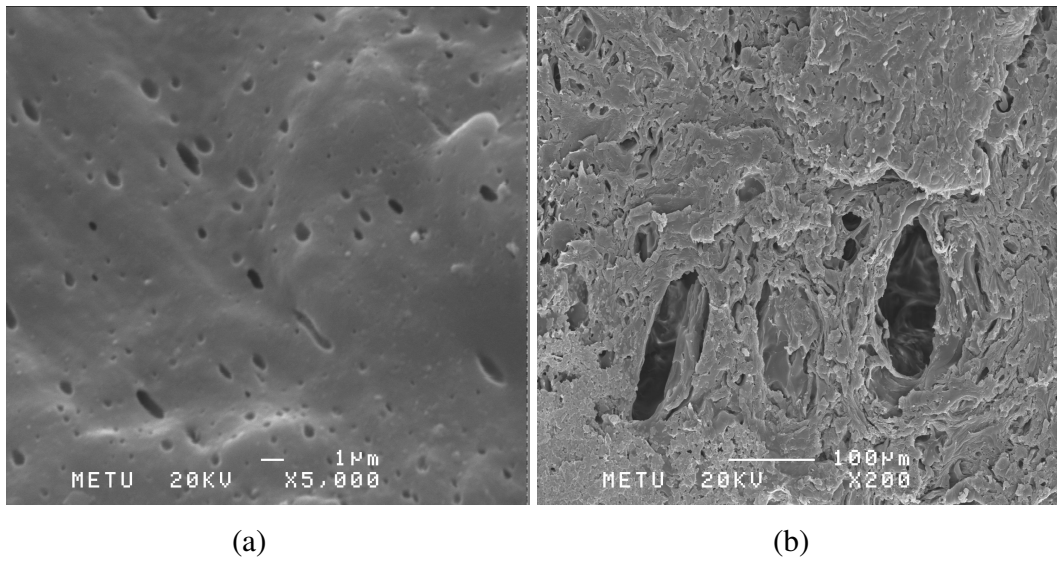
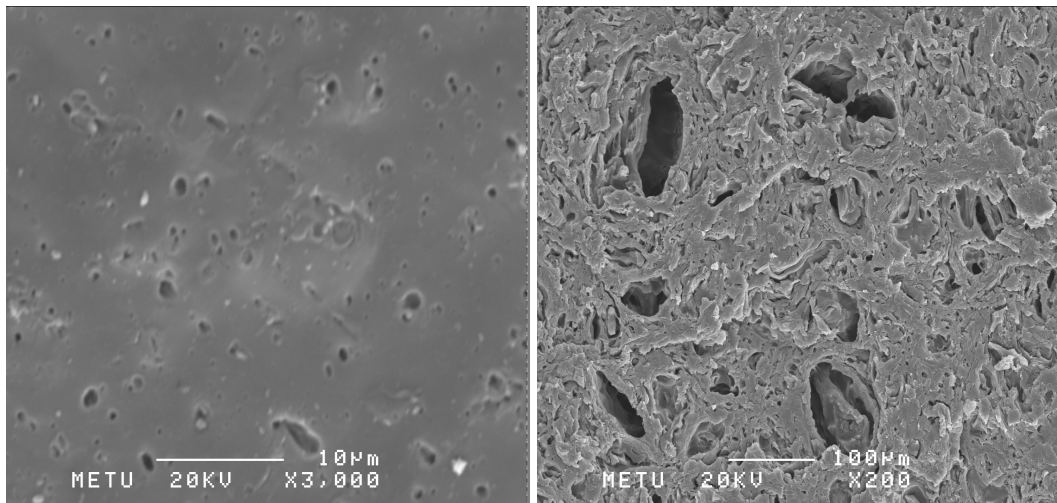


Figure 4.45 SEM micrographs of impact fractured samples of PP/PET/CNT (90/10/1) systems, etched with trifluoroacetic acid, (a) ground and (b) conventional

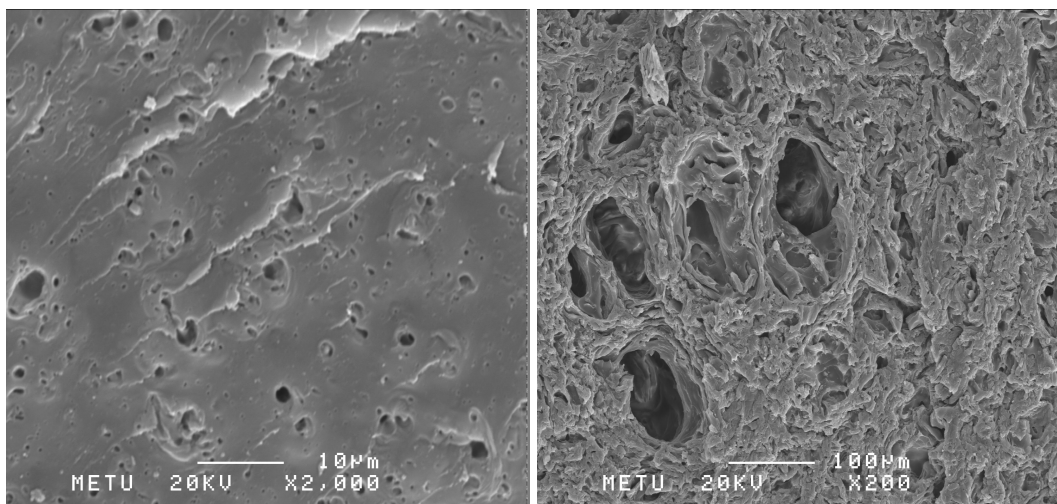
Domain size of minor phase seems to a little higher as PET content of ground systems increases from 10 to 30 wt. % (Figures 4.45-4.47) [48, 49]. The composites containing 20 and 30 wt. % PET still provide micron sized domain structures. On the other hand, conventional systems at the same PET composition leads to domain structures around 100 μm .



(a)

(b)

Figure 4.46 SEM micrographs of impact fractured samples of PP/PET/CNT (80/20/1) systems, etched with trifluoroacetic acid, (a) ground and (b) conventional



(a)

(b)

Figure 4.47 SEM micrographs of impact fractured samples of PP/PET/CNT (70/30/1) systems, etched with trifluoroacetic acid, (a) ground and (b) conventional

According to electrical resistivity and tensile test results (Figures 4.35, 4.41, 4.42), high temperature processing might slightly coarsen the domain structures of phases. However, at 10 wt. % PET composition, ground system, molded at 230 °C and ground system, molded 280 °C have similar domain structures (Figure 4.48). Hence, the microstructured blend morphology obtained by grinding is still conserved after molding process above the melting point of PET.

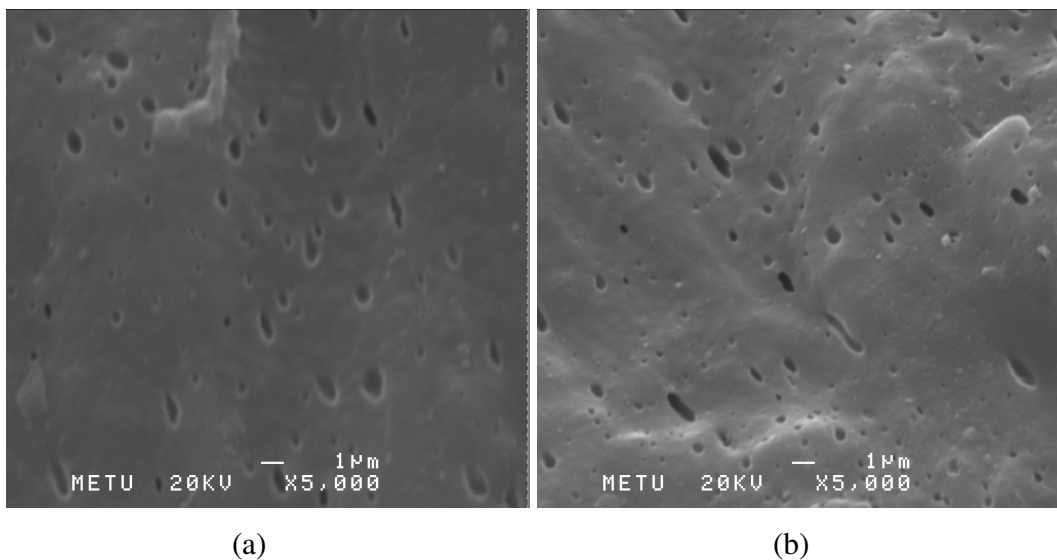


Figure 4.48 SEM micrographs of impact fractured samples of ground PP/PET/CNT (90/10/1) systems, etched with trifluoroacetic acid, (a) molded at 230 °C and (b) molded at 280 °C

4.4 Electrochemical Capacitance Performances of Pani/CNT and Pani Films on Treated Current Collectors

In addition to EMI shielding and dielectric material applications, conductive polymer composites can be used as an electrode material in electrochemical capacitors. Carbon nanotubes, possessing double-layer capacitance, and polyaniline, possessing pseudocapitance, can be combined to obtain electrode materials with enhanced capacitance performances. To assess capacitance properties of conductive polymer composites for capacitor application, polyaniline/carbon nanotubes composites were synthesized and their electrodes were prepared. Electrochemical capacitance performances of these electrodes are discussed in this part. Furthermore, alternative to polyaniline/carbon nanotubes systems, polyaniline films on treated current collectors were prepared. Their capacitance performances are also expressed in this part.

4.3.4 Fourier Transform Infrared (FTIR) Spectroscopy

Fourier Transform Infrared Spectroscopy was performed to identify synthesized carbon nanotubes and polyaniline. Besides, FTIR spectroscopy was used to reveal the interaction between composite constituents of polyaniline/carbon nanotubes. Figure 4.49 (a) presents FTIR spectrum of pure multi-walled carbon nanotubes. The peak at 3429 cm^{-1} is assigned to the presence of hydroxyl group (-OH) on the surface of carbon nanotubes, which may result either from oxidation during purification of nanotubes or from ambient moisture bound to the particles [139-142]. Another band at 1633 cm^{-1} is attributed to the C=O stretching of quinone groups on the surface of carbon nanotubes [139, 141, 142]. The peak at 1558 cm^{-1} is corroborated to characteristic stretching vibrations of C=C [143]. In addition, the peak at 1384 cm^{-1} is attributed to the bending vibration of the -OH group [141]. The appearance of a band at 1119 cm^{-1} is assigned to the stretching vibration of C-O [144].

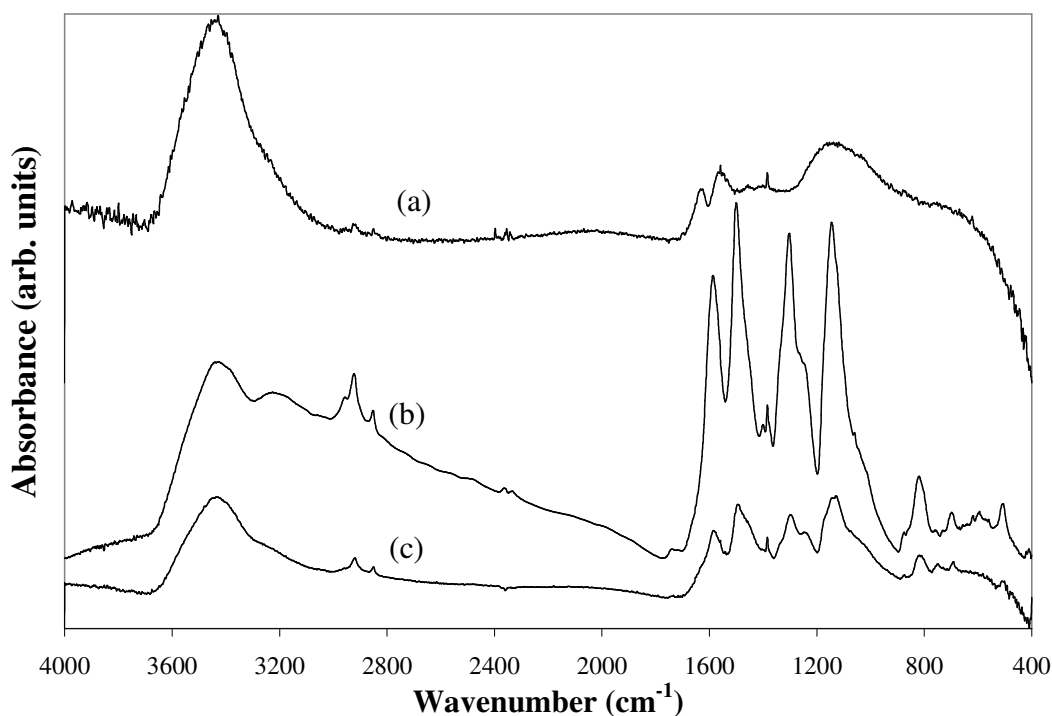


Figure 4.49 Comparison of FTIR spectra of (a) pure carbon nanotubes, (b) pure polyaniline and (c) polyaniline/carbon nanotubes composite containing 40 wt. % polyaniline

Analysis of the FTIR spectrum for polyaniline (Figure 4.49 (b)) shows the characteristic N-H peak of polyaniline at 3432 cm^{-1} [69, 145]. The peak at 2923 cm^{-1} is attributed to the stretching vibration of C-H [69, 146]. In addition, this spectrum shows peaks at 1586 and 1500 cm^{-1} for the characteristic C=C stretching of the quinoid and benzenoid rings, respectively [147]. The peak at 1384 cm^{-1} is related to the C-N stretching mode. Polyaniline sample exhibits peaks around 1303 cm^{-1} , which is corroborated with C-N stretching of tertiary aromatic amine in the quinine di-imine unit [147, 148]. Another characteristic peak at 1144 cm^{-1} is attributed to the vibration mode of $-\text{NH}^+=$ structure due to protonation [145]. The peak at 819 cm^{-1} is

assigned to the out of plane bending vibration of C-H [149]. Besides, the peak at 698 cm^{-1} is due to vibration mode of the C-C band of the aromatic nuclei [150].

It is observed that N-H peak of polyaniline at 3432 cm^{-1} becomes the most prominent peak for the composite containing 40 wt. % polyaniline (Figure 4.49 (c)) [69, 145, 151]. In addition, this peak shifts to 3436 cm^{-1} and it may combine with the peak of carbon nanotubes at 3429 cm^{-1} . The higher intensity of N-H peak means that more polymer chains grow and align in an order. This might show the trace of an accomplished polymerization reaction in the presence of carbon nanotubes [145]. FTIR spectrum of polyaniline coated carbon nanotubes exhibits two new absorption bands. One is situated at 2850 cm^{-1} and other at 750 cm^{-1} . The peak at 2850 cm^{-1} is assigned to C-H stretching vibration of chemisorbed hydrogen on carbon nanotubes [139, 152]. Other peak at 750 cm^{-1} is due to deformation vibration of the quinoid ring, which is believed to result from the formation of the following type of reaction between polyaniline and carbon nanotubes during the oxidative polymerization reaction (Figure 4.50) [132, 153]:

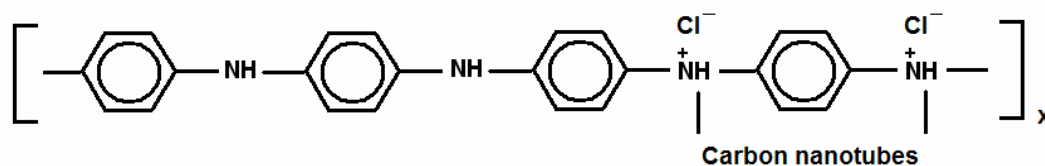


Figure 4.50 Possible reaction between polyaniline and carbon nanotubes during polymerization process [132, 153]

It is notable that the peaks observed at 1384 cm^{-1} and 818 cm^{-1} for polyaniline are virtually present for polyaniline/carbon nanotubes composite containing 40 wt. % polyaniline at the same bands (Figure 4.49 (c)) [149, 154]. The peaks noticed for polyaniline at 2923, 1586, 1500, 1303, 1144 and 698 cm^{-1} exhibit shifts to 2920, 1584, 1495, 1297, 1129, 691 cm^{-1} , respectively, for polyaniline/carbon nanotubes composites [69, 131, 146, 147, 150, 155-157]. Most of the peaks noticed for the composite show variations in positions relative to the peaks observed for the polyaniline only, which may be due to interaction between nanotubes and polyaniline [157].

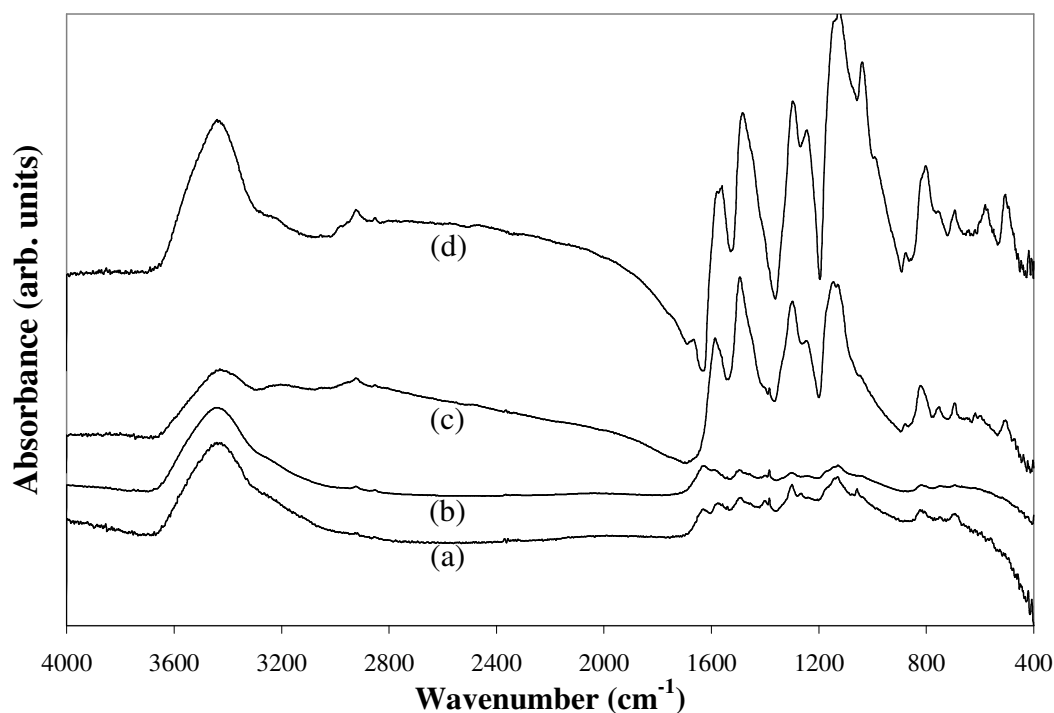


Figure 4.51 Comparison of FTIR spectra of polyaniline/carbon nanotubes composites containing (a) 10 wt. % polyaniline, (b) 20 wt. % polyaniline, (c) 60 wt. % polyaniline and (d) 80 wt. % polyaniline

FTIR spectra of polyaniline/carbon nanotubes composites, containing different amount of polyaniline, resemble each other (Figure 4.51). Only few differences in FTIR spectral characteristics are noticed among composites, containing 10, 20, 60 and 80 wt. % polyaniline, respectively. FTIR spectrum of composite containing 20 wt. % of polyaniline (Figure 4.51 (b)) shows the C=O stretching band corresponding to the carboxyl group at 1628 cm^{-1} [156]. This band is almost absent in the spectrum of the systems containing 10, 60 and 80 wt. % polyaniline. Also, FTIR spectrum of the system containing 80 wt. % polyaniline (Figure 4.51 (d)) exhibits bands at 1560, 1244 and 1038 cm^{-1} which are corroborated to N-H bending vibration [153], C-N⁺ stretching vibration in the polaron structure [131] and C-N stretching of a secondary aromatic amine [158], respectively. In addition, the bands corresponding to N-H stretching, C=C stretching of the quinoid ring and the benzenoid ring, vibration mode of -NH⁺= structure due to protonation and π -electron delocalization induced in the polyaniline by protonation illustrate variation in position among polyaniline/carbon nanotubes composites, containing different amounts of conducting polymer.

4.4.2 Electrochemical Capacitance Performances of Pani/CNT Composites

Cyclic voltammetry measurements were performed in the safe potential range for polyaniline electrode from 0 V to 0.9 V, at which range polyaniline is not exposed to degradation reaction [159]. An ideal double layer capacitor gives rise to a cyclic voltammogram in rectangular shape. The energy storage process is directly electrostatic and the resulting current is independent on potential. Upon reversal of the potential sweep, the sign of current is changed right away [124]. However, cyclic voltammetry curves of prepared electrochemical capacitors (Figures 4.52 and B.1) illustrate narrower loops far from the ideal rectangular shape owing to high internal resistance [72] and pseudocapacitance [124]. Charging with faradaic reactions is kinetically slow when compared with the electrostatic charging, resulting in a delay of potential during reversing the potential sweep [124].

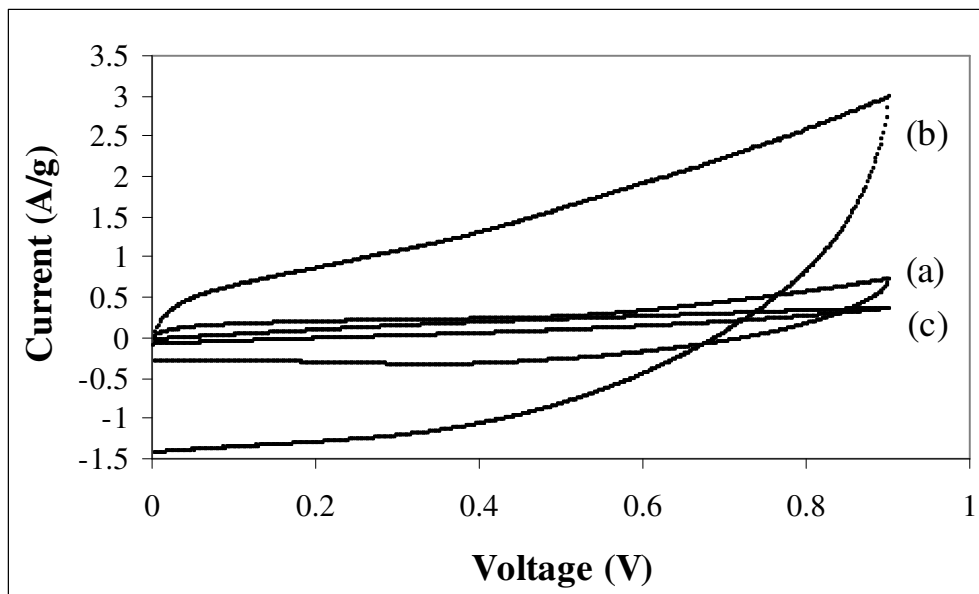


Figure 4.52 Cyclic voltammetry curves of (a) pure carbon nanotubes, (b) polyaniline/carbon nanotubes composite containing 20 wt. % polyaniline and (c) pure polyaniline

Besides, a distorted cyclic voltammetry curve can be attributed to limited diffusion of ions in the electroactive layer of electrodes. Especially, thick electrode material may limit diffusion and migration of ions in the bulk of the material, resulting in IR drop [71]. On the other hand, Zhou and coworkers [72] could not observe the symmetric and the rectangular-like current-potential responses with polyaniline/carbon nanotubes system in the neutral electrolyte medium, NaNO_3 .

Potential-time response of charge process is not the mirror image of its corresponding discharge counterpart for pure nanotubes, for pure polyaniline and for the composite (Figure 4.53). Hence, these systems do not exhibit the ideally capacitive behavior in 1 M NaNO_3 electrolyte [72]. In addition, there are rapid

voltage changes at the start of the charge and the discharge processes, known as IR drop (Figures 4.53 and B.2), which may be the result of the series resistance in the electrode system [160].

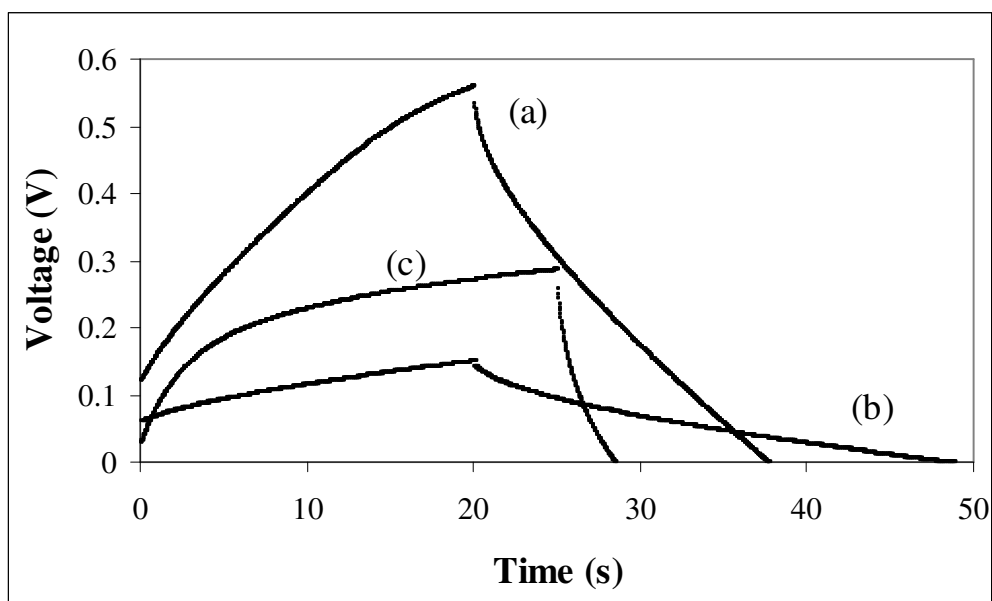


Figure 4.53 Charge-discharge plots of (a) pure carbon nanotubes, (b) polyaniline/carbon nanotubes composite containing 20 wt. % polyaniline and (c) pure polyaniline

Specific capacitances of polyaniline/carbon nanotubes composites were calculated from the galvanostatic charge-discharge plots by using the Equations 2.19 and 2.20. Pure carbon nanotubes result in low specific capacitance around 4 F/g, which is similar to the capacitance value of carbon nanotubes obtained by Show and coworker [160]. As displayed in Figure 4.54, electrochemical capacitance increases with

polyaniline content until 20 wt. % and then the capacitance values decline. The highest specific capacitance of 20 F/g is obtained with the composite system containing 20 wt. % polyaniline, which may be due to the pseudocapacitance contribution of polyaniline through oxidation-reduction reactions to the electric double layer capacitance of carbon nanotubes [162]. When compared with other systems, polyaniline at 20 wt. % composition may have more porous surface structure, which leads to a larger effective surface area and also higher electronic and ionic conductivity. Larger surface area improves double layer capacitance and pseudocapacitance behavior of electrochemical capacitor at the same time [65].

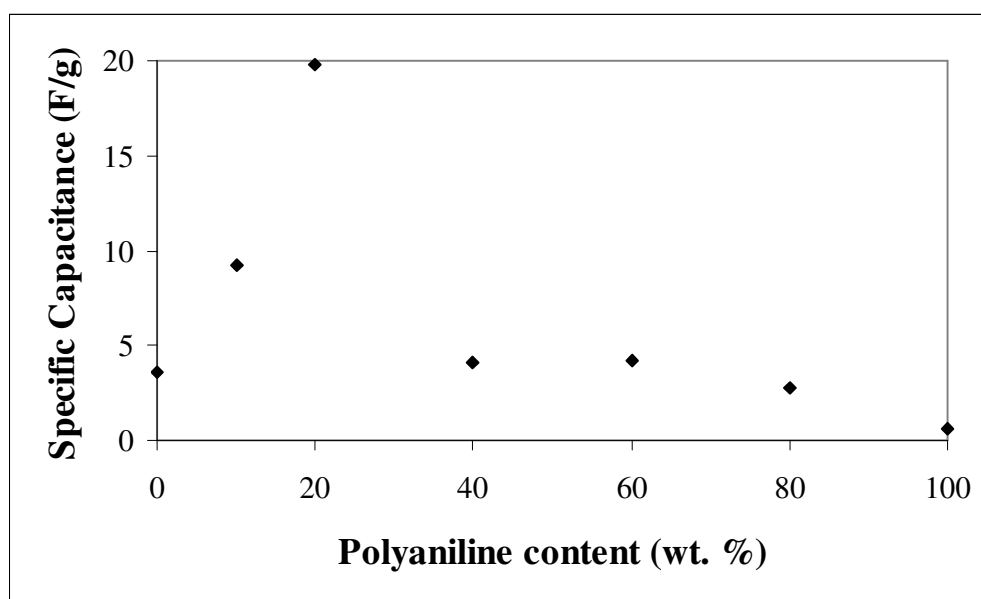


Figure 4.54 Relationship of polyaniline content of polyaniline/carbon nanotubes systems with the specific capacitance, calculated from charge/discharge plots

It is expected that the pseudocapacitance mechanism of electrochemical capacitor dominates with increasing conducting polymer content of polyaniline/carbon nanotubes systems [162]. However, the specific capacitance illustrates a reduction trend with polyaniline content after 20 wt. % composition (Figure 4.54). The only reason for this reduction may be a possible decrease in effective surface area of polyaniline on carbon nanotubes. This trend reveals the fact that the double-layer capacitance behavior of prepared capacitors is more dominant than the pseudocapacitance behavior.

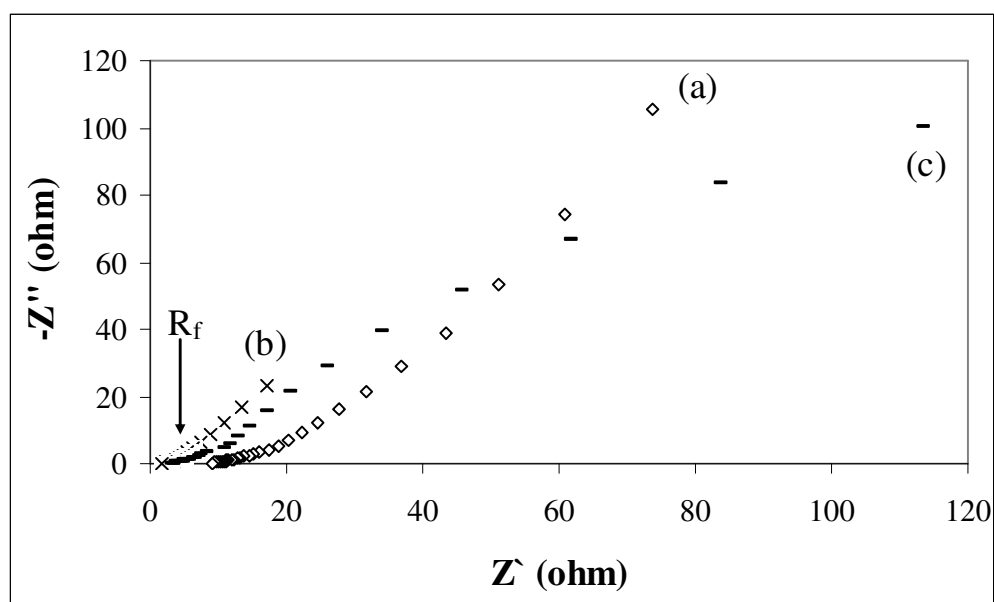


Figure 4.55 Electrochemical impedance spectra of (a) pure carbon nanotubes, (b) polyaniline/carbon nanotubes composite containing 20 wt. % polyaniline and (c) pure polyaniline

The contact resistance between the active electrode material and the current collector is a considerable factor to determine the performance of electrochemical capacitors. Pressing of electrode material directly on nickel foil might result in high contact resistance since the line parallel to the imaginary axis of the complex-plane impedance plot is not straight (Figures 4.55 and B.3). Contact resistance between electroactive electrode material and nickel foil contributes to the equivalent series resistance [54].

The inner integrated area of cyclic voltammogram of polyaniline/carbon nanotubes based capacitor, which is the power density, is higher than that of polyaniline and carbon nanotubes based capacitors (Figure 4.52). This may be due to the smaller internal resistance of polyaniline/carbon nanotubes electrodes [161]. The complex-plane impedance plot can be used to compare electrical resistance of different electrode materials when the electrolyte resistance is held constant. A decrease in R_f , which is the sum of the resistance of the electrode itself and the contact resistance between the electrode and the current collector, may indicate a decrease in electrode resistance (Figure 4.55) [54]. Hence, cyclic voltammetry and electrochemical impedance results support the same idea that the internal resistance of polyaniline/carbon nanotubes electrode is lower than those of pure carbon nanotubes and pure polyaniline electrodes (Figures 4.52 and 4.55).

In the literature, specific capacitance values of 90 and 115 F/g for Pani/CNT composites have been measured using the two-electrode cell system [73, 74]. When compared with studies performed in the literature, high capacitance could not be obtained from polyaniline/carbon nanotubes based electrochemical capacitors. As stated before, the contact resistance between polyaniline/carbon nanotubes electrode and the current collector, nickel, is important in terms of the performance of the electrochemical capacitor [54]. Possible reason for poor capacitance performances may be this contact resistance. In the continuing part of this study, it was aimed to

improve the capacitance performance of the electrochemical capacitors by reducing the contact resistance and improving the electrode material quality.

4.4.3 Scanning Electron Microscopy of Pani/CNT Composites

The surface morphology of pure carbon nanotubes, polyaniline/carbon nanotubes composites containing 20, 40 and 60 wt. % polyaniline, respectively, and pure polyaniline are shown in Figures 4.56-4.60. According to SEM Figure 4.56, the diameter of a carbon nanotube is around 20 nm. In order to benefit from both double layer capacitance behavior of carbon nanotubes and pseudocapacitance behavior of polyaniline, coated layers need to be as thin as possible to protect the nanoporous three-dimensional morphology of carbon nanotubes. However, it is difficult to coat carbon nanotubes with thin and uniform polyaniline layers since carbon nanotubes tend to agglomerate. As shown in Figures 4.57-4.59, the micrographs do not illustrate a homogeneous coating of carbon nanotubes with polyaniline, which indicates that the conducting polymer tends to grow both on itself and on carbon nanotube agglomerates. The morphologies of polyaniline/carbon nanotubes composites change with an increase in polyaniline content. The thickness of inhomogeneous polymer layers increases slightly as polyaniline content of the composites goes up. Non-uniform polyaniline layers result in reduced surface area in the electrode material to provide capacitive performance. Hence, lower specific capacitances are obtained for the polyaniline/carbon nanotubes systems.

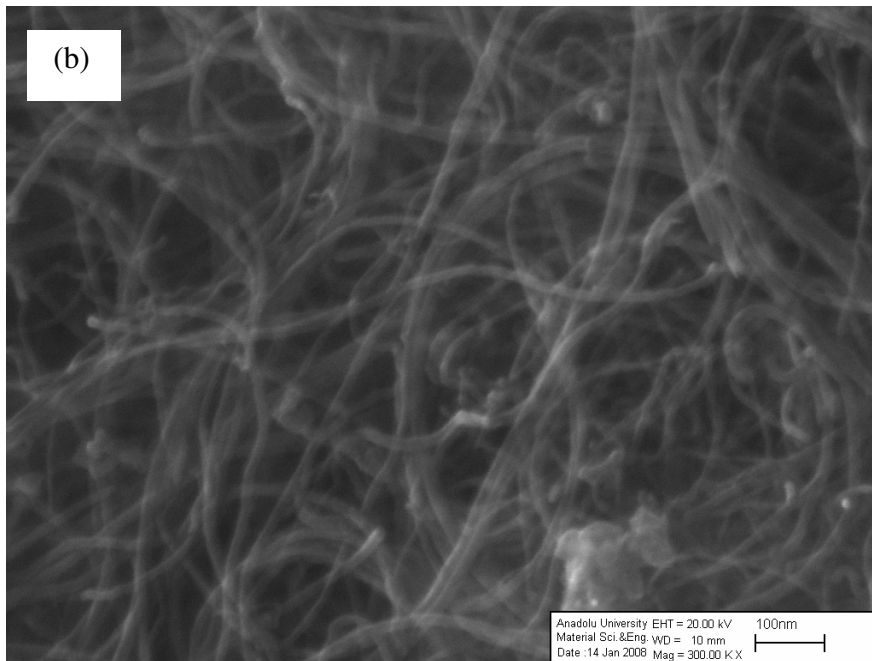
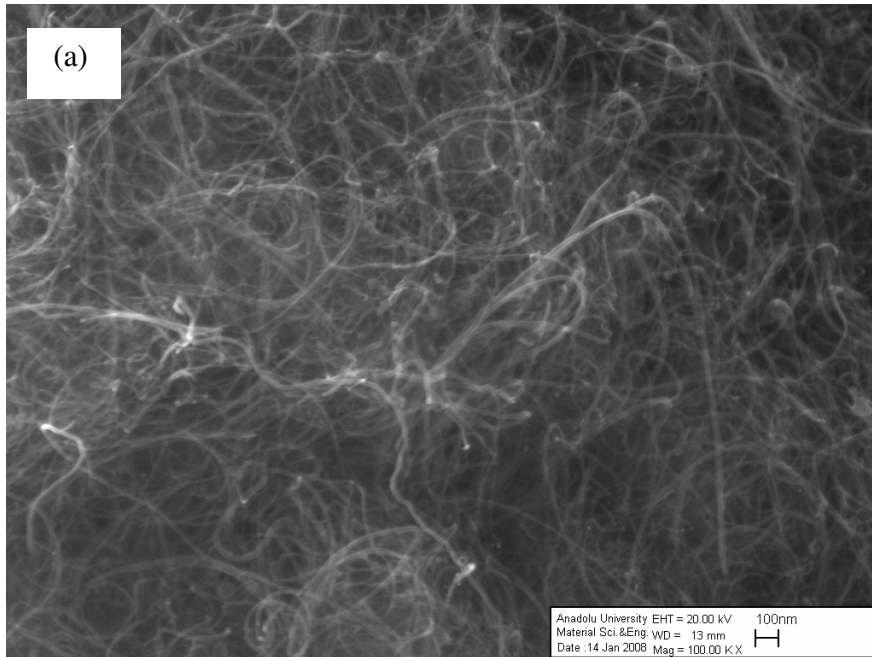


Figure 4.56 SEM micrographs of carbon nanotubes, (a) (x100000) and (b) (x300000)

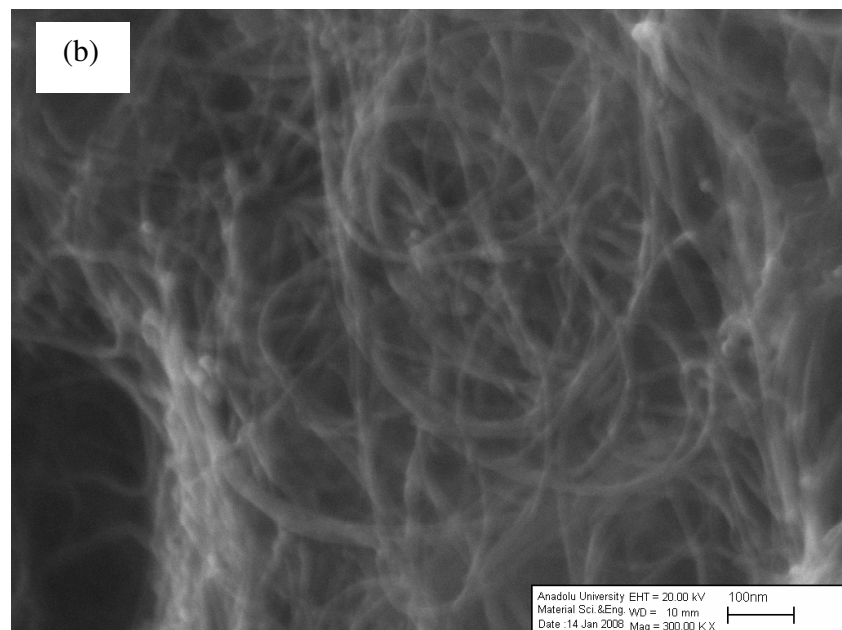
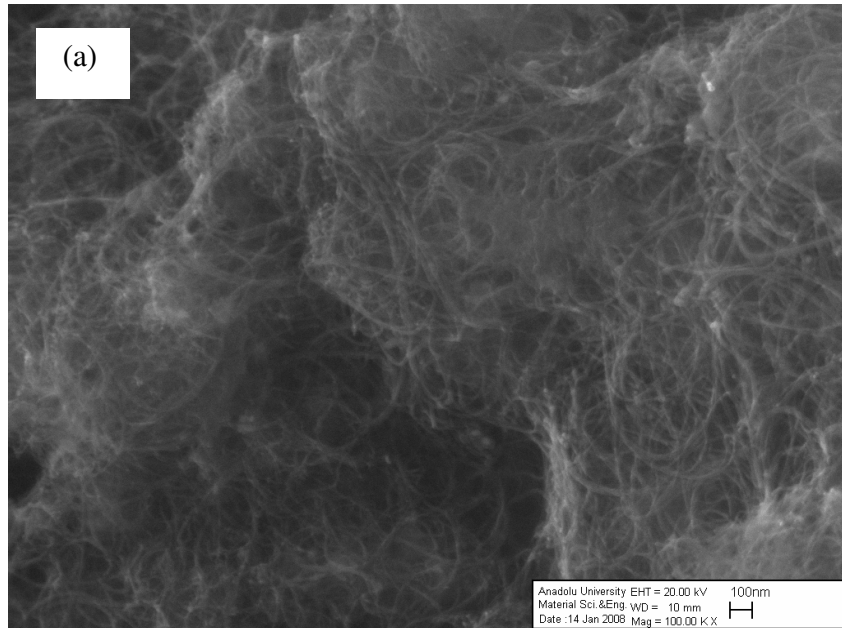


Figure 4.57 SEM micrographs of polyaniline/carbon nanotubes composite containing 20 wt. % polyaniline, (a) (x100000) and (b) (x300000)

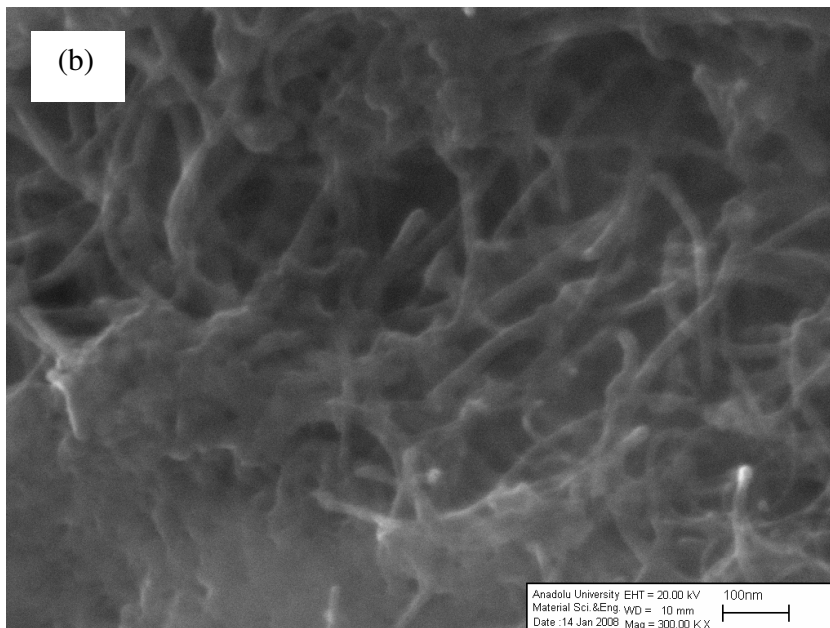
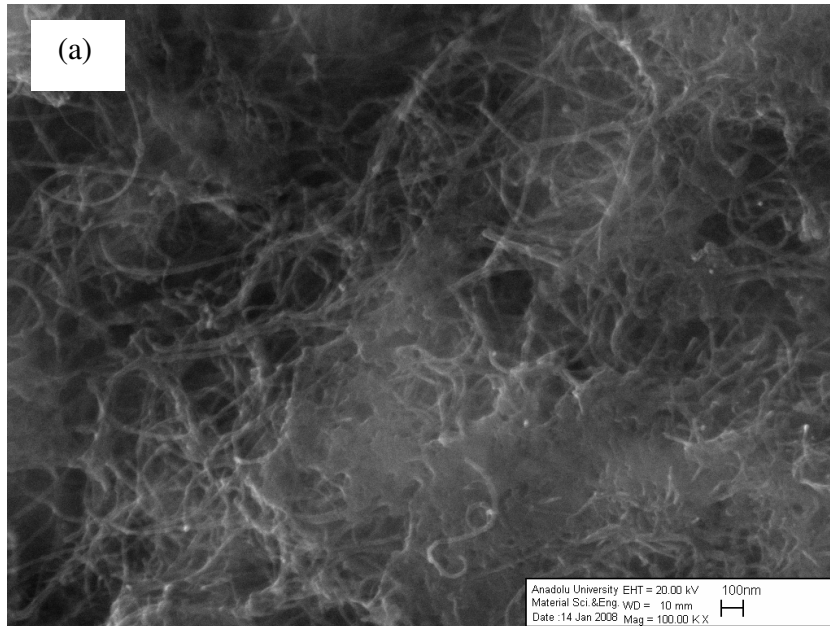


Figure 4.58 SEM micrographs of polyaniline/carbon nanotubes composite containing 40 wt. % polyaniline, (a) (x100000) and (b) (x300000)

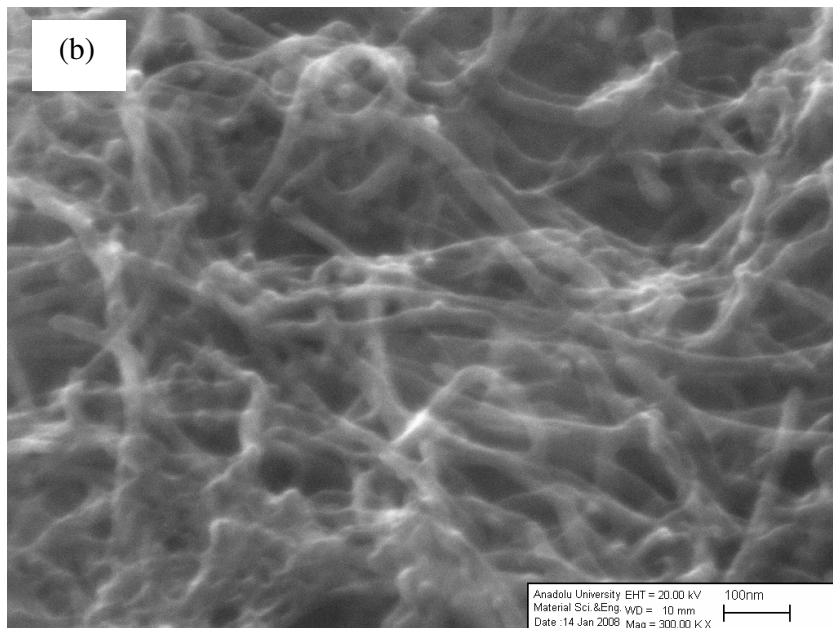
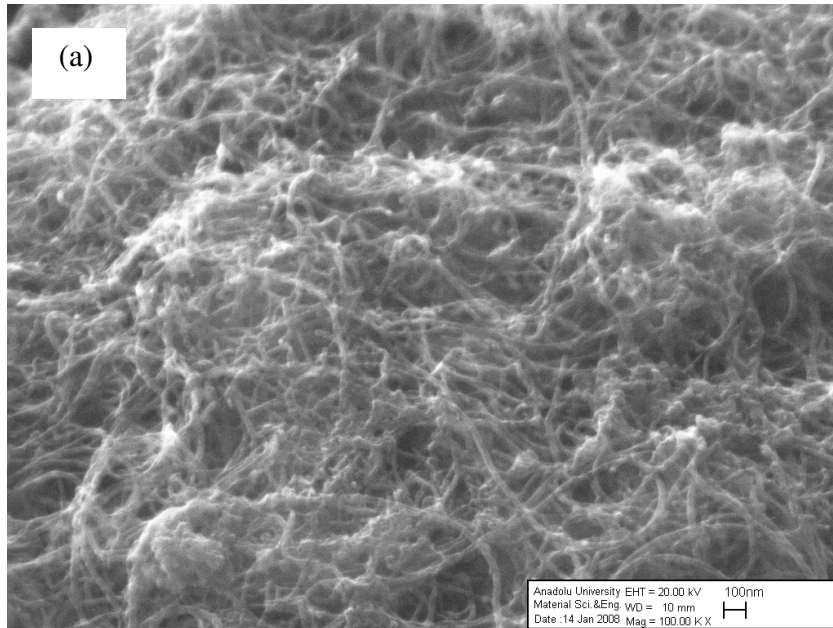


Figure 4.59 SEM micrographs of polyaniline/carbon nanotubes composite containing 60 wt. % polyaniline, (a) (x100000) and (b) (x300000)

The surface morphology of polyaniline synthesized in the absence carbon nanotubes is analyzed by scanning electron microscope as shown in Figure 4.60, which suggests that the pure polymer exhibits a porous and layered structure far from the nano-porous morphology of carbon nanotubes and Pani/CNT composites.

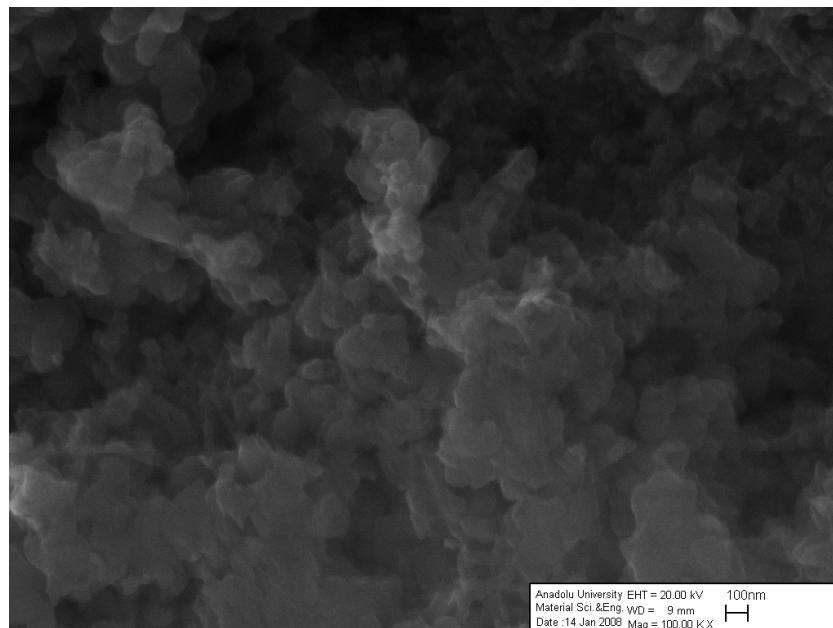


Figure 4.60 SEM micrograph of pure polyaniline, (x100000)

4.4.4 Electrochemical Capacitance Performances of Pani Films on Treated Current Collectors

It was aimed to prepare thin electrode films by depositing polyaniline/carbon nanotubes composites from their solutions on the current collectors. However, it is difficult to dissolve polyaniline/carbon nanotubes systems to prepare thin films.

Only, polyaniline films can be deposited on nickel current collectors from their solutions. Hence, in the remaining part of this application study, polyaniline films were used to fabricate electrodes for the electrochemical capacitors instead of the composite systems.

In order to reduce the contact resistance, it was aimed to improve the interaction between the electrode material, polyaniline film, and the current collector, nickel foil, by providing chemical bonding between the electrode constituents. Alizarin has the ability to bind chemically to the pre-treated nickel surface and the polyaniline film (Figures. 4.61 and 4.62) [163, 164]. For this purpose, nickel foils were treated with sulfuric acid to convert Ni to Ni⁺² and then with alizarin solution to react alizarin molecules with acid treated nickel foils, in Ni⁺² states. Alizarin molecules bonded to nickel foils can also react with polyaniline molecules in insulating form and they convert them to conducting form; that is, alizarin acts as doping agent when it bonds polyaniline molecules to nickel foil. Additionally, alizarin enhances adhesion of polyaniline film on nickel foil [163].

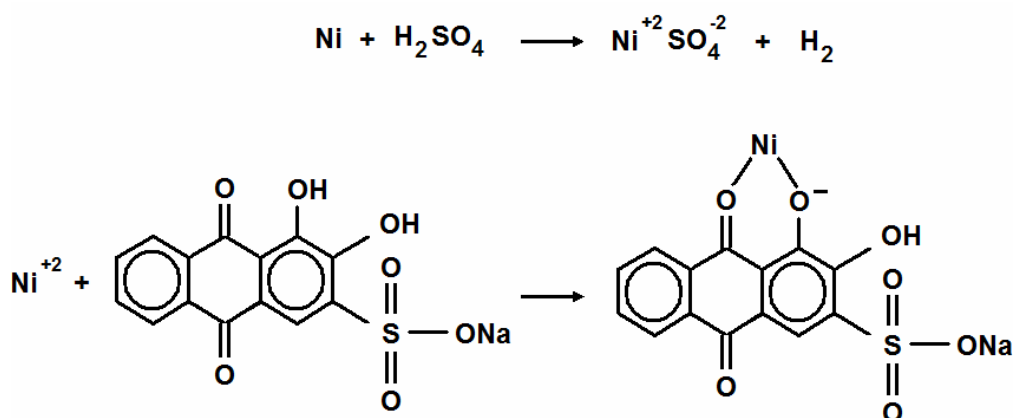


Figure 4.61 Treatment of nickel foil with sulfuric acid and then with alizarin [163, 164]

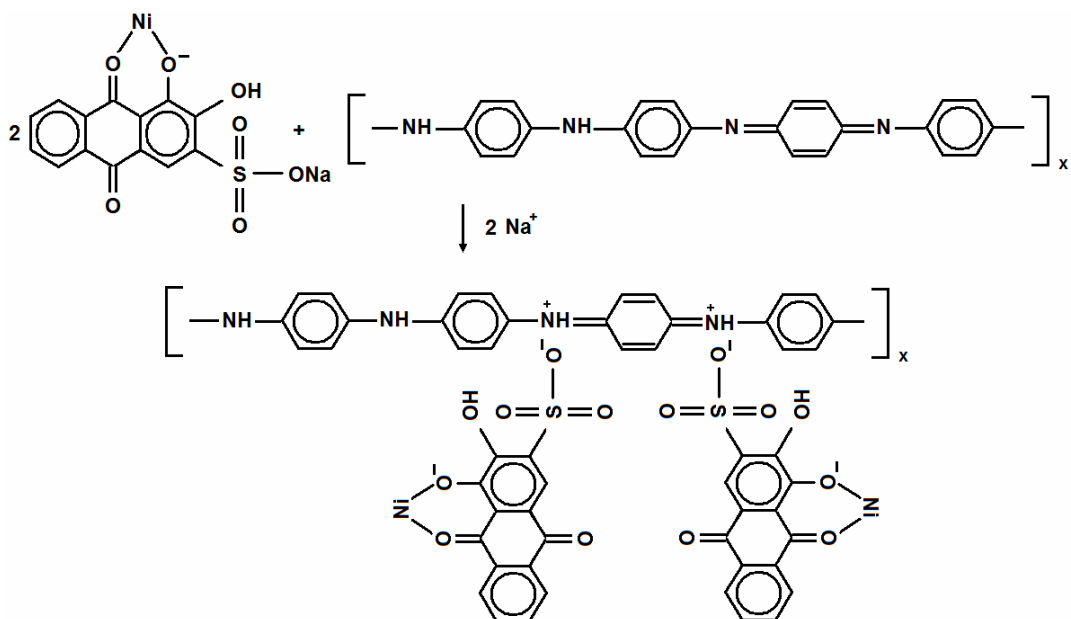


Figure 4.62 Coating of treated nickel foil with polyaniline base using alizarin [163, 164]

Capacitance results are expressed in F/g taking into account the weight of the whole electrode material, polyaniline [165]. However, the accessibility of electrolyte ions into the pores inside the electrode is limited; that is, only certain part of electrode material close to the interface between electrolyte and electrode can be used effectively during electrochemical capacitance measurements. In order to enhance the efficiency of electrochemical capacitors, the thickness of the electrode material needs to be reduced, which leads to higher specific capacitance. Electrode systems, PA100, PA50, PA25 and PA16.7 are lined up in an order that the thickness and the weight of the electrode material decrease from PA100 to PA16.7. The widest cyclic voltammetry curve and the highest specific capacitance are obtained with the electrode system PA25 (Figures 4.63 and 4.64). This system may include optimum polyaniline film thickness to provide higher specific capacitance, which is calculated

from the integration of the area of the cyclic voltammogram [165]. Specific capacitances cannot be calculated from the galvanostatic charge/discharge plots owing to fast potential-time response of discharge process (Figure 4.65). Meanwhile, electrical resistance of PA100, PA50, PA25 and PA16.7 electrode systems may not be different from each other since R_f , which is the sum of the resistance of the electrode itself, and the contact resistance between the electrode and the current collector, is similar for these electrode systems (Figure 4.66) [54].

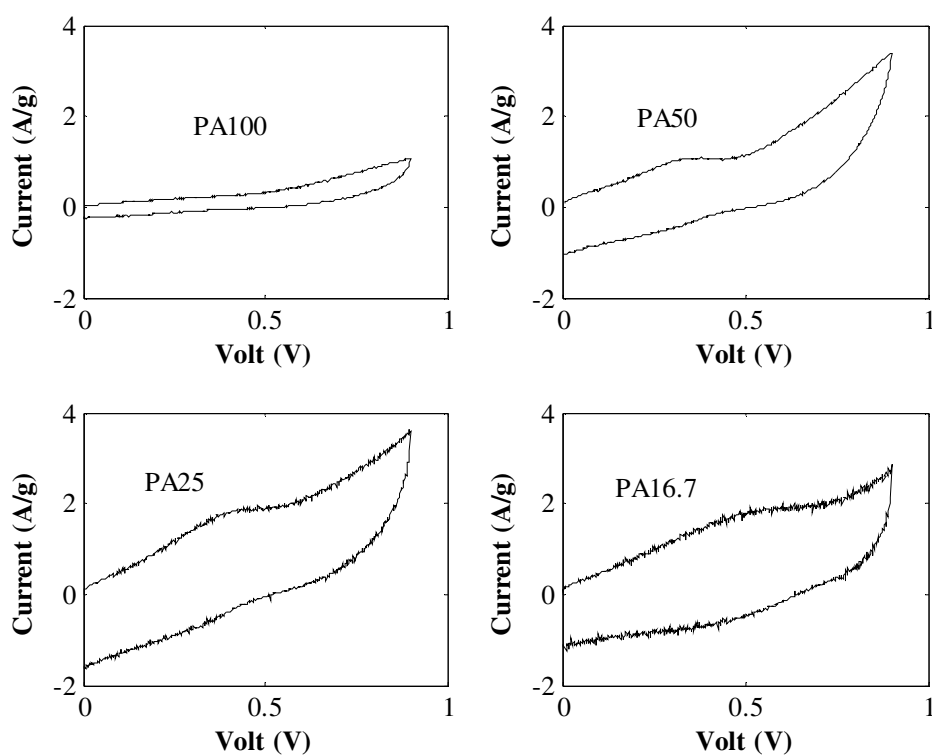


Figure 4.63 Cyclic voltammetry plots of polyaniline based electrochemical capacitors

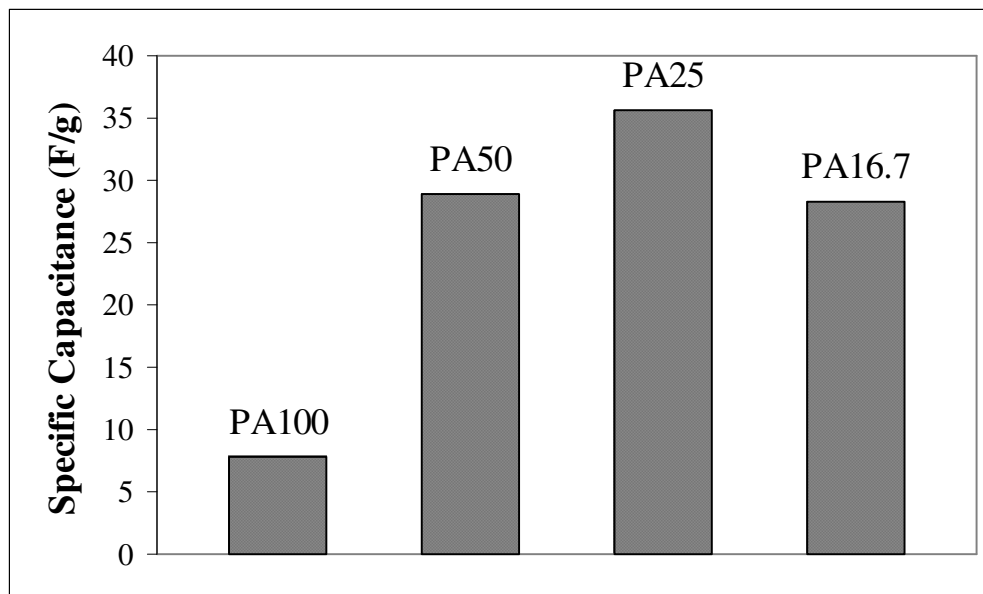


Figure 4.64 Specific capacitance values of polyaniline based electrochemical capacitors

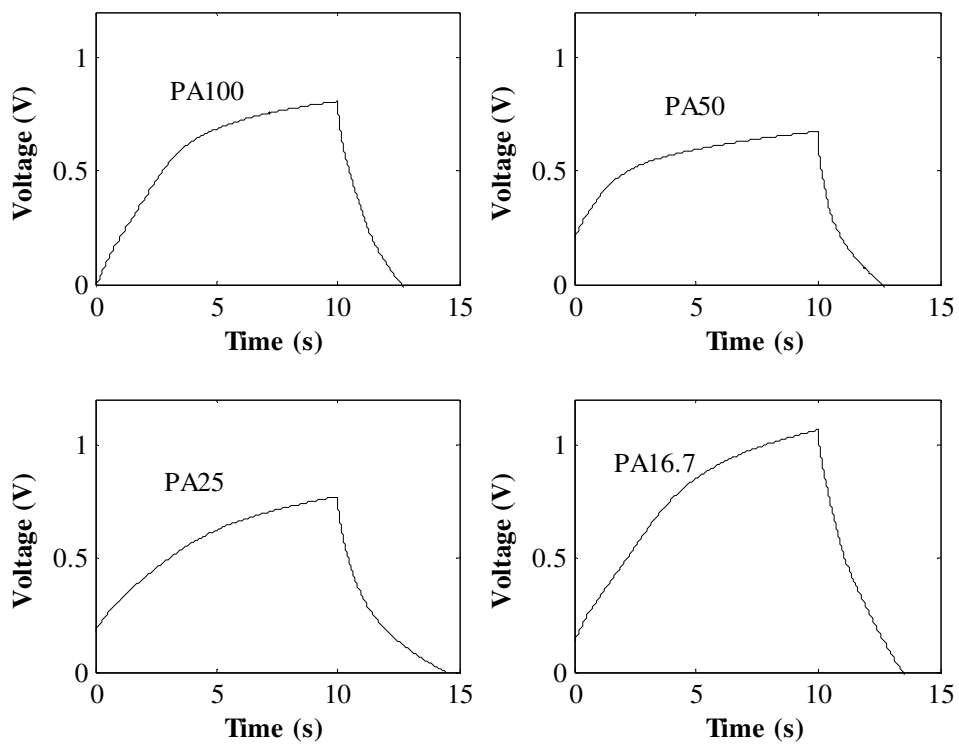


Figure 4.65 Charge/discharge plots of polyaniline based electrochemical capacitors

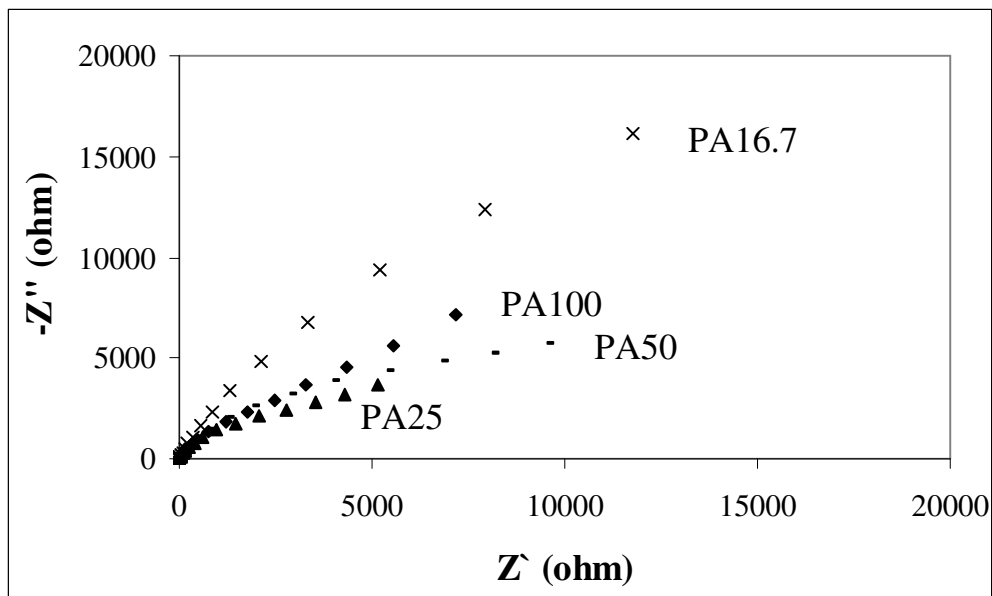


Figure 4.66 Impedance spectra of polyaniline based electrochemical capacitors

PA250, NPA25 and PA6.7 electrode systems result in narrow cyclic voltammetry curves as pure nickel current collectors do (Figure 4.67). In other words, they do not provide capacitance. NPA25 and PA25 electrode systems contain the same amount of polyaniline electrode material. Polyaniline in insulating form is deposited on untreated and treated nickel foils. Only difference between NPA25 and PA25 systems is the current collector. PA25 system possesses alizarin treated nickel foils. As stated before, alizarin may act as dopant and it turns the polymer into the conducting state. Hence, higher capacitance is obtained with PA25 system compared to NPA25 system. On the other hand, alizarin treatment does not make any sense at PA250 and PA6.7 systems. Alizarin may not be a strong dopant when compared with concentrated acids and doping effect of alizarin may be limited to a certain region close to the interface between nickel foil and polyaniline film. Besides, PA250 system possesses the thickest electrode material among other systems and the

accessibility of electrolyte ions into the pores inside the electrode is limited. Hence, PA250 system results in low capacitance. Similarly, PA6.7 system cannot be adequate to provide capacitance since it possesses a quite thin polyaniline film.

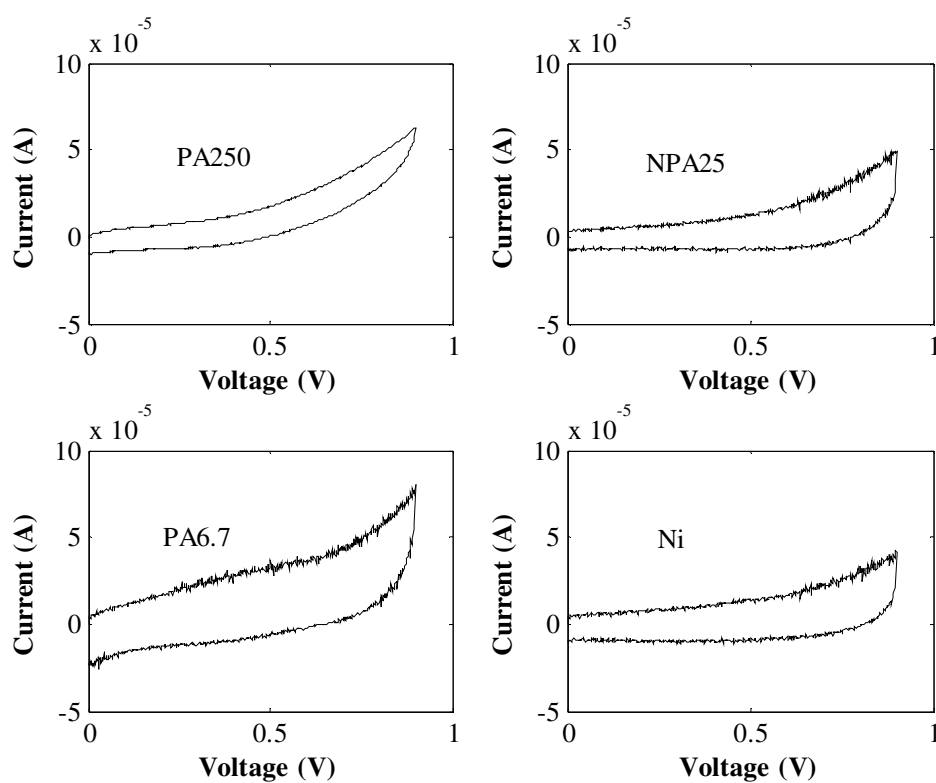


Figure 4.67 Cyclic voltammetry plots of polyaniline based electrochemical capacitors and nickel (Ni) current collectors as a reference

It is difficult to dissolve and to process polyaniline in the conducting state. On the other hand, polyaniline is not effective as electrode material in the insulating state.

By using alizarin treated nickel foil, adhesion and doping problem of polyaniline film is overcome at the same time. Additionally, polyaniline based capacitors result in higher capacitance values than those of polyaniline/carbon nanotubes composites.

CHAPTER 5

CONCLUSIONS

5.1 Preparation of Nylon 6/Carbon Black Composites

Polymer composites prepared by in-situ polymerization technique showed lower electrical resistivity at each composition of carbon black when compared with composites prepared by melt mixing method. Transition from insulator to semi conductor range was achieved at 1 wt. % carbon black content. This improvement should be the result of a reduction in agglomerate size of carbon black. Composites prepared by method A and method B did not differ so much in elongation at break values. At low compositions of the filler, method A gave higher tensile strength and impact strength results. In addition, method B gave higher tensile modulus values at intermediate compositions. According to these results and especially based on the improved electrical conductivity values, in-situ polymerization method can be chosen as the composite preparation technique alternative to melt mixing method.

5.2 Effect of Surface Treatment of Filler on LDPE/Carbon Black, Nylon 6/Carbon Black and PET/Carbon Black Composites

According to surface energy analysis and ESCA results, surface structure of carbon black was modified during chemical treatments. APS and formamide, which have amine and amide types of functional groups in their structures, increased electrical conductivity of composites by improving electrical conductivity of carbon black. According to ESCA results, nitrogen atoms of APS and formamide turned into

quaternary structure following the doping reaction between carbon black and surface modifiers. Nitrogen atoms behaved as dopant in this quaternary structure by increasing the number of charge carriers. Hence, APS and formamide treatments decreased percolation threshold concentrations of LDPE/carbon black and nylon 6/carbon black systems from 5 wt. % to 3 wt. % of carbon black content. In addition, surface treatment of carbon black did not significantly change the tensile strength and modulus of nylon 6 and LDPE composites compared to those of untreated carbon black.

In the second part of the surface treatment study, electrical resistivity of PET based composites was successfully reduced more than one order of magnitude with surface treatment of carbon black. Percolation threshold concentration of composites containing treated conductive filler shifted from 3 to 1.5 wt. % of carbon black composition. An increase in formamide solution concentration resulted in an increase in electrical conductivity of composites. In addition, microwave properties of composites containing treated carbon black were improved when compared with composites filled with untreated carbon black. Electromagnetic interference shielding effectiveness and dielectric constant increased with increasing carbon black content and formamide solution concentration. The composite containing 8 wt. % FA3-CB was shown to exhibit EMI SE of up to 27 dB and dielectric constant value of 19. Thus, application potential of conductive polymer composite as EMI shielding and dielectric material may be enhanced with surface treatment of conductive filler.

5.3 Effect of Grinding on PP/PET and PP/PET/CNT Systems

Carbon nanotubes might be selectively localized at PET phase of PP/PET/CNT composite systems. Electrical resistivity of conventional composite systems, which was in insulating range, was reduced to semiconductive level, which showed the achievement of applied grinding method. The most distinctive difference in mechanical properties of conventional and ground composite systems was observed

in the tensile strength. Ground PP/PET and PP/PET/CNT systems provided better tensile strength values for all PET compositions. During compression and injection molding processes, performed above melting temperatures of both PET and PP, average domain size of phases might coarsen a little since electrical conductivity, tensile strength and modulus values of ground composite systems molded at 280 °C were lower than those of ground composite systems molded at 230 °C. Based on the enhanced electrical conductivity and tensile strength values, grinding technique can be applied to conductive polymer composites, consisting of incompatible blend phases, after the melt compounding process.

5.4 Electrochemical Capacitance Performances of Pani/CNT and Pani Films on Treated Current Collectors

Specific capacitances of Pani/CNT based systems were higher than those of pure polyaniline based and pure carbon nanotubes based electrode systems. Thick and heavy electrodes materials with high contact resistance might be the reason for low capacitance values. To enhance the capacitance performance of the electrochemical capacitors by reducing the contact resistance and improving the electrode material quality, alizarin treatment was applied to nickel current collectors. The electrode system prepared directly by depositing polyaniline film on alizarin treated nickel foils provided higher specific capacitance than those of Pani/CNT based systems.

CHAPTER 6

RECOMMENDATIONS

It was desired to improve the electrical and mechanical properties of conductive polymer composite together. Electrical conductivity was enhanced to some extent with in-situ polymerization method by increasing the intimate contact and interaction between carbon black and nylon 6 molecules. Carbon black particles used in this study were not exposed to any surface treatment or modification. Surface treated carbon black may interact with caprolactam monomers more than untreated conductive filler does, which may result in a further reduction in carbon black agglomerate size. Hence, electrical conductivity and mechanical properties of nylon 6/carbon black composites may be improved further.

APS, which is a silane coupling agent, and formamide were selected as surface modifier of carbon black. Treated conductive filler was compounded with LDPE, nylon 6 and PET, respectively. Both tensile strength and modulus remained almost constant with APS or formamide treatment for both LDPE/CB and nylon 6/CB systems. Hence, mechanical properties of composites could not be improved with surface treatment of carbon black. It is recommended to select a suitable surface modifier, which may change the stress-strain behavior of carbon black filled composites by improving surface adhesion between the composite constituents without sacrificing electrical conductivity of the conductive filler.

High capacitances could not be obtained from polyaniline/carbon nanotube based electrochemical capacitors due to rough electrode materials and the contact

resistance between polyaniline/carbon nanotubes electrode and the current collector. Alizarin treatment solved these problems to some extent by increasing the interaction between the electrode material and the current collector. High quality, thin film polyaniline electrodes were prepared. They provided higher specific capacitances compared to polyaniline/carbon nanotubes electrodes. It is recommended to find an approach to deposit thin films of polyaniline/carbon nanotubes composites on the current collectors with good adhesion since composite can provide higher capacitance than its constituents by combining double layer capacitance behavior of carbon nanotubes with pseudocapacitance behavior of polyaniline.

REFERENCES

- [1] Tchoudakov R., Breuer O., Narkis M., “Conductive Polymer Blends With Low Carbon Black Loading: Polypropylene/Polyamide”, *Polymer Engineering and Science* 36, 1336-1346 (1996)
- [2] Gul V. E., “Structure and Properties of Conducting Polymer Composites”, VSP BV, The Netherlands (1996)
- [3] Rosen S. L., “Fundamental Principles of Polymeric Materials”, John Wiley & Sons, Inc., USA (1992)
- [4] Nielsen L. E, Landel R. F., “Mechanical Properties of Polymer and Composites”, Marcel Dekker, New York (1994)
- [5] Chodak I, Omastova M, Pionteck J., “Relation between Electrical and Mechanical Properties of Conductive Polymer Composites”, *Journal of Applied Polymer Science* 82, 1903-1906 (2001)
- [6] Koysuren O., Yesil S., Bayram G., “Effect of Composite Preparation Techniques on Electrical and Mechanical Properties and Morphology of Nylon 6 Based Conductive Polymer Composites”, *Journal of Applied Polymer Science* 102, 2520-2526 (2006)

- [7] Meincke O, Kaempfer D, Weickmann H, Friedrich C, Vathauer M, Warth H., "Mechanical properties and electrical conductivity of carbon nanotube filled polyamide 6 and its blends with acrylonitrile/butadiene/styrene", *Polymer* 45, 739-748 (2004)
- [8] Pinto G, Gonzalez C. L., Martin A. J., "Polymer Composites Prepared by Compression Molding of a Mixture of Carbon Black and Nylon 6 Powder", *Polymer Composites* 20, 804-808 (1999)
- [9] Larena A., Pinto G., "Electroconductive Nylon 6 and Copper Composites", *Polymer Composites* 16, 536-541 (1995)
- [10] Pinto G, Martin A. J., "Conducting Aluminum-Filled Nylon 6 Composites", *Polymer Composites* 22, 65-70 (2001)
- [11] Li R. J., Xu J. R., Zhang M. Q., Rong, M. Z., "Electrical Response to Organic Vapor of Conductive Composites from Amorphous Polymer/Carbon Black Prepared by Polymerization Filling", *Macromolecular Materials and Engineering* 288, 103-107 (2003)
- [12] Dong X. M., Fu R. W., Zhang M. Q., Zhang B., Li J. R., Rong M. Z., "Vapor-induced variation in electrical performance of carbon black/poly(methyl methacrylate) composites prepared by polymerization filling", *Carbon* 41, 371-374 (2003)
- [13] Li J. R., Xu J. R., Zhang M. Q., Rong M. Z., "Carbon black/polystyrene composites as candidates for gas sensing material", *Carbon* 41, 2353-2360 (2003)
- [14] Xiao P., Xiao M., Gong K., "Preparation of exfoliated graphite/polystyrene composite by polymerization-filling technique", *Polymer* 42, 4813-4816 (2001)

- [15] Pluta M., Alexandre M., Blacher S., Dubois P., Jerome R., "Metallocene-catalyzed polymerization of ethylene in the presence of graphite. II. Structure and electrical properties of the composites", *Polymer* 42, 9293-9300 (2001)
- [16] Pan Y. X., Yu Z. Z., Ou Y. C., Hu G. H., "A New Process of Fabricating Electrically Conducting Nylon 6/Graphite Nanocomposites via Intercalation Polymerization", *Polymer Physics* 38, 1626-1633 (2000)
- [17] Yoon H. G., Kwon K. W., Nagata K., Takahashi K., "Changing the percolation threshold of a carbon black/polymer composite by a coupling treatment of the black", *Carbon* 42, 1877-1879 (2004)
- [18] Yu G., Zhang M. Q., Zeng H. M., Hou Y. H., Zhang H. B., "Effect of Filler Treatment on Temperature Dependence of Resistivity of Carbon-Black-Filled Polymer Blends", *Journal of Applied Polymer Science*, 73, 489-494 (1999)
- [19] Pantea D., Darmstadt H., Kaliaguine S., Sümchen L., Roy C., "Electrical conductivity of thermal carbon blacks influence of surface chemistry", *Carbon* 39, 1147-1158 (2001)
- [20] Koysuren O., Yesil S., Bayram G., "Effect of Surface Treatment on Electrical Conductivity of Carbon Black Filled Conductive Polymer Composites", *Journal of Applied Polymer Science* 104, 3427-3433 (2007)
- [21] Koysuren O., Yesil S., Bayram G., Secmen M., Civi O. A., "Effect of a Carbon Black Surface Treatment on the Microwave Properties of Poly(ethylene terephthalate)/Carbon Black Composites", *Journal of Applied Polymer Science* 109, 152-159 (2008)

- [22] Kodali V. P., "Engineering Electromagnetic Compatibility", IEEE Press, New York (1996)
- [23] Clayton R. P., "Introduction to Electromagnetic Compatibility", John Wiley and Sons, Inc., New York (1992)
- [24] Das N. C., Khastgir D., Chaki T. K., Chakraborty A., "Electromagnetic interference shielding effectiveness of carbon black and carbon fiber filled EVA and NR based composites", *Composites: Part A* 31, 1069-1081 (2000)
- [25] Kaynak A., Polat A., Yilmazer U., "Some Microwave and Mechanical Properties of Carbon Fiber-Polypropylene and Carbon black-Polypropylene Composites", *Materials Research Bulletin* 31, 1195-1206 (1996)
- [26] Ahmad M. S., Abdelazeez M. K., Zihlif A., Martuscelli E., Ragosta G., Scafora E., "Some properties of nickel-coated carbon fibre-polypropylene composite at microwave frequencies", *Journal of Materials Science* 25, 3083-3088 (1990)
- [27] Chiang W. Y., Cheng K. Y., "Processing conditions for electromagnetic interference shielding effectiveness and mechanical properties of acrylonitrile-butadiene-styrene based composites", *Polymer Composites* 18, 748-756 (1997)
- [28] Christman J. R., "Fundamentals of Solid State Physics", John Wiley and Sons, Inc., New York (1988)
- [29] Serway R. A., "Physics for Scientists and Engineers", Saunders College Publishing, Philadelphia (1996)
- [30] Zois H., Pipekis L. and Omastova M., "Electrical Properties of Carbon Black-filled Polymer Composites", *Macromolecular Symposia* 170, 249-256 (2001)

- [31] Foulger S. H., "Reduced Percolation Thresholds of Immiscible Conductive Blends", *Journal of Polymer Science: Part B: Polymer Physics* 37, 1899-1910 (1999)
- [32] Liang G. D., Tjong S. C., "Electrical properties of low-density polyethylene/multiwalled carbon nanotube nanocomposites", *Materials Chemistry and Physics* 132, 100-105 (2006)
- [33] El-Tantawy F. E., Aal N. A., El-Daly A. A., Abdel-Daiem A. M., Bakry A., Sung Y. K., "A new phantom model and attenuation backing from epoxy resin nanosized hydroxyapatite-carbon black and multifunctional agent composites", *Materials Letters* 58, 3388-3394 (2004)
- [34] Solomon M. A., Kurian P., Anantharaman M. R., Joy P. A., "Effect of Carbon Black on the Mechanical and Dielectric Properties of Rubber Ferrite Composites Containing Barium Ferrite", *Journal of Applied Polymer Science* 89, 769-778 (2003)
- [35] Moulart A., Marrett C., Colton J., "Polymeric Composites for Use in Electronic and Microwave Devices", *Polymer Engineering and Science* 44, 588-597 (2004)
- [36] Noshay A., McGrath J. E., "Block Copolymers", Academic Press, New York, 7-10 (1977)
- [37] Fried J. R., "Polymer Science and Technology", Second Edition, Prentice Hall Pub., USA (2003)
- [38] Hu G. H., Cartier H., "Reactive Extrusion: Toward Nanoblends", *Macromolecules* 32, 4713-4718 (1999)

- [39] Ji Y., Li W., Ma J., Liang B., “A Novel Approach to the Preparation of Nanoblends of Poly(2,6-dimethyl-1,4-phenylene oxide)/Polyamide 6”, *Macromolecular Rapid Communications* 26, 116-120 (2005)
- [40] Banerjee P., Mandal B. M., “Conducting Polyaniline Nanoparticle Blends with Extremely Low Percolation Thresholds”, *Macromolecules* 28, 3940-3943 (1995)
- [41] Smith A. P., Bai C., Ade H., Spontak R. J., Balik C. M., Koch C. C., “X-ray microscopy of novel thermoplastic/liquid crystalline polymer blends by mechanical alloying”, *Macromolecular Rapid Communications* 19, 557-561 (1998)
- [42] Martin J. P., McCartney S. R., Kander R. G., “An investigation of the microstructure of a cryogenically mechanically alloyed polycarbonate-poly(aryl ether ether ketone) system”, *Journal of Materials Science* 38, 195-200 (2003)
- [43] Stranz M., Koster U., “Structural changes during cryogenic mechanical milling of iPP/sPS blends”, *Journal of Materials Science* 39, 5275-5277 (2004)
- [44] Chen Z., Wang Q., “Pan-milling mixing-a novel approach to forming polymer blends and controlling their morphology”, *Polymer International* 50, 966-972 (2001)
- [45] Chan S. H., Lin Y. Y., Ting C., “Nanoblends of Incompatible Polymers by direct Space-Confined Polymerization”, *Macromolecules* 36, 8910-8912 (2003)
- [46] Shimizu H., Li Y., Kaito A., Sano H., “Formation of Nanostructured PVDF/PA11 Blends Using High-Shear Processing”, *Macromolecules* 38, 7880-7883 (2005)

- [47] Furgieuele N., Lebovitz A. H., Khait K., Torkelson J. M., “Novel Strategy for Polymer Blend Compatibilization: Solid-State Shear Pulverization”, *Macromolecules* 33, 225-228 (2000)
- [48] Lebovitz A. H., Khait K., Torkelson J. M., “Stabilization of Dispersed Phase to Static Coarsening: Polymer Blend Compatibilization via Solid-State Shear Pulverization”, *Macromolecules* 35, 8672-8675 (2002)
- [49] Tao Y., Lebovitz A. H., Torkelson J. M., “Compatibilizing effects of block copolymer mixed immiscible polymer blends by solid-state shear pulverization: stabilizing the dispersed phase to static coarsening”, *Polymer* 46, 4753-4761 (2005)
- [50] Tao Y., Kim J., Torkelson J. M., “Achievement of quasi-nanostructured polymer blends by solid-state shear pulverization and compatibilization by gradient copolymer addition”, *Polymer* 47, 6773-6781 (2006)
- [51] Arbizzani C., Mastragostino M., Scrosati B., “Conducting Polymers for Batteries, Supercapacitors and Optical Devices”, in *Handbook of Organic Conductive Molecules and Polymers*, Nalwa H. S., (Ed.), Wiley, Chichester, England, 595-619 (1997)
- [52] Conway B. E., “Electrochemical Supercapacitors: Scientific Fundamentals and Technological Applications”, Plenum Publications, New York (1999)
- [53] Sarangapani S., Lessner P., Forchione J., Griffith A., Laconti A. B., “Advanced Double Layer Capacitor”, *Journal of Power Sources* 29, 355-364 (1990)
- [54] An K. H., Kim W. S., Park Y. S., Choi Y. C., Lee S. M., Chung D. C., Bae D. J., Lim S. C., Lee Y. H., “Supercapacitors Using Single-Walled Carbon Nanotube Electrodes”, *Advanced Materials* 13, 497-500 (2001)

- [55] Frackowiak E., Metenier K., Bertagna V., Beguin F., "Supercapacitor electrodes from multiwalled carbon nanotubes", *Applied Physics Letters* 77, 2421-2423 (2000)
- [56] Frackowiak E., Jurewicz K., Szostak K., Delpeux S., Beguin F., "Nanotubular materials as electrodes for supercapacitors", *Fuel Processing Technology* 77-78, 213-219 (2002)
- [57] Park D., Kim Y. H., Lee J. K., "Synthesis of carbon nanotubes on metallic substrates by a sequential combination of PECVD and thermal CVD", *Carbon* 41, 1025-1029 (2003)
- [58] Wen S., Mho S. I., Yeo I. H., "Improved electrochemical capacitive characteristics of the carbon nanotubes grown on the alumina templates with high pore density", *Journal of Power Sources* 163, 304-308 (2006)
- [59] Chatterjee A. K., Sharon M., Banerjee R., Spallart M. N., "CVD synthesis of carbon nanotubes using a finely dispersed cobalt catalyst and their use in double layer electrochemical capacitors", *Electrochimica Acta* 48, 3439-3446 (2003)
- [60] Yoon B. J., Jeong S. H., Lee K. H., Kim H. S., Park C. G., Han J. H., "Electrical properties of double layer capacitors with integrated carbon nanotube electrodes", *Chemical Physics Letters* 388, 170-174 (2004)
- [61] Du C., Yeh J. and Pan N., "High power density supercapacitors using locally aligned carbon nanotube electrodes", *Nanotechnology* 16, 350-353 (2005)
- [62] Du C., Pan N., "Supercapacitors using carbon nanotubes films by electrophoretic deposition", *Journal of Power Sources* 160, 1487-1494 (2006)

- [63] Conway B. E., Birss V., Wojtowicz J., “The role and utilization of pseudocapacitance for energy storage by supercapacitors”, *Journal of Power Sources* 66, 1-14 (1997)
- [64] Ryu K. S., Kim K. M., Park N. G., Park Y. J., Chang S. H., “Symmetric redox supercapacitor with conducting polyaniline electrodes”, *Journal of Power Sources* 103, 305-309 (2002)
- [65] Zhou H., Chen H., Luo S., Gewu L., Wei W., Kuang Y., “The effect of the polyaniline morphology on the performance of polyaniline supercapacitors”, *Journal of Solid State Electrochemistry* 9, 574-580 (2005)
- [66] Belanger D., Ren X., Davey J., Uribe F., Gottesfeld S., “Characterization and Long-Term Performance of Polyaniline-Based Electrochemical Capacitor”, *Journal of the Electrochemical Society* 147, 2923-2929 (2000)
- [67] Zou X., Zhang S., Shi M., Kong J., “Remarkably enhanced capacitance of ordered polyaniline nanowires tailored by stepwise electrochemical deposition”, *Journal of Solid State Electrochemistry* 11, 317-322 (2007)
- [68] Girija T. C., Sangaranarayanan M. V., “Analysis of polyaniline-based nickel electrodes for electrochemical supercapacitors”, *Journal of Power Sources* 156, 705-711 (2006)
- [69] Girija T. C., Sangaranarayanan M. V., “Polyaniline-based nickel electrodes for electrochemical supercapacitors: Influence of Triton X-100”, *Journal of Power Sources* 159, 1519-1526 (2006)

- [70] Gupta V., Miura N., “High performance electrochemical supercapacitor from electrochemically synthesized nanostructured polyaniline”, *Material Letters* 60, 1466-1469 (2006)
- [71] Fusalba F., Gouerec P., Villers D., Belanger D., “Electrochemical Characterization of Polyaniline in Nonaqueous Electrolyte and Its Evaluation as Electrode Material for Electrochemical Supercapacitors”, *Journal of the Electrochemical Society* 148, A1-A6 (2001)
- [72] Zhou Y. K., He B. L., Zhou W. J., Huang J., Li X. H., Wu B., Li H. L., “Electrochemical capacitance of well-coated single walled carbon nanotube with polyaniline composites”, *Electrochimica Acta* 49, 257-262 (2004)
- [73] Frackowiak E., Khomenko V., Jurewicz K., Lota K., Beguin F., “Supercapacitors based on conducting polymers/nanotubes composites”, *Journal of Power Sources* 153, 413-418 (2006)
- [74] Gupta V., Miura N., “Polyaniline/single-wall carbon nanotube (PANI/SWCNT) composites for high performance supercapacitors”, *Electrochimica Acta* 52, 1721-1726 (2006)
- [75] Zhou H., Chen H, Luo S., Lu G., Wei W., Kuang Y., “The effect of the polyaniline morphology on the performance of polyaniline supercapacitors”, *Journal of Solid State Electrochemistry* 9, 574-580 (2005)
- [76] Hibberd R. G., “Solid – State Electronics”, Mc Graw-Hill Book Company, Texas (1968)
- [77] Hyde F. J., “Semiconductors”, Macdonald & G. Ltd., London (1965)

- [78] Kano K., "Physical and Solid State Electronics", Addison-Wesley Pub., Reading, MA (1972)
- [79] Xanthos M., "Functional Fillers for Plastics", Wiley-VCH, Germany (2005)
- [80] Seymour R. B., "Reinforced Plastics Properties and Applications", ASM International, USA (1991)
- [81] Ebbesen T. W., "Production and Purification of Carbon Nanotubes", in Carbon Nanotubes Preparation and Properties, Ebbesen T. W., (Ed.), CRC Press, Boca Raton, 139-162 (1997)
- [82] Yumura M., "Synthesis and Purification of Multi-Walled and Single-Walled Carbon Nanotubes", in The Science and Technology of Carbon Nanotubes, Tanaka K., Yamabe T., Fukui K., (Ed.), Elsevier Science Ltd., Amsterdam, 2-13 (1999)
- [83] Dai H., "Nanotube Growth and Characterization", in Carbon Nanotubes Synthesis, Structure, Properties and Applications, Dresselhaus M. S., Dresselhaus G., Avouris P., (Ed.), Springer, Berlin, Germany, 29-53 (2001)
- [84] Mann D., "Synthesis of Carbon Nanotubes", in Carbon Nanotubes, O'Connell M. J., (Ed.), CRC Press, Boca Raton, 20-49 (2006)
- [85] Billmeyer F. W., "Textbook of Polymer Science", Third Edition, Wiley-Interscience Pub., New York, USA (1984)
- [86] "The Chemistry of Nylon 6 Synthesis" (Internet, www) Address: <http://www.Chemheritage.org/EducationalServices/FACES/teacher/poly/activity/nylon6.htm> (Accessed: December 2004)

- [87] Ram A., "Fundamentals of Polymer Engineering", Plenum Press, New York, USA (1997)
- [88] Epstein A. J., Ginder J. M., Richter A. F., MacDiarmid A. G., "Are Semiconducting Polymers Polymeric Semiconductors?: Polyaniline as an Example of Conducting Polymers", in *Conducting Polymers Special Applications*, Alcazer L., (Ed.), Reidel Publishing Company, Dordrecht, Holland, 121-140 (1987)
- [89] MacDiarmid A. G., Chiang J. C., Richter A. F., Somasiri N. L. D., "Polyaniline: Synthesis and Characterization of the Emeraldine Oxidation State by Elemental Analysis", in *Conducting Polymers Special Applications*, Alcazer L., (Ed.), Reidel Publishing Company, Dordrecht, Holland, 105-120 (1987)
- [90] Stejskal J., Kratochvil P., Jenkins A. D., "The formation of polyaniline and the nature of its structures", *Polymer* 37, 367-269 (1996)
- [91] Mohilner D. M., Adams R. N., Argersinger W. J., "Investigation of the Kinetics and Mechanism of the Anodic Oxidation of Aniline in Aqueous Sulfuric Acid Solution at a Platinum Electrode", *Journal of the American Chemical Society* 84, 3618-3622 (1962)
- [92] Wei Y., Tang X., Sun Y., "A Study of the Mechanism of Aniline Polymerization", *Journal of Polymer Science: Part A: Polymer Chemistry* 27, 2385-2396 (1989)
- [93] Mascia L., "Thermoplastic", Elsevier Applied Science, London (1989)
- [94] Joseph H. K., "Polymer Nanocomposites", McGraw-Hill, New York, 61-93 (2006)

- [95] Charrier J. M., "Polymeric Materials and Processing", Carl Hanser Verlag, Munich (1990)
- [96] Ebewe R. O., "Polymer Science and Technology", CRC Press, USA (2000)
- [97] McCabe W. L., Smith J. C., Harriott P., "Unit Operations of Chemical Engineering", Fifth Edition, McGraw-Hill, New York, 960-976 (1993)
- [98] Utracki L. A., "Polymer Alloys and Blends", Carl Hanser Verlag, Munich, 1-27 (1989)
- [99] van Oss C. J., Good R. J., Chaudhury M. K., "Additive and Nonadditive Surface Tension Components and the Interpretation of Contact Angles", Langmuir 4, 884-891 (1988)
- [100] Ozkoc G., Bayram G., Bayramli E., "Effect of polyamide 6 incorporation to the short glass fiber reinforced ABS composites: an interfacial approach", Polymer 45, 8957-8966 (2004)
- [101] Park S. J., Kim J. S., "Surface energy characterization of modified carbon blacks and its relationship to composites tearing properties", Journal of Adhesion Science and Technology 15, 1443-1452 (2001)
- [102] Shimizu R. N., Demarquette N. R., "Evaluation of surface energy of solid polymers using different models", Journal of Applied Polymer Science 76, 1831-1845 (2000)
- [103] Yosoyima R., Morimoto K., Nakajima A., Ikada Y., Suzuki T., "Adhesion and Bonding in Composites", Marcel Dekker Inc., New York (1990)

- [104] Morant M. J., "Introduction to Semiconductor Devices", Addison-Wesley Pub., London (1964)
- [105] Wu M., Shaw L. L., "On the improved properties of injection-molded, carbon nanotube filled PET/PVDF blends", Journal of Power Sources 136, 37-44 (2004)
- [106] Chen J., Chen P., Wu L., Zhang J., He J., "Enhanced fibrillation of LCP by CaCO₃ whisker in polysulfone matrix through increasing elongational stress", Polymer 47, 5402-5410 (2006)
- [107] Sumita M., Sakata K., Asai S., Miyasaka K., "Dispersion of fillers and the electrical conductivity of polymer blends filled with carbon black", Polymer Bulletin 25, 265-271 (1991)
- [108] Oswald T. A., Menges G., "Materials Science of Polymers for Engineers", Carl Hanser Verlag, Munich (1995)
- [109] Schroder D. K., "Semiconductor Material and Device Characterization", Second Edition, John Wiley & Sons, Inc., New York (1998)
- [110] Jang B. Z., "Advanced Polymer Composites: Principles and Applications", ASM International, USA, 39-40 (1994)
- [111] "Transmission electron microscopy-Wikipedia, the free encyclopedia" (Internet, www) Address: http://en.wikipedia.org/wiki/Transmission_electron_microscope (Accessed: October 2007)
- [112] Takeuchi K. J., Marschlok A. C., Lau G. C., Leising R. A., Takeuchi E. S., "Carbon structure/function relationships: Characterization and electrochemistry of carbon nanofibers", Journal of Power Sources 157, 543-549 (2006)

- [113] Park S. J., Kim J. S., “Modifications produced by electrochemical treatments on carbon black: Microstructures and mechanical interfacial properties”, Carbon 39, 2011-2016 (2001)
- [114] Lenk D. J., “Eliminating Engine Interference”, Howard W. Sons & Co., Inc., Indianapolis (1968)
- [115] Chung D. D. L., “Electromagnetic interference shielding effectiveness of carbon material”, Carbon 39, 279-285 (2001)
- [116] Harrison W. A., “Electronic Structure and the Properties of Solids”, W. H. Freeman and Company, San Francisco (1980)
- [117] Symth C. P., “Dielectric Behavior and Structure”, McGraw Hill Book Company, Inc., New York (1955)
- [118] Morrison R., “Grounding and Shielding Techniques in Instrumentation”, Wiley Interscience Pub., Canada (1977)
- [119] “Fourier transform spectroscopy-Wikipedia, the free encyclopedia” (Internet, www) Address: http://en.wikipedia.org/wiki/Fourier_transform_spectroscopy (Accessed: October 2007)
- [120] Brotherton M., “Capacitors”, D. Van Nostrand Company Inc., Canada (1946)
- [121] Livingston J. D., “Electronic Properties of Engineering Materials”, John Wiley & Sons Inc., USA (1999)
- [122] Kotz R., Carlen M., “Principles and applications of electrochemical capacitors”, Electrochimica Acta 45, 2483-2498 (2000)

[123] "Cyclic voltammetry-Wikipedia, the free encyclopedia" (Internet, www) Address: http://en.wikipedia.org/wiki/Cyclic_voltammetry (Accessed: October 2007)

[124] Frackowiak E., Beguin F., "Carbon materials for the electrochemical storage of energy in capacitors", *Carbon* 39, 937-950 (2001)

[125] "Capacitor-Wikipedia, the free encyclopedia" (Internet, www) Address: <http://en.wikipedia.org/wiki/Capacitor> (Accessed: October 2007)

[126] Brandrup J., Immergut E. H., "Polymer Handbook", Wiley Interscience Pub., New York, (1989)

[127] Akovali G., Tosun T. T., Bayramli E., Erinc N. K., "Mechanical properties and surface energies of low density polyethylene-poly(vinyl chloride) blends", *Polymer* 39, 1363-1368 (1998)

[128] Hong Y. C., Shin D. H., Cho S. C., Uhm H. S., "Surface transformation of carbon nanotube powder into super-hydrophobic and measurement of wettability", *Chemical Physics Letters* 427, 390-393 (2006)

[129] Park S. J., Seo M. K., Nah C., "Influence of surface characteristics of carbon blacks on cure and mechanical behaviors of rubber matrix compoundings", *Journal of Colloid and Interface Sciences* 291, 229-235 (2005)

[130] Stejskal J., Gilbert R. G., "Polyaniline. Preparation of a Conducting Polymer", *Pure and Applied Chemistry* 74, 857-867 (2002)

[131] Konyushenko E. N., Stejskal J., Trchova M., Hradil J., Kovarova J., Prokes J., Cieslar M., Hwang J. Y., Chen K. H., Sapurina I., "Multi-wall carbon nanotubes coated with polyaniline", *Polymer* 47, 5715-5723 (2006)

- [132] Sun Y., Wilson S. R., Schuster D., “High Dissolution and Strong Light Emission of Carbon Nanotubes in Aromatic Amine Solvents”, *Journal of American Chemical Society* 123, 5348-5349 (2001)
- [133] Cataldo F., “Carbon black nitration and nitrosation and its application to improve the mechanical hysteresis of a rubber tread compound“, *Die Angewandte Makromolekulare Chemie* 270, 81-86 (1999)
- [134] Fessenden R. J., Fessenden J. S., “Organic Chemistry”, W. Grant Press, Boston, (1982)
- [135] Hoecker F., Karcser-Kocsis J., “Surface Energetics of Carbon Fibers and Its Effects on the Mechanical Performance of CF/EP Composites”, *Journal of Applied Polymer Science*, 59, 139-153 (1996)
- [136] Zhang C., Yi X. S., Yui H., Asai S., Sumita M., “Selective localization and double percolation of short carbon fiber filled polymer blends: high-density polyethylene/isotactic polypropylene”, *Materials Letters* 36, 186-190 (1998)
- [137] Dai K., Xu X. B., Li Z. M., “Electrically conductive carbon black (CB) filled in situ microfibrillar poly(ethylene terephthalate) (PET)/polyethylene (PE) composite with a selective CB distribution”, *Polymer* 48, 849-859 (2007)
- [138] Yoon J. H., Lee H. W., Park O. O., “Properties of Poly(ethylene terephthalate) and Maleic Anhydride-Grafted Polypropylene Blends by Reactive Processing”, *Journal of Applied Polymer Science* 70, 389-395 (1998)
- [139] Chen G. X., Kim H. S., Park B. H., Yoon J. S., “Multi-walled carbon nanotubes reinforced nylon 6 composites”, *Polymer* 47, 4760-4767 (2006)

- [140] Choi J. H., Jegal J., Kim W. N., "Fabrication and characterization of multi-walled carbon nanotubes/polymer blend membranes", *Journal of Membrane Sciences* 284, 406-415 (2006)
- [141] Ma P. C., Kim J. K., Tang B. Z., "Functionalization of carbon nanotubes using a silane coupling agent", *Carbon* 44, 3232-3238 (2006)
- [142] Deng J., Zhang X., Wang K., Zou H., Zhang Q., Fu Q., "Synthesis and properties of poly(ether urethane) membranes filled with isophorone diisocyanate-grafted carbon nanotubes", *Journal of Membrane Sciences* 288, 261-267 (2007)
- [143] Liang Y., Zhang H., Yi B., Zhang Z., Tan Z., "Preparation and characterization of multi-walled carbon nanotubes supported PtRu catalysts for proton exchange membrane fuel cells", *Carbon* 43, 3144-3152 (2005)
- [144] Choi J. H., Oh S. B., Chang J., Kim II., Ha C. S., Kim B. G., Han J. H., Joo S. W., Kim G. H., Paik H. J., "Graft Polymerization of Styrene from Single-Walled Carbon Nanotube using Atom Transfer Radical Polymerization", *Polymer Bulletin* 55, 173-179 (2005)
- [145] Sengupta P. P., Adhikari B., "Influence of polymerization condition on the electrical conductivity and gas sensing properties of polyaniline", *Materials Science and Engineering A* 459, 278-285 (2007)
- [146] Qiao Y., Li C. M., Bao S. J., Bao Q. L., "Carbon nanotube/polyaniline composite as anode material for microbial fuel cells" *Journal of Power Sources* 170, 79-84 (2007)

- [147] Jing S., Xing S., Yu L., Wu Y., Zhao C., "Synthesis and characterization of Ag/polyaniline core-shell nanocomposites based on silver nanoparticles colloid", *Material Letters* 61, 2794-2797 (2007)
- [148] Sengupta P. P., Barik S., Adhikari B., "Polyaniline as a Gas-Sensor Material", *Materials and Manufacturing Processes* 21, 263-270 (2006)
- [149] Sazou D., Georgolios C., "Formation of conducting polyaniline coatings on iron surfaces by electropolymerization of aniline in aqueous solutions", *Journal of Electroanalytical Chemistry* 429, 81-93 (1997)
- [150] Huang J. E., Li X. H., Xu J. C., Li H. L., "Well-dispersed single-walled carbon nanotube/polyaniline composite films", *Carbon* 41, 2731-2736 (2003)
- [151] Amrithesh M., Aravind S., Jayalekshmi S., Jayasree R. S., "Polyaniline doped with orthophosphoric acid: A material with prospects for optoelectronic applications", *Journal of Alloys and Compounds*, in Press (2007)
- [152] Pal A. K., Roy R. K., Mandal S. K., Gupta S., Deb B., "Electrodeposited carbon nanotube thin films", *Thin Solid Films* 476, 288-294 (2005)
- [153] Lefrant S., Baibarac M., Baltog I., Mecellec J. Y., Godon C., Chauver O., "Functionalization of single-walled carbon nanotubes with conducting polymers evidenced by Raman and FTIR spectroscopy", *Diamond and Related Materials* 14, 867-872 (2005)
- [154] Wei D., Kvarnstrom C., Lindfors T., Ivaska A., "Polyaniline nanotubes obtained in room-temperature ionic liquids", *Electrochemistry Communications* 8, 1563-1566 (2006)

- [155] Jurczyk M. U., Kumar A., Srinivasan S., Stefanakos E., "Polyaniline-based nanocomposite materials for hydrogen storage", *International Journal of Hydrogen Energy* 32, 1010-1015 (2007)
- [156] Gopalan A. I., Lee K. P., Santhosh P., Kim K. S., Nho Y. C., "Different types of molecular interactions in carbon nanotube/conducting polymer composites: A close analysis", *Composites Science and Technology* 67, 900-905 (2007)
- [157] Zengin H., Zhou W., Jin J., Czerw R., Smith D. W., Echegoyen L., Carroll D. L., Foulger S. H., Ballato J., "Carbon Nanotube Doped Polyaniline", *Advanced Materials* 14, 1480-1483 (2002)
- [158] Gaikwad P. D., Shirale D. J., Gade V. K., Savale P. A., Kakde K. P., Kharat H. J., Shirsat M. D., "Potentiometric study of polyaniline film synthesized with various dopants and composite-dopant: A comparative study", *Bulletin of Material Science* 29, 417-420 (2006)
- [159] Barsukov V. Z., Khomenko V. G., Chivikov S. V., Barsukov I. V., Motronyuk T. I., "On the faradaic and non-faradaic mechanisms of electrochemical processes in conducting polymers and some other reversible systems with solid-phase reagents", *Electrochimica Acta* 46, 4083-4094 (2001)
- [160] Show Y., Imaizumi K., "Electrical double layer capacitor with low series resistance fabricated by carbon nanotube addition", *Diamond and Related Materials* 16, 1154-1158 (2007)
- [161] Wei Y. Z., Fang B., Iwasa S., Kumagai M., "A novel electrode material for electric double-layer capacitors", *Journal of Power Sources* 141, 386-391 (2005)

[162] Tamai H., Hakoda M., Shiono T., Yasuda H., "Preparation of polyaniline coated activated carbon and their electrode performance for supercapacitor", *Journal of Material Science* 42, 1293-1298 (2007)

[163] Ahmad N., MacDiarmid A. G., "Inhibition of corrosion of steels with the exploitation of conducting polymers", *Synthetic Metals* 78, 103-110 (1996)

[164] Huerta-Vilca D., Moraes E. S. R., Jesus-Motheo A., "Aspects of polyaniline electrodeposition on aluminium", *Journal of Solid State Electrochemistry* 9, 416-420 (2005)

[165] Bleda-Martinez M. J., Morallon E., Cazorla-Amoros D., "Polyaniline/porous carbon electrodes by chemical polymerization", *Electrochimica Acta* 52, 4962-4968 (2007)

APPENDIX A

X-RAY DIFFRACTION PATTERNS

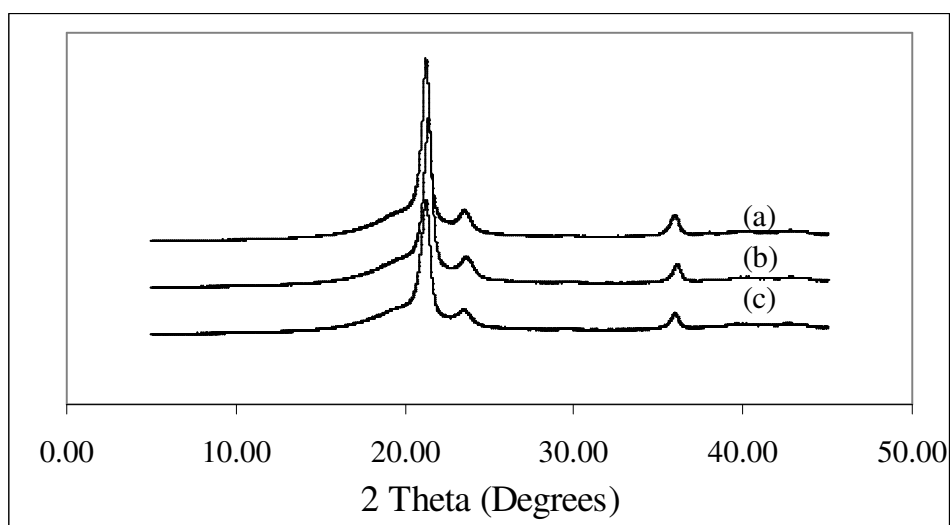


Figure A.1 Diffraction pattern of 2 wt. % (a) formamide treated carbon black, (b) untreated carbon black and (c) APS treated carbon black in LDPE

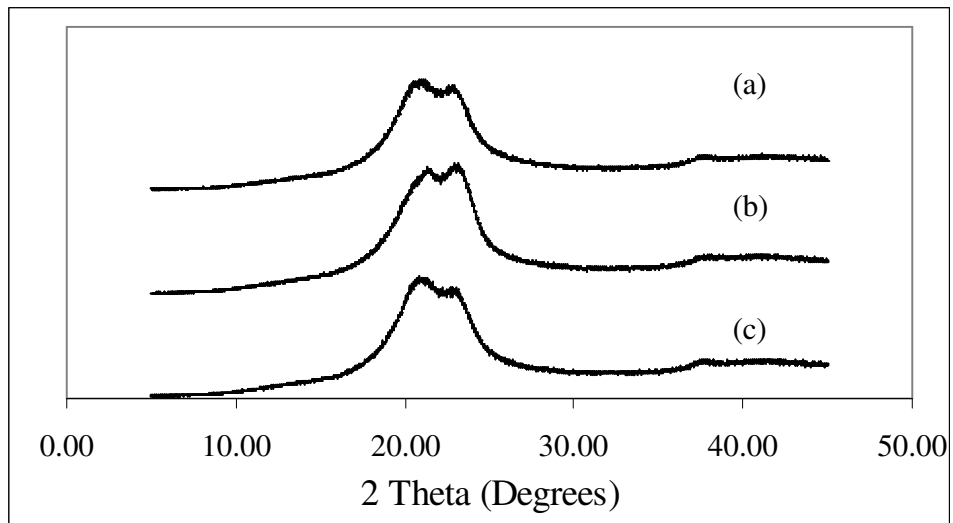


Figure A.2 Diffraction pattern of 2 wt. % (a) formamide treated carbon black, (b) untreated carbon black and (c) APS treated carbon black in nylon 6

APPENDIX B

ELECTROCHEMICAL CAPACITANCE PERFORMANCES OF POLYANILINE/CARBON NANOTUBES COMPOSITES

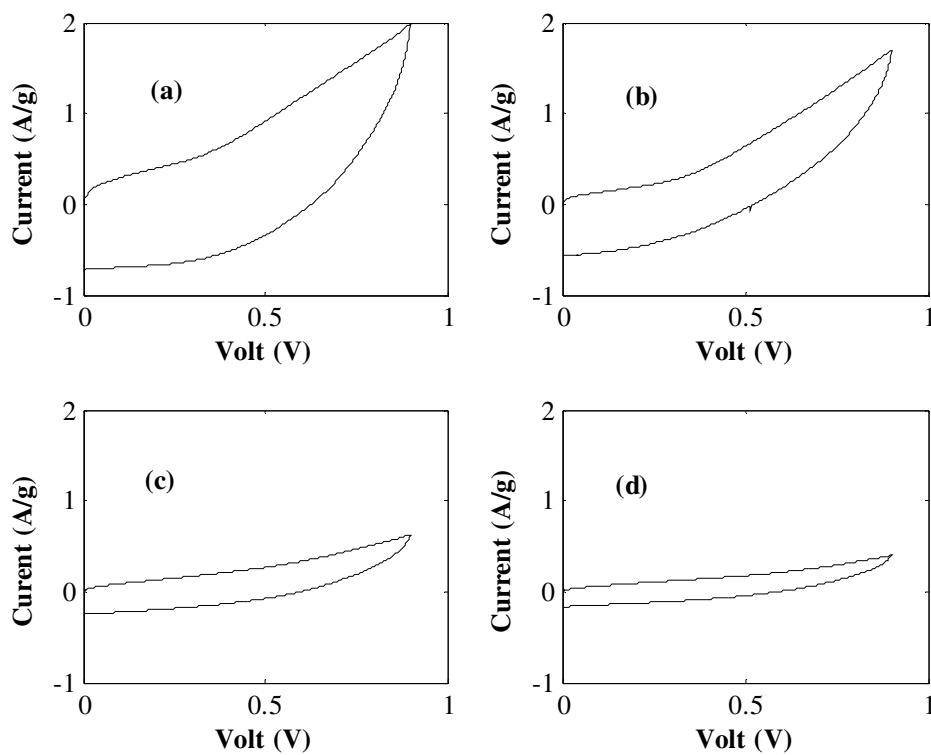


Figure B.1 Cyclic voltammety curves of polyaniline/carbon nanotubes composites containing (a) 10 wt. % polyaniline, (b) 40 wt. % polyaniline, (c) 60 wt. % polyaniline and (d) 80 wt. % polyaniline

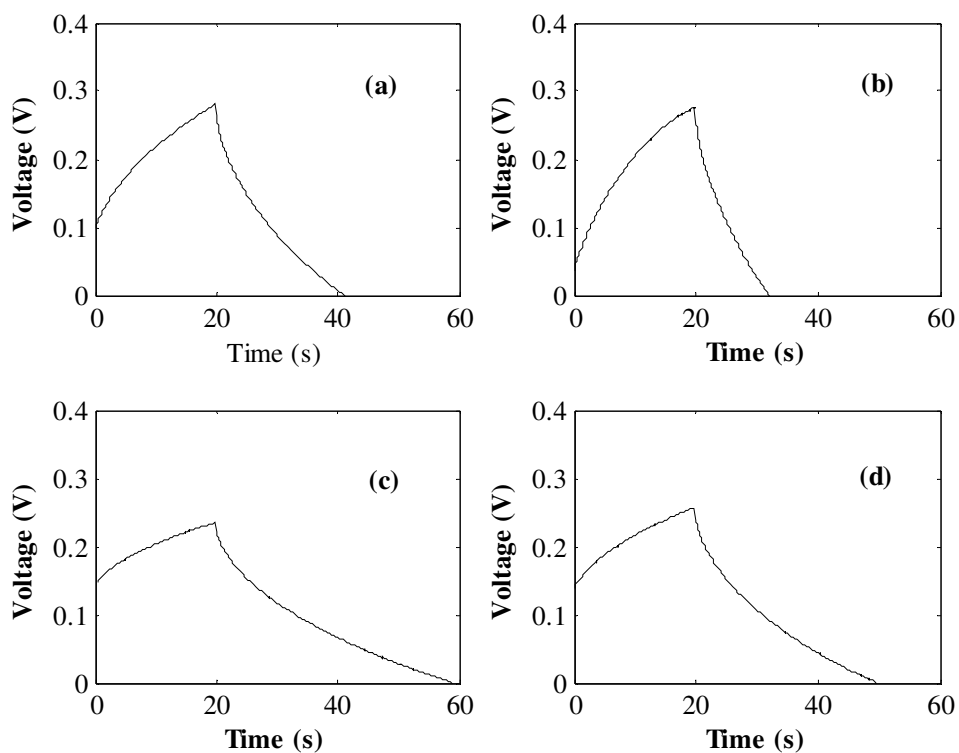


Figure B.2 Charge/discharge plots of polyaniline/carbon nanotubes composites containing (a) 10 wt. % polyaniline, (b) 40 wt. % polyaniline, (c) 60 wt. % polyaniline and (d) 80 wt. % polyaniline

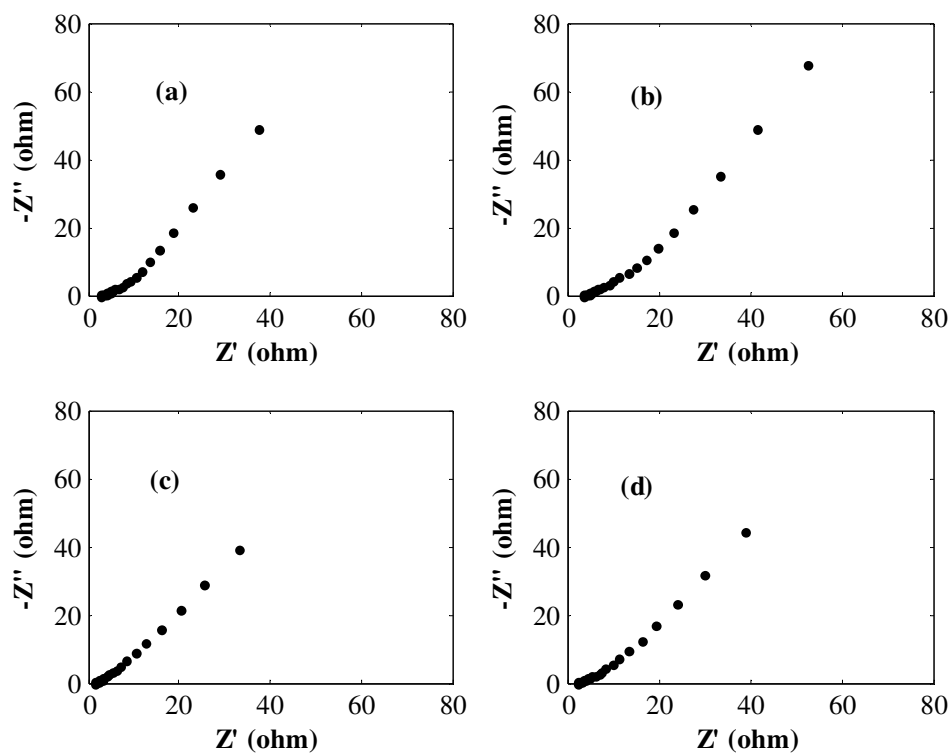


Figure B.3 Electrochemical impedance spectra of polyaniline/carbon nanotubes composites containing (a) 10 wt. % polyaniline, (b) 40 wt. % polyaniline, (c) 60 wt. % polyaniline and (d) 80 wt. % polyaniline

CURRICULUM VITAE

PERSONAL INFORMATION

Surname, Name: Köysüren, Özcan

Nationality: Turkish (TC)

Date and Place of Birth: 22 July 1979, Dinslaken (GERMANY)

Marital Status: Single

Phone: +90 312 210 43 53

Fax: +90 312 210 26 00

Email: koysuren@metu.edu.tr

EDUCATION

<u>Degree</u>	<u>Institution</u>	<u>Year of Graduation</u>
BS	METU, Chemical Engineering	2002
High School	Ankara Anadolu High School, Ankara	1997

WORK EXPERIENCE

<u>Year</u>	<u>Place</u>	<u>Enrollment</u>
2002-Present	METU, Dept. of Chemical Engineering	Teaching Assistant
2001, Summer	BOTAS, Ankara	Intern Process Engineer
2000, Summer	KORDSA, Kocaeli	Intern Process Engineer

ABROAD EXPERIENCE

<u>Place</u>	<u>Project</u>	<u>Year</u>
The University of California at Davis	Study on investigation and characterization of nano supercapacitors	March 2007- Sep. 2007

FOREIGN LANGUAGES

Advanced English and German

PUBLICATIONS

Journal Publications:

1. O. Koysuren, S. Yesil and G. Bayram, "Effect of Composite Preparation Techniques on Electrical and Mechanical Properties and Morphology of Nylon 6 Based Conductive Polymer Composites", Journal of Applied Polymer Science, 102, p. 2520, 2006.
2. O. Koysuren, S. Yesil and G. Bayram, "Effect of Surface Treatment on Electrical Conductivity of Carbon Black Filled Conductive Polymer Composites", Journal of Applied Polymer Science, 104, p. 3427, 2007.
3. O. Koysuren, S. Yesil, G. Bayram, M. Secmen and O. A. Civi, "Effect of a Carbon Black Surface Treatment on the Microwave Properties of Poly(ethylene terephthalate)/Carbon Black Composites", Journal of Applied Polymer Science, 109, p. 152, 2008.

Conference Presentations:

1. O. Koysuren, G. Bayram ve S. Yesil, “Naylon 6/Karbon Siyahı Kompozitlerinin Mekanik ve Elektriksel Özellikleri”, Ulusal Kimya Mühendisliği Kongresi (UKMK 6), İzmir, 2004, (Poster Presentation).
2. O. Koysuren, S. Yesil and G. Bayram, “Preparation and Characterization of Nylon 6 Based Conductive Composites”, Annual Technical Conference (ANTEC), Boston, U.S.A., 2005, (Poster Presentation).
3. O. Koysuren, S. Yesil ve G. Bayram, “Karbon Bazlı Dolgu Maddesi İçeren Poli(Etilen Tereftalat) Kompozitlerinin Mekanik ve Elektriksel Özellikleri”, I. Ulusal Polimer Bilim ve Teknoloji Kongresi ve Sergisi, Ankara, 2006, (Oral Presentation).
4. S. Yesil, O. Koysuren and G. Bayram, “Conductive Polymer Composites with Surface Modified Carbon Black”, 22nd Annual Meeting of Polymer Processing Society (PPS 22), Yamagata, Japan, 2006, (Poster Presentation).
5. S. Yesil, O. Koysuren ve G. Bayram, “Karbon Bazlı Dolgu Maddeleri Katkılı Polipropilen Kompozitlerinin Mekanik ve Elektriksel Özellikleri”, Ulusal Kimya Mühendisliği Kongresi (UKMK 7), Eskişehir, 2006, (Poster Presentation).
6. O. Koysuren, S. Yesil and G. Bayram, “Effect of Solid State Grinding Technique on Microstructured Blends of Incompatible Polymers”, Somer Symposium, Ankara, 2007, (Poster Presentation).
7. S. Yesil, O. Koysuren and G. Bayram, “In-Situ Microfiber Reinforcement of Conductive Polymer Composites”, Somer Symposium, Ankara, 2007, (Poster Presentation).

HOBBIES

Winter Sports, Skiing, Mountain Climbing